A GPS L5 Software Defined Vector Tracking Receiver

by

Charles Anderson Givhan

A thesis submitted to the Graduate Faculty of
Auburn University
in partial fulfillment of the
requirements for the Degree of
Master of Science

Auburn, Alabama
August 7, 2021

Keywords: GPS L5, SDR, Vector Tracking

Approved by

Scott Martin, Chair, Assistant Research Professor of Mechanical Engineering
David Bevly, Bill and Lana McNair Professor of Mechanical Engineering
Stanley Reeves, Professor of Electrical and Computer Engineering

Abstract

As the world continues towards autonomy, the need for continuous, precise, and robust navigation is becoming increasingly important. A new wave of modernized Global Navigation Satellite Systems (GNSS) signals are currently being implemented on the latest satellite blocks. The focus of this work is on the Global Positioning System (GPS) L5 signal, and while it is not yet fully available there are now windows of time where experimental data can be used to test modified algorithms exploiting the nature of the new signal structures. The GPS L5 signal is a Quadrature Phase-Shift keying (QPSK) signal that has both an in-phase (data) and quadrature (pilot) arm in the signal that are transmitted together. The pilot channel is not modulated with a data message which historically limits the length of coherent integration during tracking. This work adapts a vector tracking algorithm, which has been shown in prior works to provide a more robust navigation solution than scalar tracking architectures, to the GPS L5 signal structure. The traditional vector tracking architecture for both GPS L1 and L5 quadrature independently are compared to adapted methods. For the first method, the L5 in-phase and L5 quadrature discriminator measurements are combined before being added to the Kalman filter to update the Position, Velocity, and Timing (PVT) solution and Numerically Controlled Oscillators (NCOs). For the second method, L5 in-phase and L5 quadrature are tracked independently and both provide measurements to the same filter for PVT and NCO updates. This second method removes the limit on integration lengths for the L5 quadrature channel allowing for varying extended integration lengths on this channel. All methods are post processed on live sky data from only Block IIF and III satellites and simulated data from a Spirent GNSS simulator and evaluated. A covariance analysis is also performed comparing the methods. Lastly an ionospheric free vector tracking measurement is developed and applied to a GPS L1 GPS L5 dual frequency vector tracking

receiver. This receivers results are compared against a single frequency receiver with an ionospheric model for corrections. The GPS L5 receiver with extended integration periods provided an improvement to the stability of the receiver in degraded environments and provided better filtering of measurements and states. The GPS L5 combined receiver was able to increase the tracking threshold of the receiver by 1-3 dB-Hz over receivers with equivalent integration periods. The ionospheric free combination receiver was able to provide equivalent results to the ionospheric model in simulation, but the live sky results were not as stable as the simulated results. The linear combination of the two vector tracking measurements greatly increases the variance of the measurements.

Acknowledgments

Firstly, I would like to thank the Lord for his countless blessings. Next I would like to thank my wife, Ana, whose constant love, encouragement, and editing helped me write this thesis. I would like to thank Dr. Scott Martin for his guidance and direction while completing this paper. I also owe a thanks to Scott Burchfield, Tanner Watts, and Josh Wood for their help a long the way in my education in GNSS Navigation.

Table of Contents

List of Figures

List of Tables

List of Abbreviations

ADC Analog to Digital Converter

BPF Band Pass Filters

BPSK Binary Phase Shift Keying

C/A Coarse Acquisition

C/N0 Carrier to Noise Ratio

CDMA Code Division Multiple Access

CRC Cyclic Redundancy Check

DLL Delay Lock Loop

ECEF Earth Centered Earth Fixed

EKF Extended Kalman Filter

FEC Foward Error Correction

FFT Fast Fourier Transform

FLL Frequency Lock Loop

FPGA Field Programmable Gate Array

GNSS Global Navigation Satellite System

GPS Global Positioning System

HOW Handover Word

ICD Interface Control Document

IF Intermediate Frequency

IFFT Inverse Fast Fourier Transform

LNA Low Noise Amplifiers

NCO Numerically Controlled Oscillator

PLL Phase Lock Loop

PNT Position, Navigation, and Timing

PRN Pseudo Random Noise

PVT Position, Velocity, and Timing

QPSK Quadrature Phase Shift Keying

RF Radio Frequency

RHCP Right Hand Circularly Polarized

RTK Real Time Kinematic

SDR Software Defined Receiver

TCXO Temperature Compensated Crystal Oscillator

TLM Telemetry Word

TOW Time of Week

VCO Voltage Controlled Oscillator

VDFLL Vector Delay/Frequency Lock Loop

VDLL Vector Delay Lock Loop

VFLL Vector Frequency Lock Loop

VLL Vector Lock Loop

WNLS Weighted Non-Linear Least Squares

Chapter 1

Introduction

1.1 Background and Motivation

The Global Positioning System (GPS) is an incredible tool for modern navigational needs. Originally, the idea of Global Navigation Satellite Systems (GNSS) was created for localization and navigation. It provides an absolute position fix, and it does not have increasing error from continual use as dead reckoning methods do, such as inertial navigation. The requirement of ultra precise timing for radio signal ranging to be viable also allows for GNSS receivers to synchronize various systems to a standardized time. This has opened the use of GPS into an entirely new branch of potential applications beyond its originally intended purpose. As a result, society is becoming increasingly reliant on GNSS technologies in areas such as farming, autonomous navigation, position tracking, banking, stock trading, electrical power grids, or atmospheric science studies. Anything that requires precise position, navigation, and timing (PNT) can depend on GNSS technologies.

The dependence on GNSS PNT is problematic due to the signals being inherently weak. The satellites orbit earth at 20,000 km, and the signal they broadcast is well below the noise floor when it is received. This allows the signal to easily be degraded, either incidentally or intentionally.

Environmentally, any occlusions of line of sight disrupt the signal. Tall buildings can effectively form urban canyons that prevent GNSS position fix. In rural environments, foliage can be degrading. Not only are blockages a problem, but also reflections of the signal, called multipath, can corrupt the position solution.

Formerly attacks on GNSS receivers were only military issues. GNSS jammers operate by blasting noisy signals in the GNSS bandwidth, and spoofers operate by sending artificial

or delayed GNSS signals. Devices capable of launching such attacks can be purchased easily online. Documented issues with civilian usage of these items have already arisen. In 2008 Todd Humphreys, a professor at the University of Texas at Austin, published a paper on how to develop a portable light weight spoofer [7]. Humphreys would go on to successfully implement a real time spoofing attack on a yacht at sea, moving the vehicle off course without notice [29]. There also has been recent work showing the ability for spoofers to control the motion of commercially available autonomous automobiles [20].

As the technology continues to progress, GPS is now being updated with a new set of civil signals to help improve performance. The highly protected L5 frequency band now contains a new civil GPS signal called GPS L5. It will be stronger and more accurate than the legacy civil signal GPS L1 C/A. This new signal will not be fully available until approximately 2027. However, there are currently enough satellites available to begin experimentally examining the performance gains of the new signal, as well as investigating adaptions of legacy algorithms to the new signal structures.

This thesis focuses on enhancing the GNSS receivers navigational capabilities in degraded environments. This is to be done by implementing both a GPS L5 vector tracking software defined receiver (SDR) and a GPS L1/L5 vector tracking SDR and comparing its performance against a legacy GPS L1 C/A SDR.

1.2 Prior Art

A traditional GNSS receiver operates by determining which satellites are in the sky and assigning a single channel to track and extract measurements from an individual satellite. A satellite's signal is distinguished from the rest by a pseudo random noise (PRN) code. A channel uses this PRN code to isolate that signal from the other signals that were received at the antenna. The channel will then correlate this received signal with a local replica of the signal generated from a numerically controlled oscillator (NCO) or voltage controlled

oscillator (VCO) in the receiver. These correlator outputs will then be converted by discriminators into measurements of phase and frequency errors, which will be low pass filtered and used to update the NCO. This process of correlating and updating the local replica, known as a tracking loop, is repeated as long as the receiver is active. Successful tracking of a satellite's signal will allow for the extraction of the data message and measurements of the satellite's time and Doppler frequency. The data message provides information needed to locate the satellite, called ephemerides. Once the satellites' locations, times, and Doppler frequencies are known, the receiver can calculate the range and its derivative, range rate, from the satellite to its location. With enough measurements at a given time, the receiver will be able to calculate its position, velocity, and timing solution.

Originally this process, known as scalar tracking, was performed in hardware receivers. While hardware receivers are much more difficult to implement and alter, they were a requirement in order to have the processing speed needed to position the receiver in real time. As technology has advanced, receivers can now be programmed in software and uploaded into a programmable piece of hardware, such as a field programmable gate array (FPGA). These software defined receivers (SDR), which were popularized due to several publications in the mid 2000s, have allowed for much easier implementation and testing of new GNSS tracking and positioning algorithms [3].

Recent research directions in the area of scalar GNSS signal tracking have been in the areas of robustness and accuracy. For more resilient tracking, work has been done on designing improved tracking loops such as aiding carrier phase with carrier frequency tacking or using near optimal Kalman filter tracking loops [30] [22] [13]. As for improving accuracy, publications focus on topics such as precise point positioning or linear combinations of dual frequencies signal to remove frequency dependent errors [5] [2].

The problem with traditional receivers is that if a signal gets degraded, the discriminators no longer provides a measurement that accurately represents the error in between the replica and the signal. With a lack of meaningful feedback, the channel's tracking loop will

lose lock and will be unable to provide useful measurements to the receiver's navigator. If enough channels lose lock, the navigator will have an insufficient number of measurements to calculate the position, velocity, and timing (PVT) solution, and the receiver will fail. As already discussed, the signal is inherently weak and much research has gone in to algorithms to enable channels to withstand degradation

1.2.1 Vector Tracking

Vector tracking is a method of GNSS signal processing developed that ties all the receiver's channels together so that individual channels can better survive degradation. Vector tracking was first introduced in the 1980's and patented by James Spilker from Stanford University in the 1990's [24]. In standard scalar tracking, each channel provides range and range rate measurements to a central navigating filter. In vector tracking, each channel provides its discriminator outputs of phase and frequency error to the central filter as range and range rate residuals. The navigation solution is then propagated into the future, and estimated range and range rates are calculated from this projected PVT estimate. These estimates are then used to estimate the frequencies of the signals over the next integration period. Vector tracking allows for the update of all channel's NCOs to come from the PVT solution. This allows for degraded channels to have quality updates to the local replicas based off current and projected PVT solutions despite some channels inability to provide a useful update individually. The shortcomings of vector tracking are that the weak channels can also add noise to stronger channels, and an initial position estimate is required for vector tracking. A diagram of vector tracking is shown in Figure 1.1.

The benefits of vector tracking, in comparison to scalar tracking, has been well documented in the literature. Matthew Lashley and David Bevly have published multiple works on vector loops outperforming equivalent scalar loops by 2-6 dB and surviving signal outages, low carrier to noise ratio (C/N0) tracking, and degraded urban environments [10] [11] [12]. Works by Zhao and Akos also show a gain in C/N0 from vector tracking, as well as increased

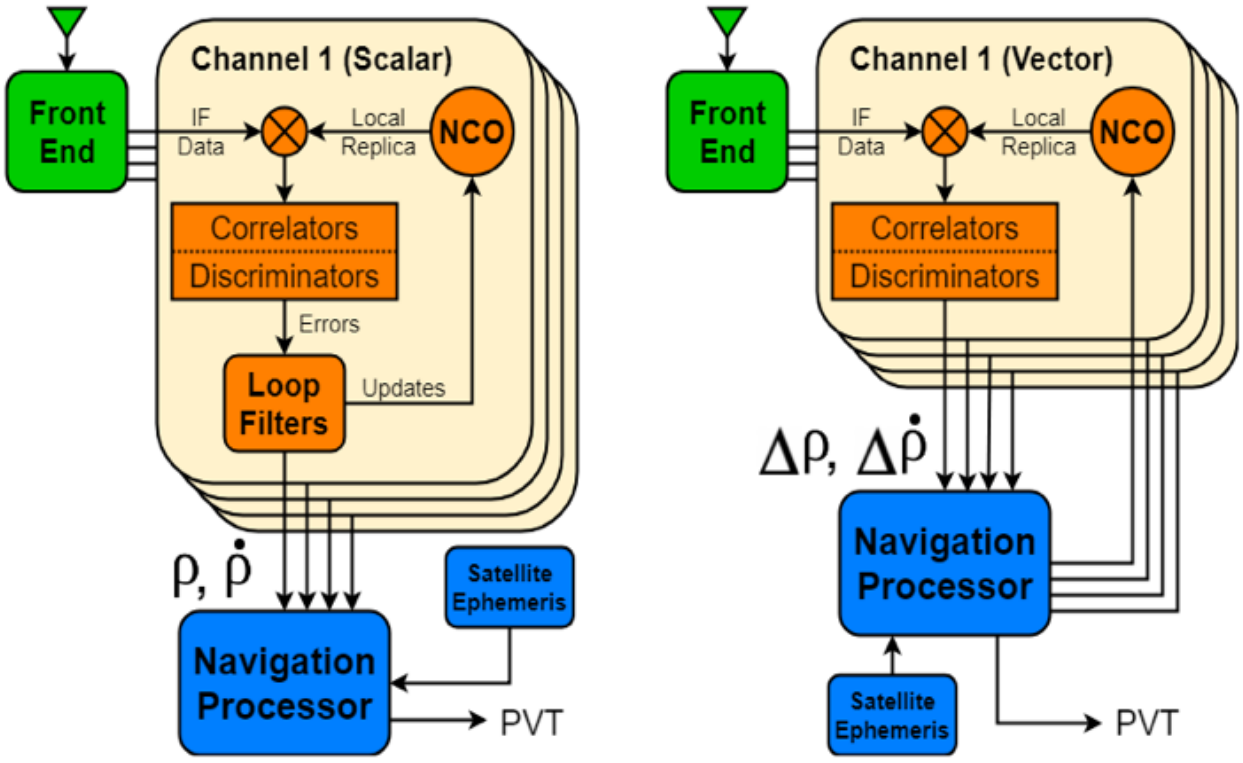

Figure 1.1: Scalar and vector tracking architectures [31].

survivability of degraded environments [32]. Work by Benson has shown the vector tracking architecture to be more resilient to interference than scalar architectures [1].

1.2.2 GPS L5

The GPS L5 signal is one of two modern civil signals being added to the GPS suite of signals. The second signal is GPS L2C, a civil signal in the L2 frequency band. The majority of the research on the signal's performance was conducted not long after the plan for the modern signal structure was announced. James Spilker and A.J. Van Dierendonck published works discussing the theoretical improvement of the GPS L5 PRN codes over legacy codes [25]. Michael Tran and Christopher Hegarty, as well as others from the MITRE Corporation, produced a series of papers on GPS L5 algorithms for acquiring and tracking with the new signal structure [27]. In addition, simulated performance evaluations also showed the new signals to perform well in noisy environments [28]. The Position, Location, and Navigation

(PLAN) Research Group out of the University of Calgary produced several works testing various acquisition and dual channel tracking algorithms in a hardware simulator as well as Kalman filter tracking schemes [15] [16] [17] [33]. The French Space Agency developed a GPS L5 SDR and investigated acquisition, dual channel tracking, L1/L5 dual frequency tracking, and Galileo signal interference [23]. Lastly the South Korean Electronics and Telecommunication Research Institute published SDR design schemes for a GPS L5 receiver [8]. Most of these works focus on heavily on code improvements and acquisition schemes. There is very little additional research put towards improved tracking algorithms for the new signal.

1.3 Research Contributions

There has been much research conducted with vector tracking algorithms on legacy GNSS signals, most notably GPS L1 C/A. However, there is now a new slate of civil GPS signals that have enough availability to test experimentally. While there has been some theoretical discussion of performance gains from the modernized signal, there has been little to no research into experimental performance gains for these modern signals. There has been no research done on adapting vector tracking algorithms to the modern signal architecture. Several contributions to the field of GNSS signal tracking are made in this thesis:

- Implement a GPS L5 vector tracking software defined receiver and a dual frequency GPS L1 C/A & GPS L5 vector tracking software defined receiver
- Compare the results from a GPS L5 vector tracking software defined receiver from live sky data to simulated data
- Analyze GPS L5 vector tracking algorithm adaptions including extended integration periods and pilot/data channel combinations as compared to legacy signal results in degraded environments
- Develop a ionospheric free combination of dual frequency vector tracking measurements

- Analyze a dual frequency vector tracking receiver against single frequency vector tracking receivers for mitigation of frequency dependent errors
- Published and presented the results shown in this work in the ION GNSS+ conference in September 2020 [6]

1.4 Thesis Outline

This thesis will describe the process of developing, implementing, and analyzing a GPS L5 and a GPS L1/L5 dual frequency vector tracking software defined receiver on experimental live sky data. While the algorithms described herein could be implemented in hardware, everything is implemented in software due to ease of development and testing. Chapter 2 will go into detail on the signal structure of the GPS signals. First, the legacy signal, L1 C/A, will be presented, then the GPS L5 signal will be shown in comparison. The key differences will be highlighted, showing their potential for improvement over the legacy signal. Chapter 3 will go into the architecture of the software defined receiver. It will cover front end processes, acquisition of the signal, tracking loop design, measurement calculation, and PVT algorithms. Chapter 4 will provide an overview of vector tracking and proposed adaptions to the algorithm for the L5 signal. Chapter 5 will examine experimental results from degraded environments encountered by the standard user of the GPS L5 vector tracking SDR and a covariance analysis. Chapter 6 will examine experimental results of the GPS L1/L5 dual frequency vector tracking SDR, ionospheric error mitigation in simulated and clear sky data, and a covariance analysis. Chapter 7 will present conclusions from this thesis as well as proposed future work to be pursued.

Chapter 2

GNSS Signal Structures

GPS currently broadcasts several signals from their satellites. As the need for improved satellite navigation becomes more prevalent, GPS has continued to add new generations of signals to improve upon shortcomings of earlier signals. The purpose of this chapter is to explain the structure of the legacy civilian signal GPS L1 C/A, compare it to the new civil signal GPS L5, and explain how the new structure potentially allows for improvement.

The GPS Signals have three main components to their structure: the carrier wave, the pseudo random noise code, and the data message. Each component will be discussed in their own section for both signals.

2.1 GPS L1 C/A

2.1.1 L1 Carrier

The GPS L1 C/A signal broadcasts a sinusoidal carrier wave a 1575.42 MHz. This is within the L1 frequency band, which is its name sake. The L-Band is a range of frequencies from 1-2 GHz that is optimal for GNSS signals due to its ability to not only pass through earth's atmosphere but to do so with limited atmospheric delays.

2.1.2 L1 Code

The GPS L1 C/A signal has a binary code modulated on to the carrier wave; it is called the Coarse Acquisition (C/A) Pseudo Random Noise (PRN) code. The code is a sequence of 1023 bits that are generally referred to as chips. It is broadcast at 1.023 MHz, so the PRN code completes a full cycle every millisecond. Sometimes referred to as the ranging code, the

PRN is used to keep track of the satellite's time to calculate the range measurement. Since the code is tracked to the sub chip level, it allows for the receiver to keep time to under a microsecond for ranges accurate to under 300 meters.

Each satellite broadcasts a unique PRN code so as to distinguish themselves from the other satellites. This is a method known as Code Division Multiple Access (CDMA) where multiple signals can be distinguished from one another despite being broadcast at the same frequency. This is possible due to the PRN codes being Gold Codes which have strong cross-correlation and auto-correlation properties. The PRN code will only have a high correlator output if the code is being correlated with a replica of the same code with less than a one chip offset. Figure 2.1 shows the the auto-correlation and cross-correlation of GPS L1 C/A PRN codes.

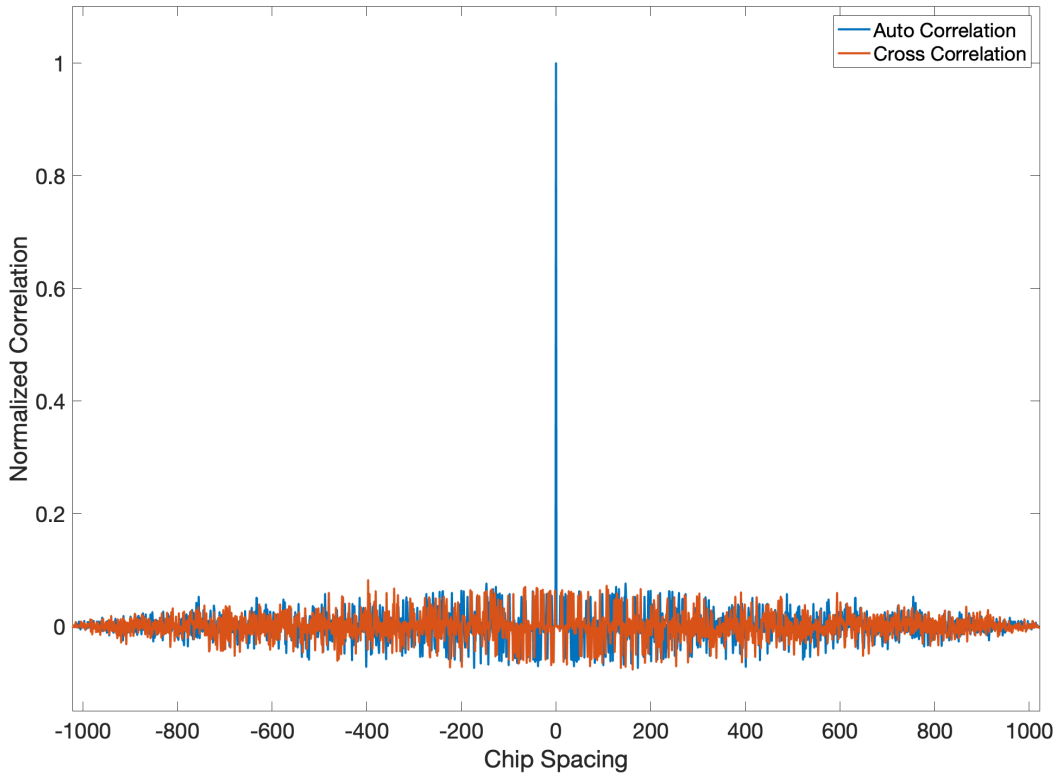

Figure 2.1: GPS L1 C/A PRN Code Auto-Correlation and Cross-Correlation

Within one chip, the PRN code auto-correlation is modeled as a linear increase from zero, at a full chip spacing, to a normalized value of one for a zero chip spacing. The auto-correlation function is shown in Equation 2.1 as a function of the error of a partial chip length, known as the code phase ϵ.

$$R(\epsilon) = \begin{cases} 1 - |\epsilon| & \epsilon \leq 1 \\ 0 & \epsilon > 1 \end{cases} \tag{2.1}$$

A plot of the auto-correlation function is also provided in Figure 2.2.

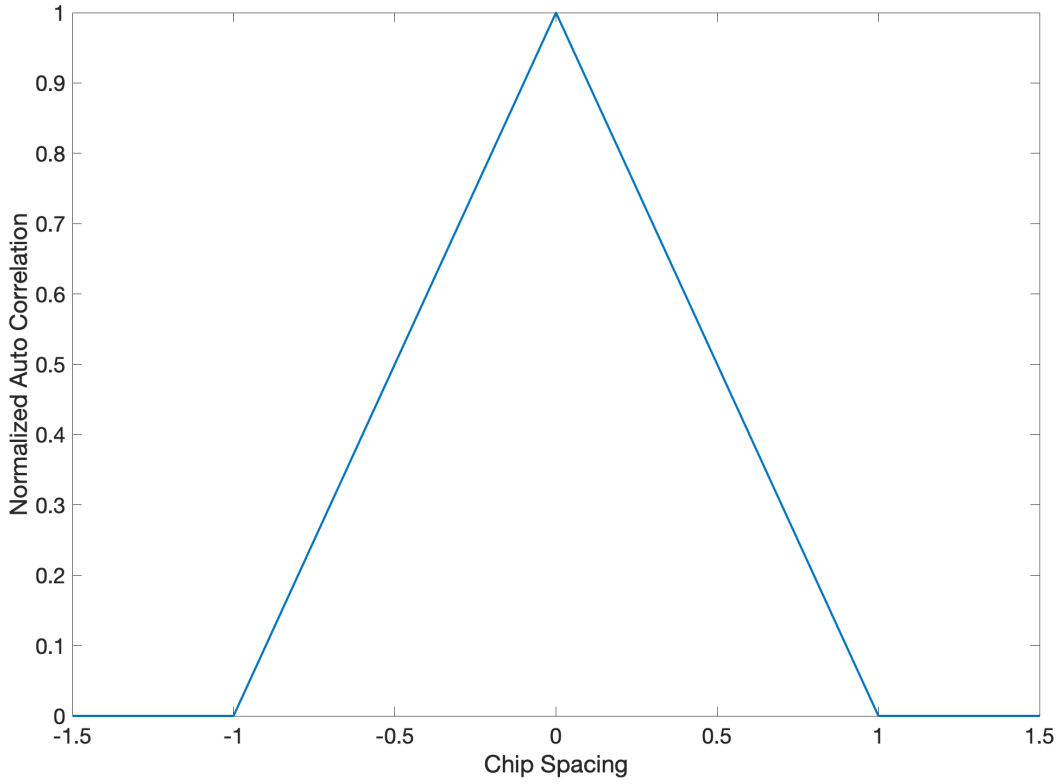

Figure 2.2: Modeled Auto-Correlation Function for GPS PRN Code

All of the PRN codes can be generated following a simple algorithm involving modulo-2 summation of a pair of ten element code registers. Certain values are passed from the register to create the next value to be inserted into the register, while the last value is removed from the register. While the register indices used to update the register are constant for both

registers, the register indices needed to calculate the next element of the PRN sequence are satellite dependent. This way a receiver can store a map of a pair of single digit integers for each satellite and quickly create the PRN code, rather than having to have each 1023 bit code programmed into every receiver. This was developed when memory was a limiting factor. With current technology, the storage of codes is no longer a problem. A complete algorithm for the PRN code generation for GPS L1 C/A can be found in the GPS Interface Control Document (ICD) IS-GPS-200L [18].

The PRN code, being a series of bits, becomes a square wave when it is transmitted. When this code is multiplied onto the carrier wave, bit transitions cause sudden π radians shifts in the transmitted phase, allowing for constant frequency waves to carry data messages. This is a process known as Binary Phase Shift Keying (BPSK). Another effect of multiplying a square wave onto a sinusoid is that it smears the frequency spectrum. Since a square wave is made up of an infinite number of sine waves of varying frequencies, the spectral content of the multiplied signal will reflect that. This is why the PRN code is sometimes referred to as the spreading code. The spreading effect actually makes the signal more robust as it provides the signal a greater bandwidth that can not be easily overpowered by a signal at the nominal carrier signal frequency. The spreading effect of the PRN code can be seen in Figure 2.3.

2.1.3 Data Message

The GPS L1 C/A data message is a 50 Hz binary code containing all the satellite, atmospheric, and timing information necessary to calculate the PVT of the satellite. The satellite information is called ephemeris. The ephemeris is used to calculate the position and velocity of the transmitting satellite at a given time according to an algorithm defined in the ICD [18]. The satellite also broadcasts corrections to the satellite clocks that are needed for accurate ranging, model parameters for atmospheric delay reduction, and an almanac full of useful information, although not necessarily pertinent to the standard users needs. The

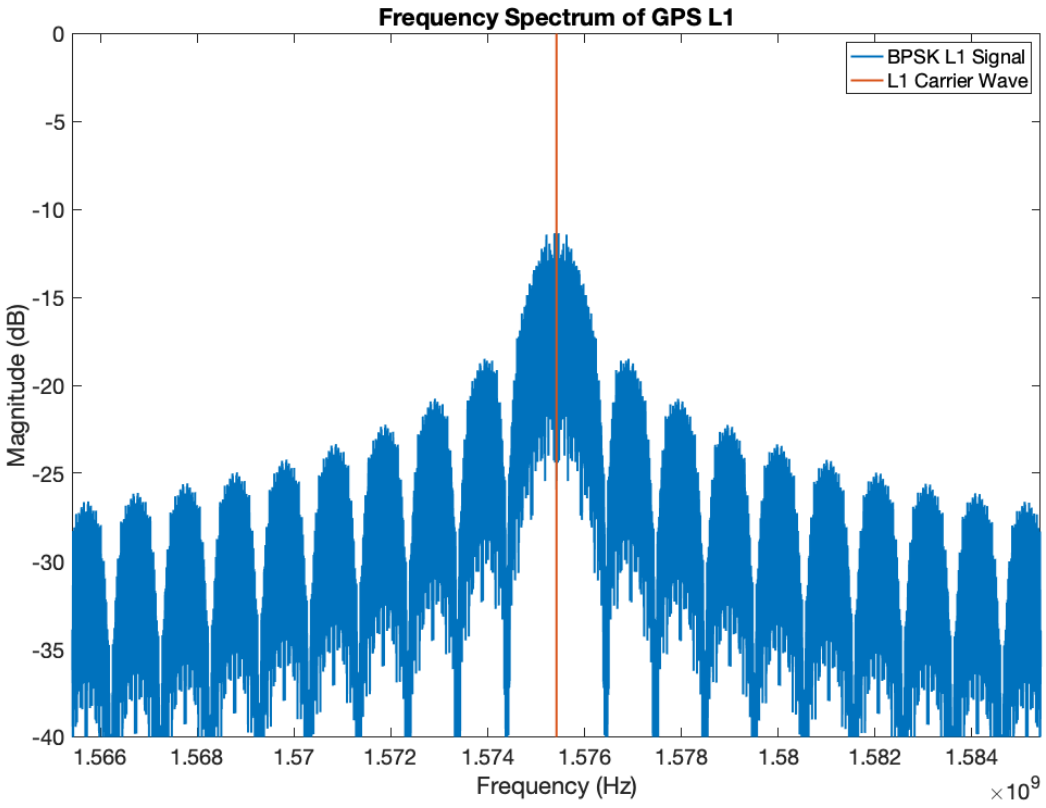

Figure 2.3: Magnitude of the Frequency Spectrum for GPS L1 C/A

GPS L1 C/A data message consists of 25 frames, where each frame has 5 subframes. Each subframe has 10 words, where each word contains 30 bits. The entire message takes 12.5 minutes to transmit. However, for the standard user, all the information needed to position is in subframes 1-3 from any frame. Subframe 1 contains clock information for timing corrections due to satellite errors. Subframe 2 and 3 contain the ephemerides necessary for the satellite position and velocity calculation. Subframe 4 and 5 contain almanac information. Subframe 1-3 are repeated in each frame for as long as the ephemerides within them are valid. Generally, ephemeris information is valid for around 4 hours. Subframe 4 and 5 each carry 25 pages of information, which is why the full message takes 12.5 minutes to broadcast. Every subframe begins with a telemetry word (TLM) that contains a preamble, so the start of the message can be located in the bit stream. The TLM is then followed by a handover word (HOW) that transmits time of week (TOW), so that the time of each satellite can be

kept by the receiver. A parity check algorithm is also provided to ensure correct translations of the data message. A full discussion of the data message can be found in the ICD [18]. The data bit takes 20 ms to broadcast and therefore has 20 repetitions of the PRN sequence during one bit transmission. These two codes are modulo-2 summed before being multiplied onto the carrier wave and broadcast.

The final continuous model of the GPS L1 C/A signal can be seen below in Equation 2.2

$$s(t)_{SVL1} = \sqrt{2P_{L1}}D(t)C(t)sin(2\pi f_{L1}t) \tag{2.2}$$

where P_{L1} is the signal power, $D(t)$ is the data bit value, $C(t)$ is the C/A PRN code bit value, and f_{L1} is the nominal GPS L1 transmission frequency.

2.2 GPS L5

The new civil signal GPS L5 is a Quadrature Phase Shift Keying (QPSK) signal, meaning that it has two data bits on its carrier wave rather than one, as in BPSK. The two bits are modulated onto the carrier with two unique PRN codes for each satellite at a $\pi/2$ radians phase difference. Normally, QPSK is used to transfer data at twice the rate of BPSK, but the second channel has no data message modulated onto it, only PRN code bits. This dataless secondary channel, called the quadrature channel or pilot channel, has phase shifts only caused by codes modulated onto it, which occur at predictable intervals. Sudden phase shifts from modulated bits cause sign changes that are detrimental to the integration of the signal, and since the data bit change causes unknown phase transitions, it is usually the limiting element in the integration duration. Integration period length is important because extended integration periods allow for the accumulation of power from weak signals, which improves the quality of the update necessary to track that signal. The signal also is broadcast at a power 3 dB higher than GPS L1 C/A to overcome the fact that the QPSK signal splits its power evenly across the two channels.

2.2.1 L5 Carrier

GPS L5 is broadcast at 1176.45 MHz, which is within the L5 frequency band that is highly protected by the Federal Aviation Administration. The signal was created to be used in conjunction with GPS L1 C/A for accurate and robust navigation for safety of flight navigation purposes.

2.2.2 L5 Code

The GPS L5 signal is modulated with two codes. First is the PRN code used for ranging and spreading the signal. The secondary code is the Neuman Hoffman code which is used for syncing the two channels.

PRN

The L5 PRN code is broadcast at 10.23 MHz. This is 10 times the rate of the L1 PRN code, which results in much more accurate time keeping and therefore range measurements. Each satellite has two PRN codes of 10230 bits with one on the in-phase channel and one on the quadrature channel. The two GPS L5 PRN codes, shown in 2.4, have better correlation properties than L1's PRN codes that were shown in Figure 2.1. The signal also has 10 times the bandwidth due to the faster code rate, as shown by the spectrum in Figure 2.5. The width of the center lobe for GPS L5 is 20.46 MHz, as opposed to GPS L1's 2.046 MHz center lobe. The larger center lobe makes the signal more robust, as interference must cover a wide frequency range to drown out the signal. The L5 PRN code is modeled with the same auto-correlation function as L1 for spacing within a chip width.

The L5 PRN codes are again generated by an algorithm of modulo-2 summations. There are three 13 bit shift registers; one is common to both quadrature and in-phase, and one is for each individually. Unlike how GPS L1 passes out bit values from satellite dependent register indices, GPS L5 provides initial states to the channel dependent shift registers, thereby providing a unique PRN for the quadrature channel and in-phase channel for each satellite.

A complete explanation of the algorithm can be found within the ICD IS-GPS-705G, which covers the new civil signals [19].

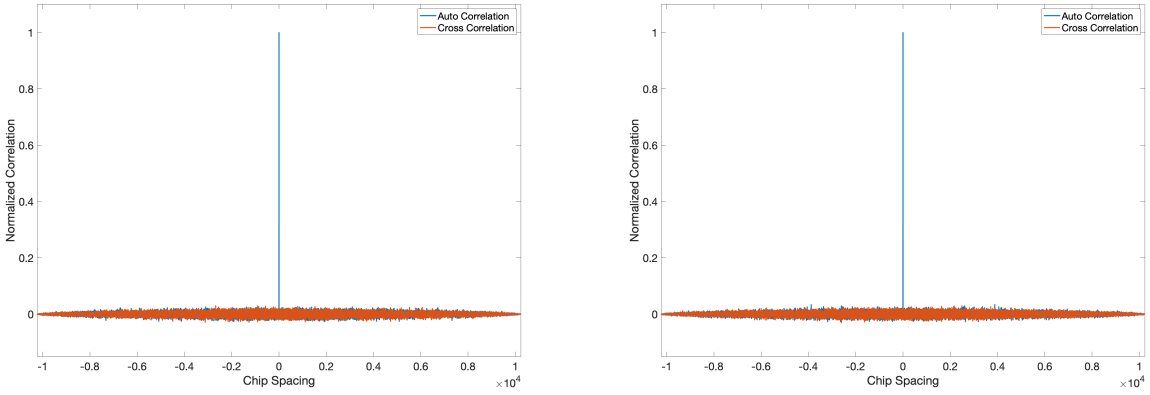

(a) GPS L5 In-phase

(b) GPS L5 Quadrature

Figure 2.4: GPS L5 Auto-Correlation and Cross-Correlation for In-phase and Quadrature PRN Codes

Neuman Hoffman

The Neuman Hoffman codes are a pair of 1 kHz binary codes that are modulo-2 summed onto the data message and PRN codes before being multiplied onto the signal. The Neuman Hoffman code on the in-phase channel is a 10 bit long repeating code, where one bit is as long as a full PRN code repetition (i.e. 1 ms). This Neuman Hoffman code effectively groups the in-phase signal into 10 ms bins. The quadrature channel has a different code that is 20 bits and is of the same rate as the in-phase Neuman Hoffman code. This code effectively groups the quadrature channel into 20 ms bins. Every full cycle of the quadrature Neuman Hoffman code exactly aligns with two in-phase Neuman Hoffman cycles. The importance of these groupings will be explained in the GPS L5 data message section.

2.2.3 Data Message

The structure of GPS L5 CNAV data message is similar to that of GPS L1 with several key differences. The data bits are broadcast at 50 Hz, but they undergo a process called

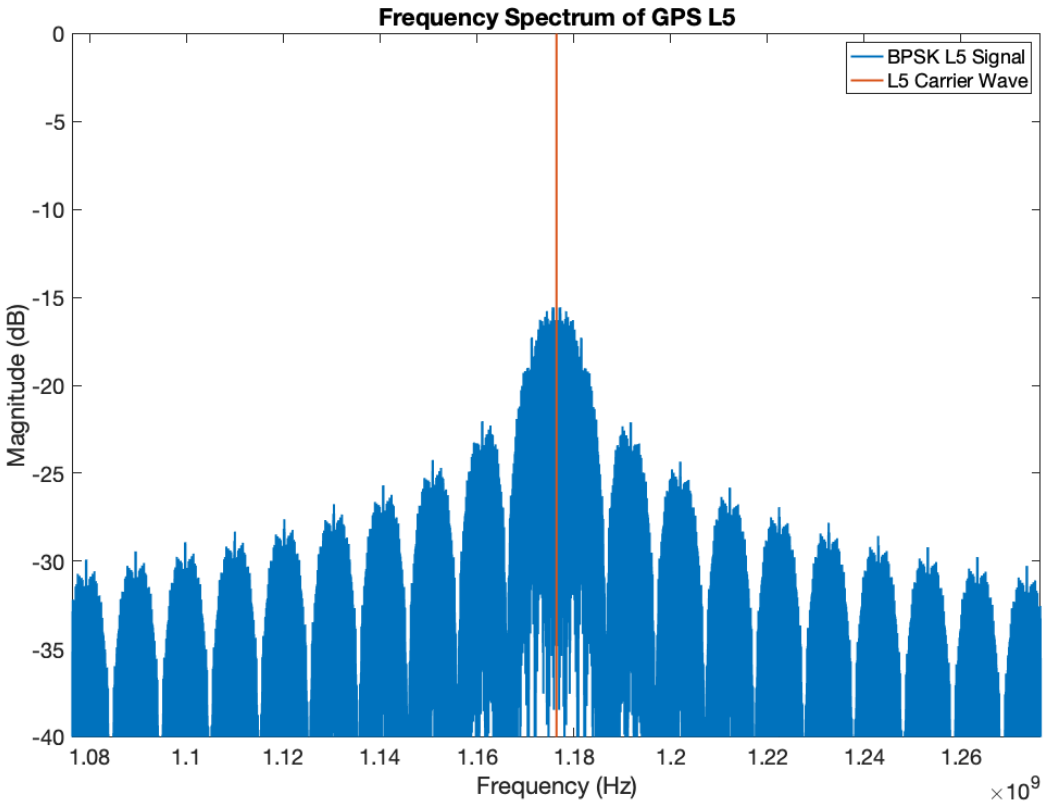

Figure 2.5: Magnitude of the Frequency Spectrum for GPS L5

forward error correction (FEC) encoding. This method helps to prevent the incorrect translation of data bits. FEC encoding splits the data bit into two data symbols each at 100 Hz. The in-phase Neuman Hoffman code aligns with the data symbol, and the quadrature Neuman Hoffman code aligns the two symbols together so that they can be used to regroup into a single data bit upon decoding. The FEC encoding is done by an 8 bit shift register. The suggested method of decoding is a Viterbi algorithm to choose a potential path of decoding that results in the minimum error. This method allows for incorrect data bits to be correctly filled with higher accuracy. This thesis does not use a Viterbi, but rather a brute force method similar to that done on L1 to locate and confirm a preamble location in the bit stream. All decoding possibilities of the message are preformed for each initialization of the shift register, and the decoded bits are searched for preamble sequences. If multiple preamble sequences are found full message lengths, which is 300 bits, apart repeatedly,

then the shift register is initialized to the values that would create the preamble. The FEC encoding is then wiped off the data message starting from the end of the preamble. The decoded message is then passed through a Cyclic Redundancy Check (CRC), which uses the last 24 bits of the message to run a parity check to ensure the rest of the message was decoded correctly. Unlike L1 whose parity check depends on bits from the last word, the L5 message parity check is completely handled within one message. Once the message is confirmed as valid, its message number is determined. There are multiple types of messages with IDs ranging from 0-63. The majority of message IDs have nothing affiliated with them yet. Message type 10 and 11 broadcast the ephemerides, while message type 30's broadcast clock corrections. These messages are repeated at a maximum of a 24 second interval as opposed to L1's 30 second interval. Also, message type 30 contains ionospheric correction terms for dual and single frequency users. This message type occurs at a maximum of 144 second interval, as opposed to L1's 750 second interval for ionospheric model parameters. The rest of the message type 30's contain almanac information, as well as repetitions of the clock corrections. For a complete explanation of CNAV message contents and intervals, as well as decoding methods and satellite PVT algorithms, please look to the ICD IS-GPS-705G [19].

The final continuous model of the transmitted GPS L5 signal can be seen below in Equation 2.3

$$s(t)_{SVL5} = \sqrt{2P_{L5_i}}D(t)NH_{10}(t)C_i(t)cos(2\pi f_{L5}t) + \sqrt{2P_{L5_q}}NH_{20}(t)C_q(t)sin(2\pi f_{L5}t) \quad (2.3)$$

where P_{L5_x} is the signal power of that channel, $D(t)$ is the data bit value, $C_x(t)$ is the PRN code bit value, $NH_x(t)$ is the Neuman Hoffman code bit value, and f_{L5} is the nominal GPS L5 transmission frequency.

2.3 Conclusions

The GPS L5's modern signal design offers exciting opportunities for the improvement of GNSS navigation and signal processing algorithms. The key features that this thesis looks to exploit are the dual channel nature of GPS L5, and the dataless quadrature channel. With the ability to get higher powered signals from the combination of the two channels, better ranging measurements from the increased code frequency, and increased integration lengths to accumulate more power, GPS L5 should offer improved performance over that of GPS L1 C/A, particularly in degraded environments.

Chapter 3

GNSS Software Defined Receiver Architecture

GNSS receivers have four key components that will be examined in this chapter. First will be the front end, where the the receiver converts the received analog signal into a digital signal that is usable by the computer. The computer will then process the data with a series of software written algorithms. The second item of discussion is the first algorithm encountered in the receiver, which is acquisition. This algorithm is where the incoming signal is searched for all satellites in the constellation to determine which are in view. Acquisition then passes its results to the next algorithm which is signal tracking. In signal tracking, each acquired signal is assigned a channel in the receiver where it is to be processed. The results of this processing is the data message and measurements. These observables are then passed to the final section, the navigator, that calculates the user PVT solution.

3.1 Front End

The purpose of the front end is to amplify and filter the received signal so that it can be processed. First, the signal is received by a right hand circularly polarized (RHCP) antenna. This antenna is not necessarily active, but for uses that require long cables with notable signal losses, active antennas with amplifiers are needed. The signal is then passed through a series of low noise amplifiers (LNA) and band pass filters (BPF) before going through an analog to digital converter (ADC) to convert the continuous signal into digitized samples. During this process, the signal is mixed with a local oscillator that is normally made from a temperature compensated crystal oscillator (TCXO) and a phase lock loop (PLL) that also controls the sampling of the ADC block of the front end. The mixing process is to down convert the signal from its L band frequency into a more manageable intermediate frequency

(IF) for the receiver while still maintaining the same modulation and Doppler frequency. A diagram is shown below in Figure 3.1 depicting the process of converting the analog received RF signal into a digital IF signal for processing.

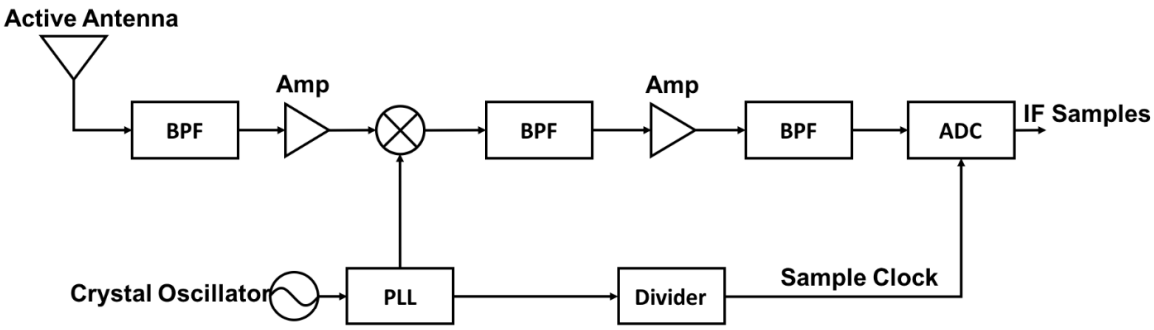

Figure 3.1: Block Diagram of typical Software Receiver Front-End [14]

3.2 Acquisition

Once the received signals have been processed by the front end and digitized, the computer must then determine which satellites are being received. To do this, an acquisition algorithm correlates local replicas of the signal against what was received. Due to the PRN code correlation properties, the local replica must be within one chip of of the received signal for there to be a nonzero correlation. Also, for there to be a strong correlation, the frequency of the carrier wave must be accurately estimated. Because the satellite is in motion, and potentially the user as well, the receiver and satellite's relative velocities cause a Doppler shift in the received carrier frequency. In order for the acquisition algorithm to determine which satellite is broadcasting to the receiver, the algorithm must check for a correlation spike of every satellite in the constellation, at every possible code offset, and at every possible Doppler offset.

Searching all of these possibilities is computationally intensive, so generally the acquisition space is divided up into large bins to limit the number of correlations required. For the most direct and simple acquisition algorithm, called the Serial Search Algorithm, the

code phase offsets are generally blocked into half chip spacings so that only 2047 chip offsets need to be searched for GPS L1 C/A and 20461 for GPS L5. Because of the auto-correlation function for GPS PRN codes, a peak will be present with a maximum error of a half chip which will be within the pull in range of the discriminator. Generally, the Doppler shifts are broken into 500 Hz spacings from the range of -5000 to 5000 Hz. Again, this spacing is chosen for the pull in range of the tracking algorithm. If the expected velocity of the receiver is high, then the range is usually extended from ± 5 kHz to ± 10 kHz.

The Serial Search Algorithm is performed on at least 1 ms of data to guarantee a full cycle of the PRN code is contained. The versions of the local replica are then created for each frequency and code offset. Because the phase of the received signal is unknown, each bin must have two replicas with phases that are $\pi/2$ radians apart to remove the phase ambiguity. Each replica is then multiplied with the incoming signal and integrated. The results of the two correlations for each code and Doppler offset bin, called the in-phase and quadrature correlators, are then squared and summed in order to remove any phase caused sign errors. The maximum final value of the code and frequency search space is then compared against a threshold. If it passes the criteria, the signal is considered acquired. The location of the peak determines the initial estimates of code phase and carrier frequency that are passed to the signal receiver channel for initializing the local replica. A diagram of the Serial Search Algorithm is shown in Figure 3.2.

For the acquisition of weak signals, longer correlation times can be used. Integrating over a longer time period will give a larger correlator output that will stand further above the noise. For GPS L1 the maximum coherent integration time is two periods of 10 ms. If you know where the data bit transition is, the maximum integration period is 20 ms, which is the length of a data bit. Since it is unknown in acquisition, consecutive integration periods of 10 ms will guarantee that one period will not contain a data bit transition. Another way to increase signal power is to add consecutive non-coherent integration periods. This method effectively stacks integration periods, usually of 1 ms, so data bit transitions are not a factor.

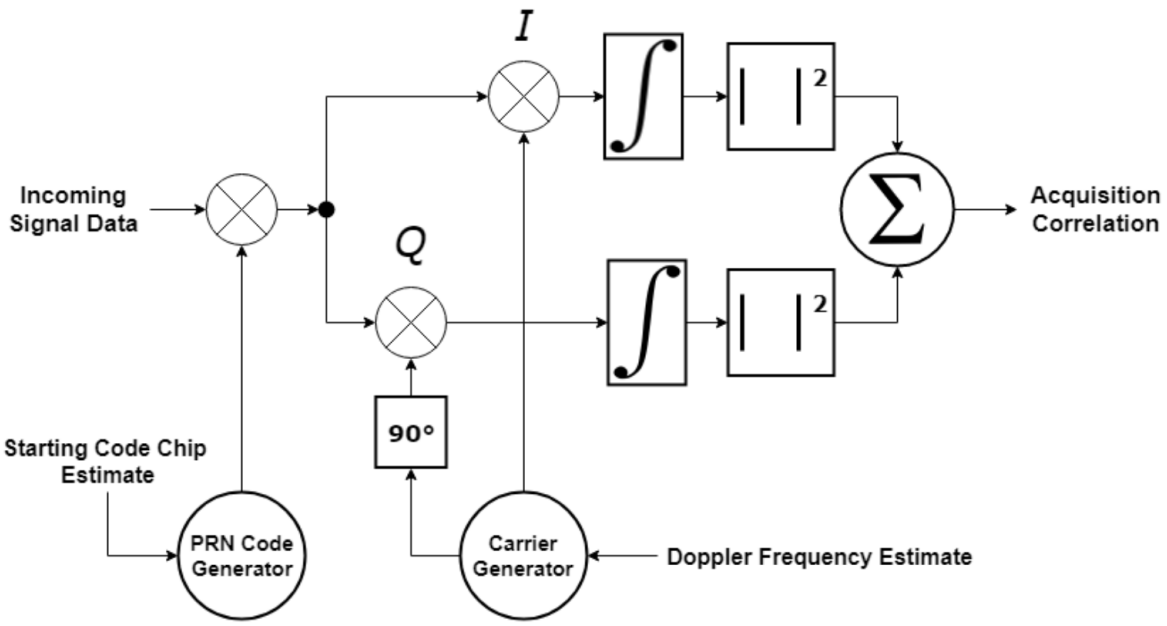

Figure 3.3: Diagram of the Serial Search Acquisition Algorithm

Figure 3.2: Diagram of Serial Search Acquisition Algorithm [31]

Non-coherent acquisition accrues less power since it sums multiple integration periods after squaring, but it has no limit to the total integration length. The Neuman Hoffman code creates issues for GPS L5 since its bit value is not known at acquisition. The change of bit values every millisecond limits the L5 coherent integration to 1 ms. For accumulation of power in acquisition, the GPS L5 signal requires non-coherent integration.

While the Serial Search Algorithm is useful for understanding what the receiver is trying to accomplish during acquisition, it is inefficient. This work uses a Parallel Code Search Algorithm that parallelizes the PRN code offset search space by using the frequency domain. A diagram of the algorithm is shown in Figure 3.3. First the carrier replica, both in-phase and quadrature, are multiplied with the signal and summed in a complex fashion with the quadrature becoming the imaginary portion and the in-phase becoming the real portion. The result of the summation is then passed through a fast Fourier transformation (FFT) taking the search space into the frequency domain. The transformed result is then multiplied by

the the complex conjugate of the FFT of the code replica. An inverse fast Fourier transform (IFFT) is then performed and the magnitude of the results are taken, converting the values from complex to real. The results of this process is an array with a maximum value at the point of the start of the PRN sequence with sample level resolution on the code start point. This process must be repeated for all possible Doppler offsets, and then the final search space is examined for a acquisition peak. If found, the results are passed to the tracking algorithm.

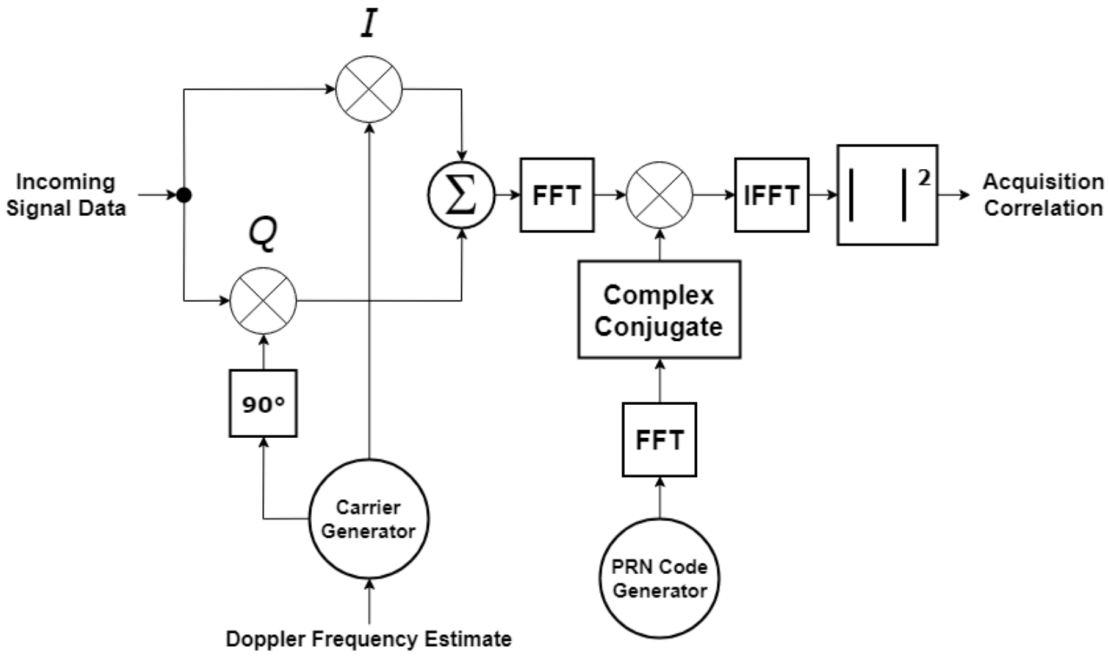

Figure 3.3: Diagram of Parallel Code Search Acquisition Algorithm [31]

The Parallel Code Search Algorithm allows for better resolution on the code offset with a more efficient algorithm than Serial Search Acquisition. The increase in efficiency can also allow the shrinking of the frequency bins to 100 Hz for a more refined Doppler estimate. The acquisition algorithm can also be parallelized on the Doppler shift dimension rather than the code dimension of the search space, but for GPS purposes, parallelized code is more efficient since there are more bins in that dimension and the resolution on the code is more useful than resolution on the frequency.

3.3 Tracking Loops

Once the Acquisition Algorithm has determined the initial estimates of code phase and carrier frequency for all present satellites, a dedicated channel is provided for each satellite signal where it is to be tracked. The tracking process is performed by: correlating local replicas with the incoming signal, transforming the correlator outputs into a measurement of error via discriminator, filtering the measurement, and then updating the replica's frequencies and phases. As this process is performed, the tracking loops lock the replica to the true signal. The correlator outputs will contain the carrier phase shifts caused by the data bits. With the data bits, the user can calculate the satellite PVT information.

The receiver must accurately track the carrier and code phase. The code phase is tracked using a Delay Lock Loop (DLL) initialized by the acquisition estimate of code phase. The carrier phase is tracked by the Phase Lock Loop (PLL). Unlike the code, there is no initial estimate on carrier phase to initialize the tracking loop. If the Doppler estimate is very fine, then the PLL can lock the phase without an intermediate step. However, if the initial frequency estimate is coarse or the signal is noisy, the carrier frequency estimate must be refined first using a Frequency Lock Loop (FLL). The FLL is more robust than the PLL, but it cannot provide the phase estimate needed to determine bit values. Once the data bits have been collected and the ephemeris decoded, only code phase lock and carrier frequency lock are necessary for standard position and velocity estimation. The code phase lock provides the time keeping needed to form the range measurements, and the carrier frequency lock provides the Doppler frequency needed to estimate user velocity.

A correlator is the resulting value after mixing a replica signal with the true signal and integrating the results. This correlation process is refereed to as an integrate and dump period and usually has an integration period that is a integer number of full code cycles. For GPS, this means integration periods are in millisecond intervals. The correlator outputs are functions of the error of the states being tracked: code phase, carrier frequency, and carrier phase. A standard receiver uses six correlators to track both carrier and code. Two

are required for tracking the carrier phase, and two are required for tracking the code phase if the carrier phase is locked. If the carrier phase is not locked, then the code will require four correlators. The carrier phase tracking requires two correlators with accurate code estimates at $\pi/2$ radians carrier phase separation. These correlators are called quadrature and in-phase. The code requires two correlators with time shifted codes, one early and one late. The standard code shift is half a chip, but anything less than one chip is possible. Because the code tracking should be independent of carrier phase lock, the code tracking can combine in-phase and quadrature correlators to remove carrier phase dependency resulting in four correlators. This results in the six total correlators, which are called the in-phase prompt IP, the quadrature prompt QP, the in-phase early IE, the quadrature early QE, the in-phase late IL, and the quadrature late QL. The models for these correlators can be seen below in Equation 3.1.

$$\begin{aligned}
IP(k) &= AR(\epsilon)D(k)cos(\pi f_{err}T + \theta_{err}) + \eta_{IP} \\
QP(k) &= AR(\epsilon)D(k)sin(\pi f_{err}T + \theta_{err}) + \eta_{QP} \\
IE(k) &= AR(\epsilon + d)D(k)cos(\pi f_{err}T + \theta_{err}) + \eta_{IE} \\
QE(k) &= AR(\epsilon + d)D(k)sin(\pi f_{err}T + \theta_{err}) + \eta_{QE} \\
IL(k) &= AR(\epsilon - d)D(k)cos(\pi f_{err}T + \theta_{err}) + \eta_{IL} \\
QL(k) &= AR(\epsilon - d)D(k)sin(\pi f_{err}T + \theta_{err}) + \eta_{QL}
\end{aligned} \tag{3.1}$$

$$A = \sqrt{2T\frac{C}{N_0}}\frac{sin(\pi f_{err}T)}{\pi f_{err}T} \tag{3.2}$$

where, T is the integration period over which the correlation is integrated (summed), f_{err} is the error in the carrier frequency, θ_{err} is the error in the carrier phase, $R(\epsilon)$ is the auto-correlation function defined in Equation 2.1, d is the code delay spacing, C/N_0 is the carrier to noise density ratio that will be explained later in this chapter, and η is noise.

Once these correlators have been calculated, they must be converted by discriminators into errors. The discriminator is different for each state being tracked. The following sections

will discuss the discriminators used for each of the tracking loops. The diagram in Figure 3.4 shows the architecture of a standard tracking loop and four aspects covered in this section in block diagram form.

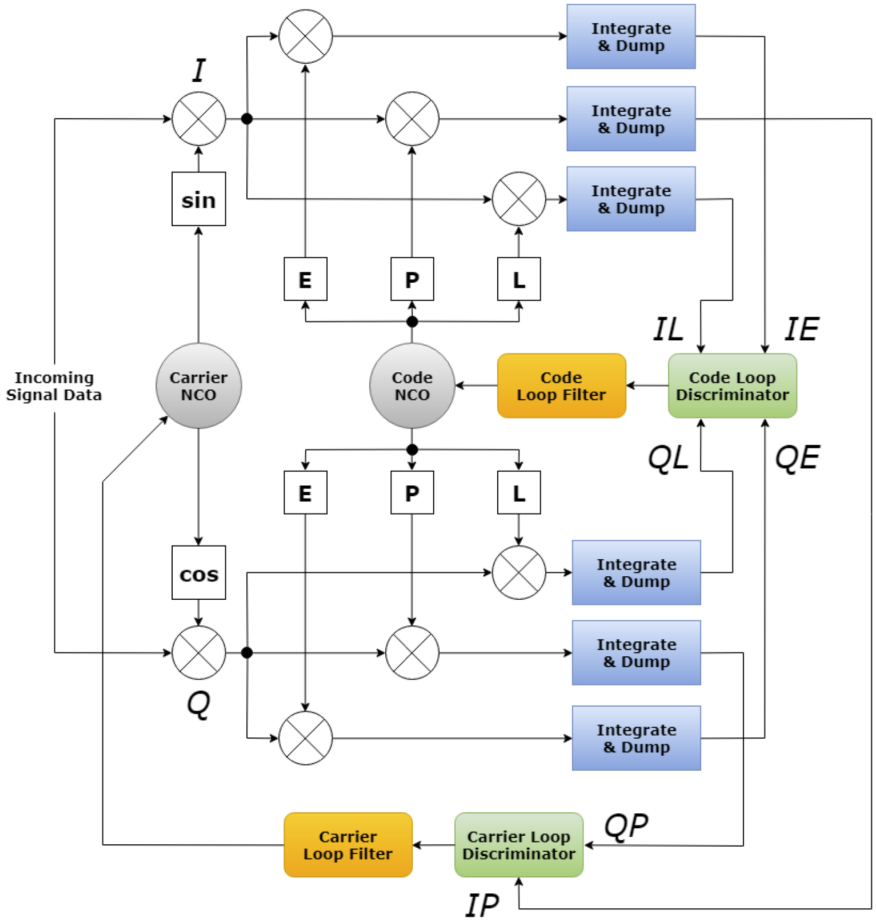

Figure 3.4: Diagram of Tracking Loop Architecture [31]

Once the discriminators have been calculated, the result is low pass filtered before updating the replica. Generally, second order or higher under-damped low pass filters are designed classically and discretized, but, for this work, all filters are second order discrete standard under-damped low pass filters of the form shown in Equation 3.3.

$$\delta = K_0[K_1(\phi(k) - \phi(k-1)) + K_2\phi(k)] \tag{3.3}$$

The update δ is calculated by gain K_0 set by the user to decrease convergence time, filter coefficients K_1 and K_2 chosen from a table in [26] based on desired bandwidth and integration period, and $\phi(k)$ the discriminator update from time index k. The FLL has a chosen filter bandwidth of approximately 30 Hz, the PLL 20 Hz, and the DLL 10 Hz for 1ms integration periods. Note that the code and carrier phase updates are in units of phase and should be divided by the integration period before updating the replica frequency.

3.3.1 Carrier Frequency Tracking

The carrier frequency can be tracked by either a PLL or an FLL. Both loops require in-phase and quadrature prompt correlators. The FLL works by effectively looking at the time rate of change of the carrier phase error across the integration period T which gives a representation of the carrier frequency error. In this work, the FLL uses a cross-dot arc-tangent discriminator that takes a set of consecutive in-phase and quadrature prompt correlators with no updates to frequency applied in between to calculate the carrier frequency error as shown in Equations 3.4 and 3.5.

$$\begin{aligned} cross &= IP_1QP_2 - IP_2QP_1 \\ dot &= IP_1IP_1 + QP_1QP_2 \end{aligned} \tag{3.4}$$

$$\phi_{FLL} = \frac{arctan2(cross, dot)}{2\pi T} \approx f_{err} + \eta_{FLL} \tag{3.5}$$

The linear range of the discriminator, where true error is linearly mapped to output error, is determined by the integration period, but the discriminator can handle around 500 Hz of error, which is why coarse acquisition bins are usually set to that size.

3.3.2 Carrier Phase Tracking

Once the FLL is accurately tracking the carrier frequency, the carrier phase tracking can be handled by a PLL. The PLL in this work uses a Costas loop discriminator. This

discriminator uses an arc-tangent function on the quadrature and in-phase correlators to find the phase error of the replica as shown in Equation 3.6.

$$\phi_{PLL} = \frac{arctan(\frac{QP}{IP})}{2\pi} \approx \theta_{err} + \eta_{PLL} \tag{3.6}$$

The output is divided by 2π to convert the phase error from radians to cycles. The two quadrant arc-tangent function has half the linear range of the four quadrant arc-tangent function, but it is immune to data bit flips. This is why the Costas loop is the most common PLL discriminator, but in challenging environments, the receiver may have to lean on the FLL for carrier tracking due to the PLL's sensitivity and limited range.

3.3.3 Code Phase Tracking

The code phase is tracked by using the auto-correlation model shown in Equation 2.1. The correlators are shifted by a set chip spacing to either side of the tracked phase and compared. If one side is higher than the other, the phase needs to be shifted towards the high side to place the prompt code phase evenly between them atop the auto-correlation peak. In this work, the code phase error is determined by a normalized early minus late power discriminator that is shown in Equation 3.7.

$$\phi_{DLL} = \frac{\sqrt{IE^2 + QE^2} - \sqrt{IL^2 + QL^2}}{2(\sqrt{IE^2 + QE^2} + \sqrt{IL^2 + QL^2})} \approx \epsilon + \eta_{DLL} \tag{3.7}$$

The inclusion of quadrature correlators removes the need for carrier phase lock to track the code. This discriminator provides a linear range equal to the delay spacing up to one chip. It also has a pull in range of a chip and a half.

Once the carrier and code phases are being accurately tracked, the value of the in-phase prompt correlator will reflect the data bit value as can be seen in Figure 3.5. It is possible that the PLL locked onto a π radians phase shift of the carrier, so the bit values could be inverted. When searching for the preamble in the data bits, searches for inverted preambles

must be done as well. The repetition of the preamble and the parity checks prevent the inversion of data bits from causing an error in translation.

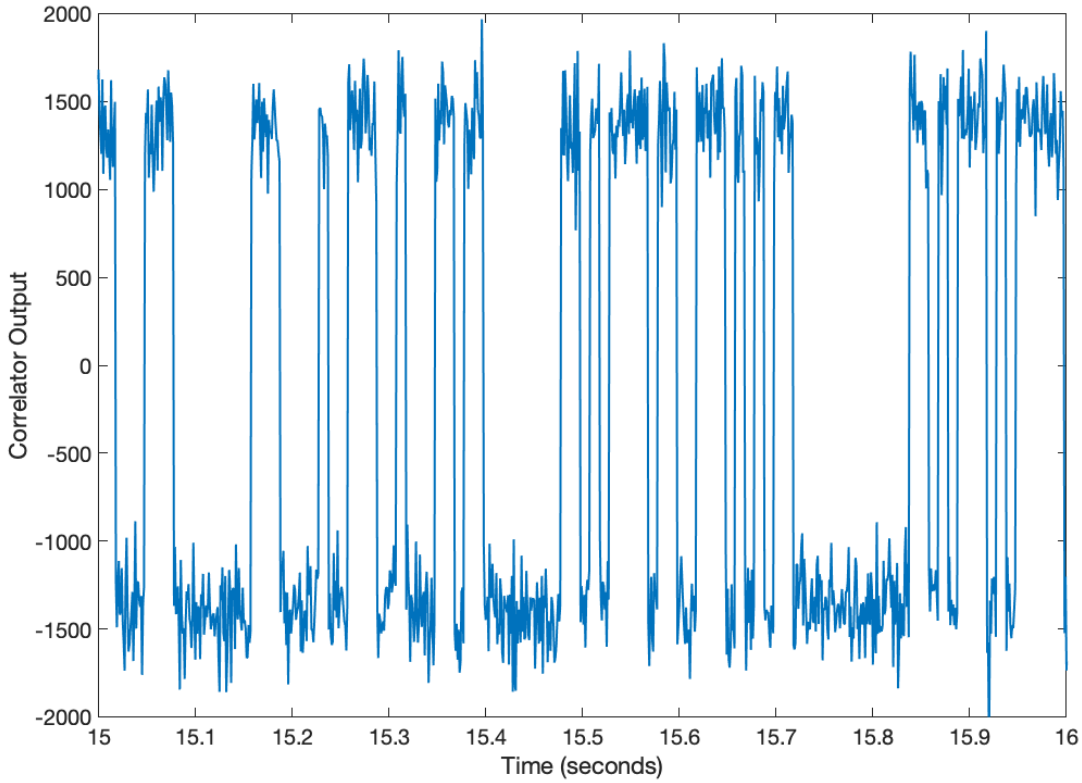

Figure 3.5: In-Phase Prompt Correlator Output Showing Data Symbols on GPS L5

3.4 Position Velocity and Timing

Once the signals are being accurately tracked and the data message has been decoded, the navigator can begin calculating the user PVT solution. GNSS positioning works due to the principle of trilateration. If there are three unique ranges from known locations measured at a point, then that point can be located. Similarly, this process can be done with range rates to find the receiver velocity. This section seeks to show how the measurements are developed and used to calculate the PVT solution.

3.4.1 Measurements

Pseudorange

The pseudorange is the primary measurement from the GNSS satellite. It is calculated by taking the time of the satellite transmission of the signal as estimated by signal tracking and subtracting it from the time it reached the receiver. The resulting value is the transit time of the signal, which is then multiplied by the speed of light in a vacuum to get the range. The equation is shown below in Equation 3.8.

$$\tilde{\rho}^j = (t_r - t_t^j)c \tag{3.8}$$

Here, t_r is the receiver time, t_t^j is the transmit time of the j^{th} satellite, c is the speed of light in a vacuum, and $\tilde{\rho}^j$ is the measured pseudorange from the user to the j^{th} satellite. The pseudorange would be the true range if the times were measured accurately at both the receiver and the satellite and if the signal traveled through a vacuum for its entire transit. Neither of those assumptions are true, so instead it is called a pseudorange. The model of the pseudorange is shown in Equation 3.9.

$$\rho_j = r_u^j + ct^j + ct_u + I_u^i + T_u^i + M_u^i + \eta_{\rho_i} \tag{3.9}$$

$$r_u^j = \sqrt{(x^j - x_u)^2 + (y^j - y_u)^2 + (z^j - z_u)^2} \tag{3.10}$$

Here r_u^j is the geometric range of the user (u) to the satellite (j) that is shown in Equation 3.10, ct_u is the clock bias of the user, ct^j is the clock bias of satellite j, I is the atmospheric delay from the ionosphere, T is the atmospheric delay from the troposphere, M is the multipath delay, and η is additive Gaussian noise.

GNSS positioning is only possible due to the high level of stability of the satellite clock. The time of each satellite is able to be kept at the receiver due to the TOW being given by the data message and the satellite reproducing the PRN sequence every millisecond precisely.

By accurately tracking the code, the user is able to keep the satellite time to whatever sample level resolution the the receiver can provide of the code phase. While incredibly stable, the satellite clock is not able to perfectly repeat the PRN sequence at millisecond intervals but its error is modeled and broadcast in the ephemeris, so ct^j can be removed by the user from the pseudorange.

The receiver time, however, is not known at activation, and the receiver clock is not as stable as the atomic clock on board the satellite. To handle this problem, the receiver time is initialized to the first received satellite time plus a nominal offset, usually 70 ms, and a receiver clock bias must be estimated. Fortunately, the clock bias is assumed to be constant across all pseudoranges taken at a time, allowing for a position solution to be solvable. The unknown bias of the receiver clock effectively adds a fourth dimension to the receiver position. In order for the receiver to position itself, it requires at minimum as many ranges as the receiver has states, which are the three geometric states x_u, y_u, and z_u as well as the temporal state ct_u.

Pseudorange Rate

While the primary purpose of GNSS is localizing the user anywhere on the planet, it also provides an excellent source of velocity estimation. The measurement to calculate velocity is the derivative of the pseudorange with respect to time. The measurement is called the pseudorange rate and it is modeled in Equation 3.11.

$$\dot{\rho}_j = \dot{r}_u^j + c\dot{t_u} + \dot{I}_u^i + \dot{T}_u^i + \eta_{\dot{\rho}_i} \tag{3.11}$$

In the pseudorange rate model, the pseudorange rate is equal to the time derivative of the geometric range shown in Equation 3.10, the derivative of the user clock bias, which is called the clock drift, and the derivative of the atmospheric delays. The satellite clock is considered

stable enough for its clock drift to be ignored by the model, and the atmospheric errors can either be ignored as they are small or modeled.

The pseudorange rate is the measurement of the users relative line of sight velocity which can be calculated directly from the Doppler frequency. The Doppler frequency between the user and the satellite is shown in Equation 3.12.

$$f_d = -\frac{\dot{r}_u^j * f_t}{c} \tag{3.12}$$

Here the Doppler frequency f_d is equal to the negative geometric range rate times the transmitting frequency f_t divided by the speed of light. If the receiver is frequency locked, then it has a good estimate of the carrier frequency that can be used to directly calculate the pseudorange rate. The equation for the measured range rate is shown in Equation 3.13.

$$\tilde{\dot{\rho}}_j = -\frac{(f_c - f_{IF}) * c}{f_t} \tag{3.13}$$

Here the pseudorange rate is equal to the negative difference of the estimated carrier frequency f_c and the intermediate frequency f_{IF} times the speed of light divided by the transmit frequency.

If the user clock was perfect, the user would only need pseudorange rates from three satellites to estimate velocity. However the drift of the user clock biases the frequencies. This in turn biases the range rates, and, just like position, a fourth state must be estimated in order for the velocity to be estimated accurately. So, a fourth satellite is needed at minimum to estimate the clock drift and the user's three velocity states.

Carrier to Noise Ratio

The last measurement the satellite channel provides to the navigator is an estimate of the noise on the channel. The receiver uses a value called carrier to noise density ratio (C/N0) to quantify the quality of the range and range rates being provided. This value is

calculated by comparing the amplitude of the tracked signal to the variance of correlators that are hundreds of chips away from the tracked peak. The formula used for C/N0 in this work is shown in Equation 3.14

$$\frac{C}{N_0} = 10log_{10}\left(\frac{\tilde{A^2} - 4\hat{\sigma}_\eta^2}{2T\hat{\sigma}_\eta^2}\right) \tag{3.14}$$

$$\tilde{A}^2 = (IE^2 + IL^2) + (QE^2 + IL^2) \tag{3.15}$$

$$\hat{\sigma}_\eta^2(k) = (1-\alpha)\hat{\sigma}_\eta^2(k-1) + \alpha\tilde{\sigma}_\eta^2 \tag{3.16}$$

The C/N0 is a function of the amplitude of the signal, A^2, as represented in Equation 3.15 by the correlators, and the variance, σ_η^2, that is referenced in Equation 3.16 and filtered with a moving average with an α coefficient of 0.99. The variance does not change much over time and is able to be heavily filtered to filter the noise estimate. The variance measurement itself is the variance of correlators offset by 100 chip intervals and is computationally intensive for the receiver.

3.4.2 PVT Algorithms

Once measurements and ephemeris data have been made available for at least four different satellites, the receiver can begin to position the user. In this work two common PVT algorithms are used: weighted nonlinear least squares (WNLS); and the extended Kalman filter (EKF). The weighted nonlinear least squares algorithm is the simpler estimation algorithm and is useful for initializing the PVT estimate. Once there is a position estimate, the extended Kalman filter can be used to apply a propagation model to the states that filters measurements and creates a smoother estimate than WNLS.

Weighted Nonlinear Least Squares

There are eight states being estimated by the receiver in this work, which are the three position states in Earth Centered Earth Fixed (ECEF) coordinates, the three velocity states, the user clock bias, and the user clock drift, and they are displayed in Equation 3.17.

$$\hat{\boldsymbol{x}} = [\hat{x}_u \quad \hat{\dot{x}}_u \quad \hat{y}_u \quad \hat{\dot{y}}_u \quad \hat{z}_u \quad \hat{\dot{z}}_u \quad \hat{ct}_u \quad \hat{\dot{ct}}_u]^T \tag{3.17}$$

However, the WNLS tries to estimate the error between the true state and the estimated state. These error states, shown in Equation 3.18, are then related to the measurements residuals by Equation 3.19.

$$\delta\hat{\boldsymbol{x}} = [\delta\hat{x}_u \quad \delta\hat{\dot{x}}_u \quad \delta\hat{y}_u \quad \delta\hat{\dot{y}}_u \quad \delta\hat{z}_u \quad \delta\hat{\dot{z}}_u \quad \delta\hat{ct}_u \quad \delta\hat{\dot{ct}}_u]^T \tag{3.18}$$

$$\boldsymbol{Y} = \boldsymbol{H}\delta\hat{\boldsymbol{x}} \tag{3.19}$$

The geometry matrix, $\boldsymbol{H}$, is defined by the Jacobian of the measurement model with respect to the four position states for the pseudorange and the four velocity states for the pseudorange rate. The measurement models are nonlinear, so the geometry matrix must be evaluated with the most recent state estimate. This results in a unit vector pointing from the user to the satellite for the geometric states and a one in place of the appropriate clock term. The geometry matrix can be seen in Equation 3.20 with a corresponding measurement residual vector as seen in Equation 3.21, which is a difference of the current measurements and the

estimate of the measurements from their models.

$$\boldsymbol{H} = \begin{bmatrix} -a_{x1} & 0 & -a_{y1} & 0 & -a_{z1} & 0 & 1 & 0 \\ 0 & -a_{x1} & 0 & -a_{y1} & 0 & -a_{z1} & 0 & 1 \\ \vdots & \vdots & \vdots & \vdots & \vdots & \vdots & \vdots & \vdots \\ -a_{xm} & 0 & -a_{ym} & 0 & -a_{zm} & 0 & 1 & 0 \\ 0 & -a_{xm} & 0 & -a_{ym} & 0 & -a_{zm} & 0 & 1 \end{bmatrix}_{\hat{\boldsymbol{x}}^-} \tag{3.20}$$

$$\boldsymbol{Y} = [\tilde{\rho}_1 - \hat{\rho}_1 \quad \tilde{\dot{\rho}}_1 - \hat{\dot{\rho}}_1 \quad \dots \quad -\hat{\rho}_m \quad \tilde{\dot{\rho}}_m - \hat{\dot{\rho}}_m]^T \tag{3.21}$$

$$a_{lj} = \frac{(l^j - l_u)}{r_u^j} \tag{3.22}$$

$$r_u^j = \sqrt{(x_{SV}^j - x_u)^2 + (y_{SV}^j - y_u)^2 + (z_{SV}^j - z_u)^2} \tag{3.23}$$

In the equations above, the indices on the unit vectors and measurements run from one to m, where m is the number of measurements available at the given reception time. Because there are two measurements from each satellite, $\boldsymbol{H}$ will be a 8 by $2m$ matrix, and $\boldsymbol{Y}$ will be a 1 by $2m$ vector. The unit vector in the geometry matrix is explained in Equation 3.22 where the l^{th} geometric dimension of the unit vector pointing towards the j^{th} satellite is equal to the difference of the satellite and the user's l^{th} state normalized by the geometric range.

Next, a weighting matrix is created to place higher value on satellites with better tracking performance as characterized by the C/N0. The models for the variance of the range and range rate are shown in Equations 3.24 and 3.25 and are used to compose a diagonal matrix that is called the measurement covariance matrix shown in Equation 3.26 whose inverse is the least squares weighting matrix in Equation 3.27.

$$\sigma_{\delta\rho}^2 = \frac{\lambda_{code}^2}{2T^2(\frac{C}{N_0})^2} + \frac{\lambda_{code}^2}{4T\frac{C}{N_0}} \tag{3.24}$$

$$\sigma^2_{\delta\dot{\rho}} = \left(\frac{\lambda_{carrier}}{\pi T}\right)^2 \left(\frac{2}{T^2(\frac{C}{N_0})^2} + \frac{2}{T\frac{C}{N_0}}\right) \tag{3.25}$$

$$\boldsymbol{R} = diag\left([\sigma^2_{\delta\rho 1}\sigma^2_{\delta\dot{\rho}1} \ldots \sigma^2_{\delta\rho m}\sigma^2_{\delta\dot{\rho}m}]\right) \tag{3.26}$$

$$\boldsymbol{W} = \boldsymbol{R}^{-1} \tag{3.27}$$

In the variance equations, the λ is the wavelength of the code or carrier frequency, T is the integration period for the measurements, and C/N0 is the carrier to noise ratio in units of Hz.

Once all the above matrices have been created and the states have been initialized at some previously known position or some nominal start condition, typically a vector of zeros, the weighted nonlinear least squares algorithm can be performed iteratively until the error states converge. The equations for estimating the value of the error states and updating the PVT state estimates are shown in Equations 3.28 and 3.29.

$$\delta\hat{\boldsymbol{x}} = (\boldsymbol{H}^T\boldsymbol{W}\boldsymbol{H})^{-1}\boldsymbol{H}^T\boldsymbol{W}\boldsymbol{Y} \tag{3.28}$$

$$\hat{\boldsymbol{x}}^+ = \hat{\boldsymbol{x}}^- + \delta\hat{\boldsymbol{x}} \tag{3.29}$$

Upon each iteration of the least squares algorithm, the geometry matrix and the residual vector must be recalculated using the latest state estimates. Generally, the algorithm will converge in five iterations, if starting from zero.

Extended Kalman Filter

Once an initial state has been found, the extended Kalman filter is used to filter the estimated states. If the measurement models were linear, the Kalman filter would be the optimal estimator. However, the models are nonlinear, so an extended Kalman filter proves to be a very good estimator.

For the EKF, the estimator is broken into two parts: state propagation and measurement correction. First, the states are propagated from the last estimate to the time the next measurement is available by a state transition matrix that is shown in Equation 3.30.

$$\boldsymbol{A} = \begin{bmatrix} 1 & dt & 0 & 0 & 0 & 0 & 0 & 0 \\ 0 & 1 & 0 & 0 & 0 & 0 & 0 & 0 \\ 0 & 0 & 1 & dt & 0 & 0 & 0 & 0 \\ 0 & 0 & 0 & 1 & 0 & 0 & 0 & 0 \\ 0 & 0 & 0 & 0 & 1 & dt & 0 & 0 \\ 0 & 0 & 0 & 0 & 0 & 1 & 0 & 0 \\ 0 & 0 & 0 & 0 & 0 & 0 & 1 & dt \\ 0 & 0 & 0 & 0 & 0 & 0 & 0 & 1 \end{bmatrix} \tag{3.30}$$

Here dt is not the integration period of the correlators as it has been used previously. Instead it is the difference in time from when the last measurement was applied until the next measurement is ready to be applied. The state transition matrix used in this work is a constant velocity model. Other models can be used instead for varying dynamic constraints. Once the state estimates are propagated forward, the state covariance matrix, $\boldsymbol{P}$, must be propagated forward as well. The state covariance matrix is a square matrix with its size equal to the number of states. Typically, it is initialized as a diagonal matrix with conservative estimates of the states variances. The state covariance matrix also has a process noise covariance matrix, $\boldsymbol{Q}$, added to it. The constant velocity model assumes a zero mean acceleration state. The process noise covariance matrix is where the variance of the zero mean acceleration is accounted for in the filter, and it will determine the how much the filter will weight in favor of the model rather than the measurement. The process noise covariance

matrix is modeled in Equation 3.31.

$$\boldsymbol{Q} = \begin{bmatrix} \sigma_x^2\boldsymbol{U} & \mathbf{0} & \mathbf{0} & \mathbf{0} \\ \mathbf{0} & \sigma_y^2\boldsymbol{U} & \mathbf{0} & \mathbf{0} \\ \mathbf{0} & \mathbf{0} & \sigma_z^2\boldsymbol{U} & \mathbf{0} \\ \mathbf{0} & \mathbf{0} & \mathbf{0} & \boldsymbol{\beta} \end{bmatrix} \tag{3.31}$$

$$\boldsymbol{U} = \begin{bmatrix} \frac{T^3}{3} & \frac{T^2}{2} \\ \frac{T^2}{2} & T \end{bmatrix} \tag{3.32}$$

$$\boldsymbol{\beta} = \begin{bmatrix} \sigma_b^2 T + \frac{\sigma_d^2 T^3}{3} & \frac{\sigma_d^2 T^2}{2} \\ \frac{\sigma_d^2 T^2}{2} & \sigma_d^2 T \end{bmatrix} \tag{3.33}$$

In the above equations, σ_x^2, σ_y^2, and σ_z^2 are variance terms that can be tuned by the user. The three geometric terms are set equal in this work, but that is not necessary. The value of those variances are usually around 2 m^2/s^3 for situations where the constant velocity model is accurate and higher if the dynamics suggest the model is inaccurate. The clock variances of bias and drift, σ_b^2 and σ_d^2, are defined based on the power spectral density coefficients of the local oscillator. Their equations are shown in below in Equations 3.34 and 3.35.

$$\sigma_b^2 = \frac{c^2 h_0}{2} \tag{3.34}$$

$$\sigma_d^2 = 2c^2\pi^2 h_{-2} \tag{3.35}$$

The values of h_0 and h_{-2} change depending on the oscillator. For data sets that use a Temperature Compensated Crystal Oscillator (TCXO), the values used in this work are $2 * 10^{-19}$ and $2 * 10^{-20}$ respectively. For data sets that were aided by a Rubidium Oscillator, the values used are $2 * 10^{-22}$ and $1 * 10^{-30}$ respectively. Both sets of coefficients were taken from [4].

With the state transition and process noise matrices established, the state propagation step in the extended Kalman filter is shown in Equations 3.36 and 3.37.

$$\hat{\boldsymbol{x}}_k^- = \boldsymbol{A}\hat{\boldsymbol{x}}_{k-1}^+ \tag{3.36}$$

$$\boldsymbol{P}_k^- = \boldsymbol{A}\boldsymbol{P}_{k-1}^+\boldsymbol{A}^T + \boldsymbol{Q} \tag{3.37}$$

The measurement correction step is then done using matrices developed in the previous section. An extended Kalman gain $\boldsymbol{K}$ is calculated from the geometry matrix, the state covariance matrix, and the measurement covariance matrix. The Kalman gain is then multiplied by the residual vector and added to the propagated state estimate to correct the state. The Kalman gain is also used to correct the state covariance matrix. The equations for the measurement corrections are presented in Equations 3.38 , 3.39, and 3.40.

$$\boldsymbol{K}_k = \boldsymbol{P}_k^-\boldsymbol{H}^T\left(\boldsymbol{H}\boldsymbol{P}_k^-\boldsymbol{H}^T + \boldsymbol{R}\right)^{-1} \tag{3.38}$$

$$\hat{\boldsymbol{x}}_k^+ = \hat{\boldsymbol{x}}_k^- + \boldsymbol{K}_k\boldsymbol{Y} \tag{3.39}$$

$$\boldsymbol{P}_k^+ = \left(\boldsymbol{I} - \boldsymbol{K}_k\boldsymbol{H}\right)\boldsymbol{P}_k^- \tag{3.40}$$

In the extended Kalman filter, the tuning is handled by the process noise matrix, the measurement noise matrix, and the initial states of the state covariance matrix. In this work the process and measurement noise matrices are modeled and limited to a single tuning parameter. For each data set presented the geometric variance will be given as well as the clock type. The initial state covariance matrix is the same for all experiments.

3.5 Conclusions

This chapter explains the inner working of a software defined receiver. There are much more thorough explanations of scalar tracking receivers and advanced algorithms that are

available in the literature. This work focuses on creating vector tracking architectures rather than scalar, so this chapter was meant to provide the reader with an understanding of tracking loops as opposed to a guide to design a flawless scalar tacking software defined receiver.

Chapter 4

Vector Tracking Algorithms and Adaptions

Now that an overview of a scalar software defined receiver has been presented, this chapter seeks to explain the changes to the tracking loops made by a vector tracking architecture. For a scalar tracking architecture, the tracking loop is entirely contained within a single channel, which operates independently from all other channels. In a vector tracking architecture, the loop closure occurs in the central navigator, which tethers all the channels together through the PVT solution. The vector tracking architecture is broken into two sections: a vector delay lock loop (VDLL) to track the code and a vector frequency lock loop (VFLL) to track the carrier. Each tracking loop will be explained below, and the chapter will conclude with proposed adaptions to the legacy algorithm to be applied on GPS L5.

4.1 Vector Delay Lock Loop

The main change of the vector delay lock loop from the standard scalar delay lock loop is where the loop closure occurs. The VDLL will require the same number of correlators as the DLL and can use the same discriminators. This work uses the normalized early minus late power discriminator that was described in the previous chapter in the vector tracking loop as well. However, instead of passing the discriminator output through a low pass filter and directly updating the channel code frequency replica, the discriminator is applied to the centralized navigation extended Kalman filter as a range measurement residual. This is shown in Equation 4.1.

$$\delta\rho_j = \lambda_{code}\phi^j_{DLL} \tag{4.1}$$

Here the residual pseudorange $\delta\rho_j$ is equal to the code discriminator output ϕ^j_{DLL}, converted from units of chip phase into units of distance by the code wavelength λ_{code}. The integration periods of the individual loops do not necessarily align. In scalar tracking, pseudoranges can be pulled from every channel at anytime, but vector tracking channels must wait until the end of the integration period before the discriminator is available. Then the vector measurement must be applied immediately so that the corrected states can be used to estimate the local replica frequencies for the next integration period. Therefore, the error being represented by the discriminator is related to the state that initialized its replica frequencies. However, these states may have already been corrected by another measurement before the integration period is finished. So, the error the measurement is representing corresponds to a state that has changed, and the discriminator measurement represents the error most accurately at the middle of the integration period at a time that has already passed. Figure 4.1 shows the asynchronous elements of the vector tracking measurements.

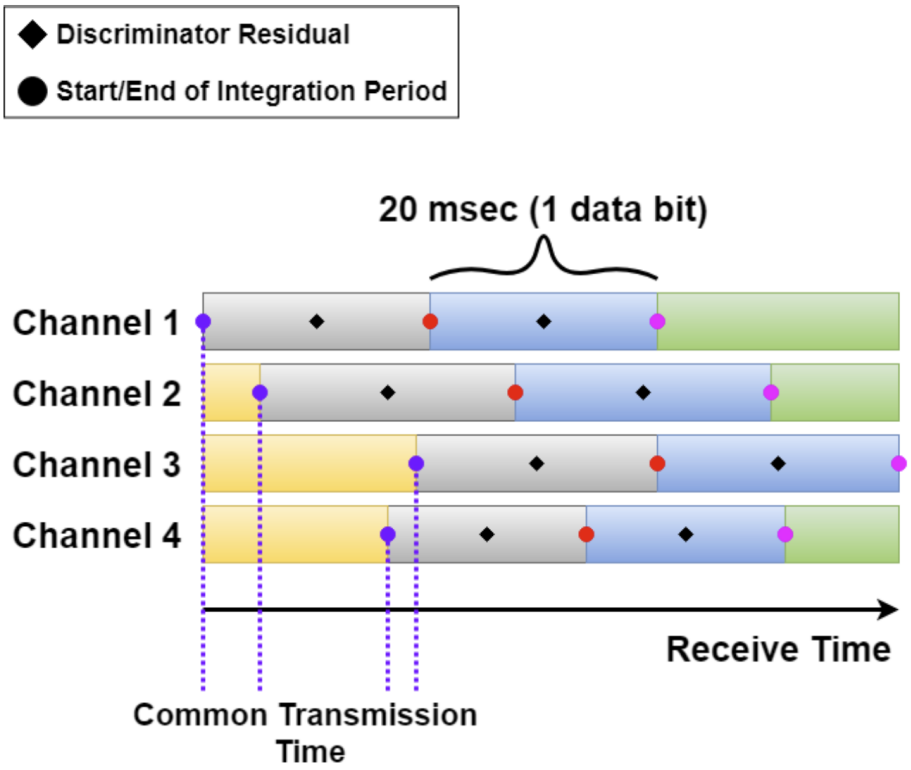

Figure 4.1: Vector Discriminator Measurements with Respect to Receive Time [31]

For example channel 1 in Figure 4.1 gets a measurement of error that is best applied in the middle of the blue integration period, but it is not available until the end of that integration period. The measurement gives the error of the state at the beginning of the integration period, but channels 2-4 have measurements that need to be applied to the states before channel 1 has finished integrating. As the length of integration periods increase, the measurement becomes a more inaccurate representation of the current error. Since the measurement is not available until the end of the integration period, the measurement cannot be applied at its most accurate location. There is a method of back tracking the state estimate and removing and re-adding previous corrections so as to accurately apply measurements, but it is overly complex for a negligible return. For an explanation of this method, see [12]. In order to account for these errors, this work adds the scalar tracking residual to correct the measurement to the current state that is presented in Equation 4.2.

$$\delta\rho_j = \lambda_{code}\phi^j_{DLL} + (\tilde{\rho}_j - \hat{\rho}_j) \tag{4.2}$$

Once the measurement has been applied and the state has been corrected, the replica code frequency must be updated before the next integration period can begin. The code frequency is updated based off of the predicted change in pseudorange over the next integration period. The equation for estimating the code frequency is shown in Equation 4.3.

$$f_{code}(k+1) = f_{chip} - \frac{\hat{\rho}(k+1) - \hat{\rho}(k)^+}{\lambda_{code}T} \tag{4.3}$$

The code frequency for the next integration period $f_{code}(k+1)$ is determined by taking the difference of the current estimate of the pseudorange, after the measured states have been corrected $\hat{\rho}(k^+)$ and a projected estimate of the pseudorange $\hat{\rho}(k+1)$, then dividing by the wavelength of the code and the length of time between the estimates to convert the range to frequency. Finally, subtract this value from the nominal code frequency f_{chip}.

4.2 Vector Frequency Lock Loop

For carrier tracking, a vector architecture in a standalone receiver is incapable of predicting the carrier phase from the position solution. There are works that show combining a vector frequency lock loop with a scalar phase lock loop provides a strong estimate of carrier frequency [31]. Furthermore, additional works also show the plausibility of a vector phase lock loop in combination with a Real Time Kinematic (RTK) system for carrier phase processing [14]. However, this work will use only a vector frequency lock loop. The discriminator used is a four quadrant arc-tangent that is the same as the one described in Chapter 3. The frequency error from the discriminator is used as the pseudorange rate residual as shown in Equation 4.4. The same errors that were in the VDLL are again present here. To correct these, the scalar residual is added to the measurement as done previously.

$$\delta\dot{\rho}_j = -\lambda_{carrier}\phi^j_{FLL} + \tilde{\dot{\rho}}_j - \hat{\dot{\rho}}_j \tag{4.4}$$

Once the measurements have been added and the states have been corrected, the carrier frequency needs to be updated for the next integration period. This is done by using the current corrected state estimate to estimate a pseudorange rate. The estimated measurement is then converted into an estimate of Doppler frequency and added to the IF to give the next integration period estimate of carrier frequency. This is shown in Equation 4.5

$$f_{carrier}(k+1) = f_{IF} - \frac{\hat{\dot{\rho}}(k)^+}{\lambda_{carrier}} \tag{4.5}$$

4.3 Combined Vector Lock Loop

The VDLL and VFLL can be implemented individually or in unison. In this work, the receiver will be running purely scalar until position fix is achieved, and then the receiver will transition to a vector delay/frequency lock loop (VDFLL). The only difference between the vector tracking loops and the scalar tracking loops is how the measurements are created and

how the replica frequencies are updated. The positioning algorithms used are the same as in Chapter 3.

4.4 Algorithm Adaptions for GPS L5

The main benefit of the vector tracking architecture is the added robustness it provides. This work identifies a 2 potential modifications to the traditional vector tracking architecture made possible by the GPS L5 signal structure.

4.4.1 Combined Channel Tracking

The first adapted method works by combining the in-phase and quadrature channels at the discriminator level. This method uses the standard six correlators for each signal, but creates them all from a common replica signal. The correlators then create discriminators and noise estimates for each channel. These measurements are then combined in a weighted fashion using the C/N0 from both channels. The weight for each measurement is the channel C/N0 divided by the sum of both channels C/N0. The measurements are then applied to the navigation filter, and the common replica frequencies are updated normally from the navigation filter. Ideally, the averaging of two measurements will act as a filter and provide more robust measurements. A diagram of this tracking method can be seen below in Figure 4.2.

A version of this combination was implemented on a scalar tracking loop in [23]. The work found that the combination extended the tracking threshold of the measurement by 1 dB and it improved the position performance at high C/N0. At low C/N0 it tended to degrade position performance slightly. The shortcoming of this method is that the integration period will be 10 ms, and therefore the thermal noise filtering on the measurements will be poor.

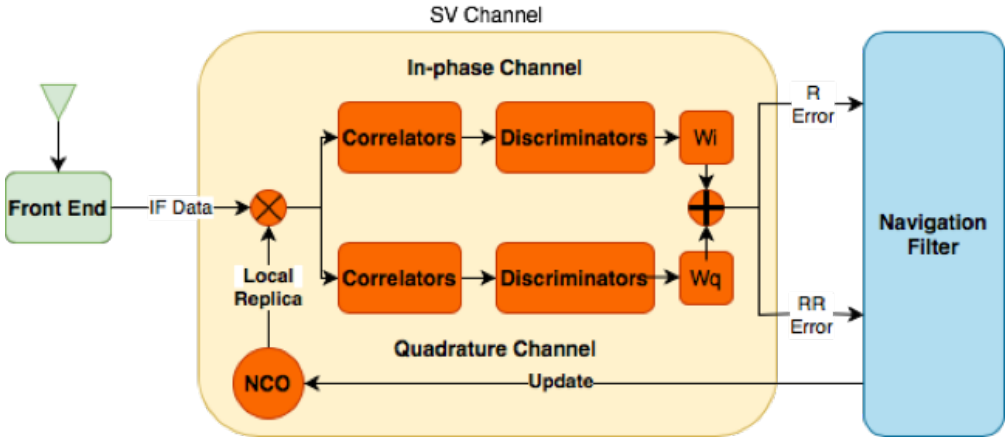

Figure 4.2: Combined Vector Tracking Architecture for GPS L5

4.4.2 Separate Extended Channel Tracking

The second method tracks both the in-phase and quadrature channels separately. Both channels maintain their own local replica and apply two measurements directly to the central filter. The quadrature channel has no limit on integration period length due to the lack of a data message. Therefore, the integration period of the quadrature can be extended well passed that of the in-phase. This allows for a tighter bandwidth on the carrier frequency estimate as well as a longer period to accumulate weak signals. Figure 4.3 shows a diagram of the algorithm.

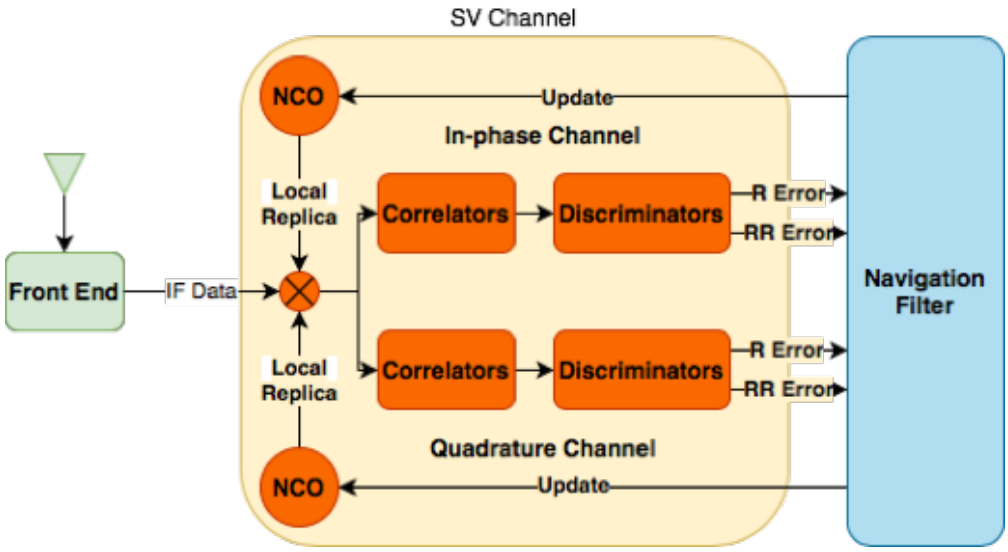

Figure 4.3: Separate Vector Tracking Architecture for GPS L5

This idea of extended integration has been applied in acquisition where the signal is squared to remove the data bit phase shifts. This allows for the accumulation of power to acquire the signal in low C/N0. The GPS L5 quadrature can used in a similar fashion but without the need for squaring. This extended integration will have a much lower measurement variance with that will in turn cause the extended Kalman filter to track the frequencies with very tight bandwidths. The tight bandwidths will remove the majority of the thermal noise and will allow the receiver to continue producing quality measurements in degraded environments. There is a shortcoming in that the extended integration period will shorten the bandwidth to a point it will fail to capture the user dynamics of some platforms. For this work, the separate method will have an integration period of the 10 ms maximum on the GPS L5 in-phase signal and will have an integration period of 100 ms on the GPS L5 quadrature signal.

This work will also present a GPS L5 quadrature only vector tracking receiver with 20 ms integration periods. This receiver will be identical to the GPS L1 receiver and will allow for a direct comparison of the two signals in a vector tracking mode.

4.5 Conclusion

This chapter has presented an overview of the implementation of vector tracking as done in this work, as well as proposed some variations to the traditional vector tracking architecture that was made available by the new signal structure. The following chapters will compare these implementations against each other, as well as against traditional architectures, on both modern and legacy signals in static live sky, dynamic live sky, and simulated experiments.

Chapter 5

GPS L5 Vector Tracking Implementation and Results

This chapter presents the results from implementations of the algorithms and adaptions described previously on live sky and simulated data. There will be a presentation of a covariance analysis that will show the theoretical gains of the proposed methods. The methods will then be tested on simulated and live sky data. The success of the algorithms will be determined by how robust the receiver is in degraded environments.

5.1 Covariance Analysis

This section presents a covariance analysis of the methods described in the previous chapter to evaluate theoretical gains in positioning accuracy at varying carrier to noise levels. The analysis is done by utilizing the satellite geometry of the experimental data collected for this work and iterating the Kalman filter for defined process noise, state propagation, and measurement covariance matrices until the state covariance matrix converges. This is done over a range of C/N0 values for the GPS L5 combined, GPS L5 separate with extended quadrature integration periods, GPS L5 quadrature only with extended integration periods, and GPS L1 C/A methods.

For each covariance analysis, the state covariance matrix $\boldsymbol{P}$ is initialized to an identity matrix multiplied by 100. The geometry matrix $\boldsymbol{H}$ is held constant while the filter is iterated. There are six satellites in the data set, and a sky plot of the satellites in Figure 5.1 shows the geometry. The state covariance matrix was propagated in time by the extended Kalman filter by a constant velocity state propagation matrix $\boldsymbol{A}$ with a time step of the measurement integration period and a process noise matrix $\boldsymbol{Q}$ that was tuned with a parameter of 20 m^2/s^3 and the same time step as the state propagation matrix. The measurement covariance

matrix $\boldsymbol{R}$ was the element that changed with C/N0 level and integration period length of the tracking loop. For each given C/N0 level and integration period the extended Kalman filter was iterated until the position states along the diagonal went to steady state.

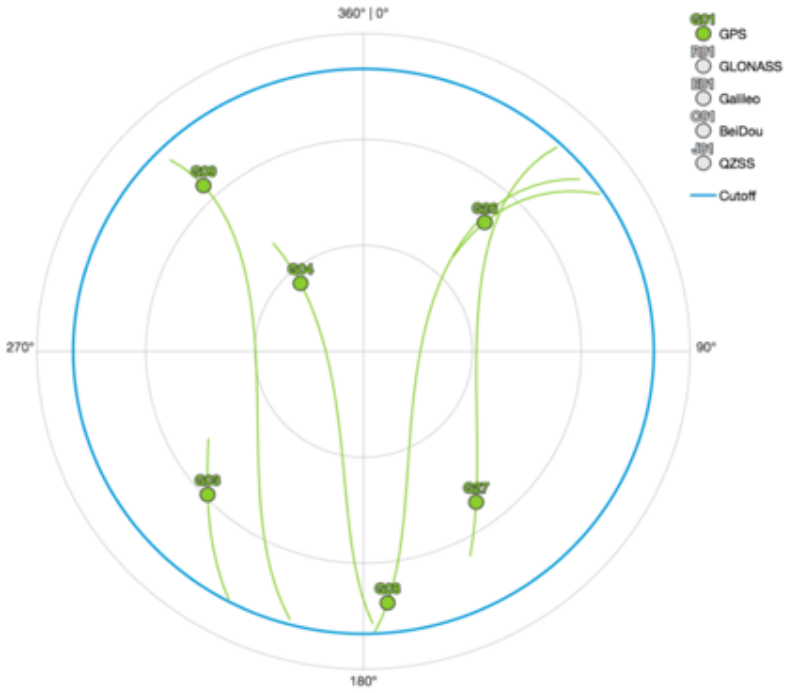

Figure 5.1: Sky Plot of the Satellite Geometry Used in the Covariance Analysis

The variance of the measurements only considers the thermal noise of the measurements. As the integration period increases, the measurement will be more heavily filtered, but the dynamics will begin to be filtered out as well if they are high enough. The variance of the dynamics is captured in the process noise covariance. From Equation 3.31, the process noise is dependent on the integration period and will increase non-linearly as the integration period increases. However, from Equation 5.2 the dominating term in the pseudorange measurement covariance is linearly dependent on the integration period. As the integration period increases at high C/N0, the filter will begin to favor the shorter integration periods as the increased filtering on the measurements is unnecessary. As the process noise tuning coefficient is increased, the value of extended integration periods decreases. The extension of

integration periods is a trade of accuracy for precision. At low dynamics the trade is viable, but at high dynamics the accuracy is needed for the tracking loops to function.

Figures 5.2 and 5.3 show the variance of the pseudorange and pseudorange rate as a function of C/N0 and integration period length. The variances shown on these graphs make up the diagonal of the measurement covariance matrix used in the covariance analysis. The GPS L5 pseudorange variance is lower across all noise levels than GPS L1 due to the shorter wavelength of the GPS L5 PRN code. The increased chipping rate of GPS L5 provides more accurate ranges. As the GPS L5 integration period is extended from 10 ms to 100 ms, the variance on the measurement continues to decrease. With the increase and chipping rate there comes a decrease in the maximum allowable pseudorange variance for a successful tracking loop. The tracking threshold for the VDLL is half the wavelength of the PRN code. Using this $\lambda/2$ threshold as a 3σ value, a maximum variance for both signals is plotted as well. While the GPS L5 is more accurate at all integration periods, it needs an extended integration period to track the code at levels lower than GPS L1.

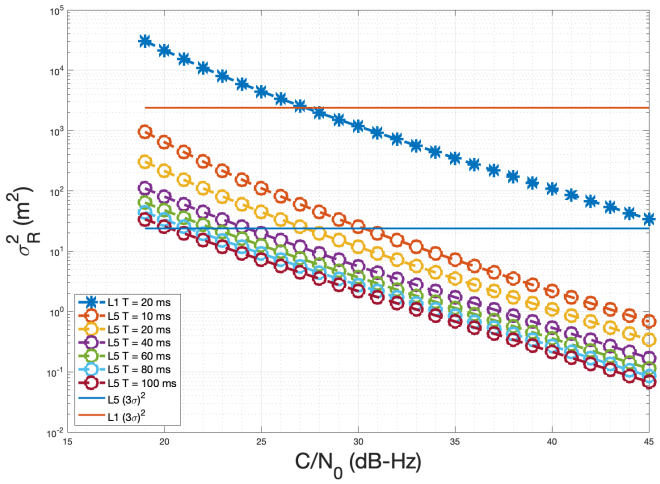

Figure 5.2: Variances of Pseudorange Measurements as a Function of C/N0

A similar effect is seen in the pseudorange rate variance. Here, the GPS L1 signal outperforms the GPS L5 signal of equivalent or lesser integration period lengths due to its shorter carrier wavelength. However, the further extended integration periods allow the GPS

L5 measurements to out perform GPS L1. There is no tracking threshold comparison for the pseudorange rate variance because the VFLL discriminator linear region is a function of the integration period length.

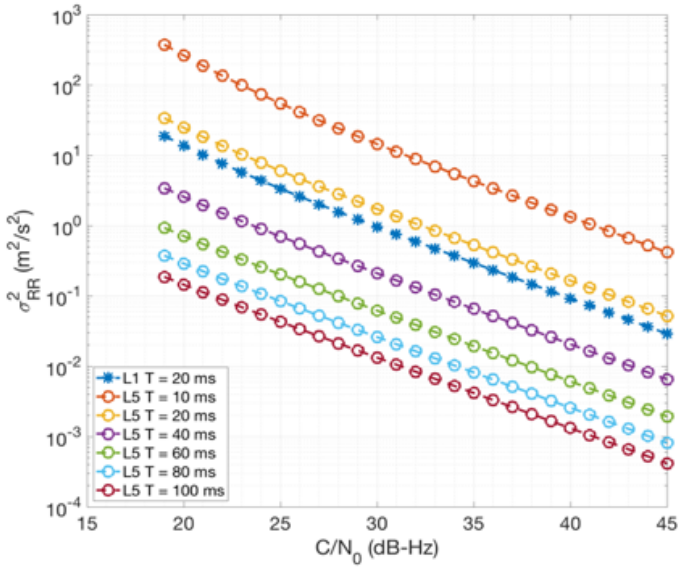

Figure 5.3: Variances of Pseudorange Rate Measurements as a Function of C/N0

Figures 5.4 and 5.5 show the ECEF X dimensional position and velocity results of a covariance analysis for GPS L1 and GPS L5 Quadrature solutions with varying integration lengths. The covariance follows similar trends to that of the measurements. The extended integration periods offer performance gain at low C/N0 for the positions, but at high C/N0s every method over 40 ms converges to approximately the same value. The velocity variance follows closely with the measurement covariance, decreasing with increasing integration periods.

In Figures 5.6 and 5.7, the covariance analysis is shown for a receiver that has measurements from both the GPS L5 in-phase and the GPS L5 quadrature being applied to the filter. This receiver is compared to the GPS L1 receiver from the previous covariance analysis. the GPS L5 in-phase signal update rate is restricted to 100 Hz due to the data symbol rate, while the GPS L5 quadrature signal update rate is changed from 100 Hz to 10 Hz as is was shown in the previous results. The net effect is the position covariance no

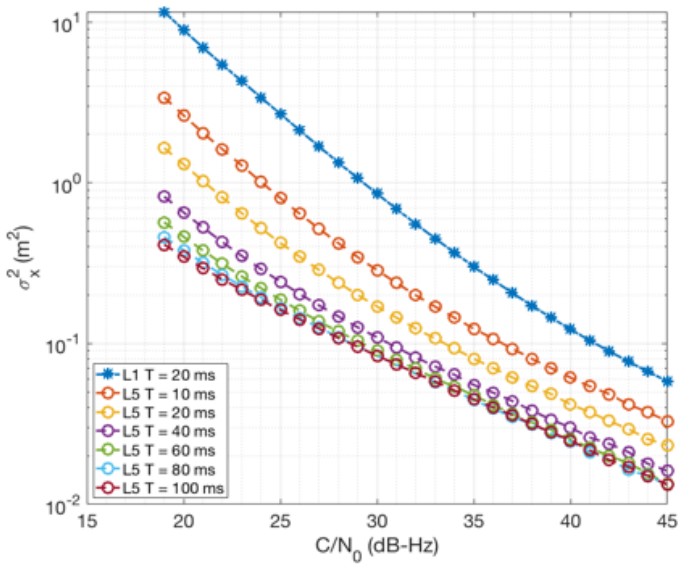

Figure 5.4: Covariance of ECEF X Position as a Function of C/N0 for GPS L1 and L5 Quadrature

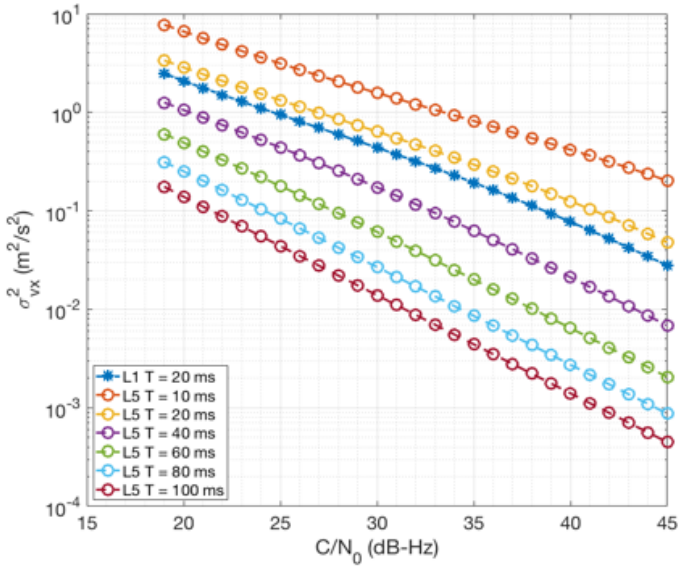

Figure 5.5: Covariance of ECEF X Velocity as a Function of C/N0 for GPS L1 and L5 Quadrature

longer improves with extended integration, but instead is constrained by the faster update rate of the in-phase channel. For the velocity covariance, the covariance oscillates between a value more in line with the in-phase update, and then drops radically when the extended quadrature measurement is applied due to the weight the filter places on that measurement. In Figure 5.3 there is an approximately three orders of magnitude change in the variance of the measurements being applied at 100ms quadrature integration periods versus 10 ms in-phase integration periods. The velocity covariance in Figure 5.7 depicts these drops rather than the oscillating intermediate values.

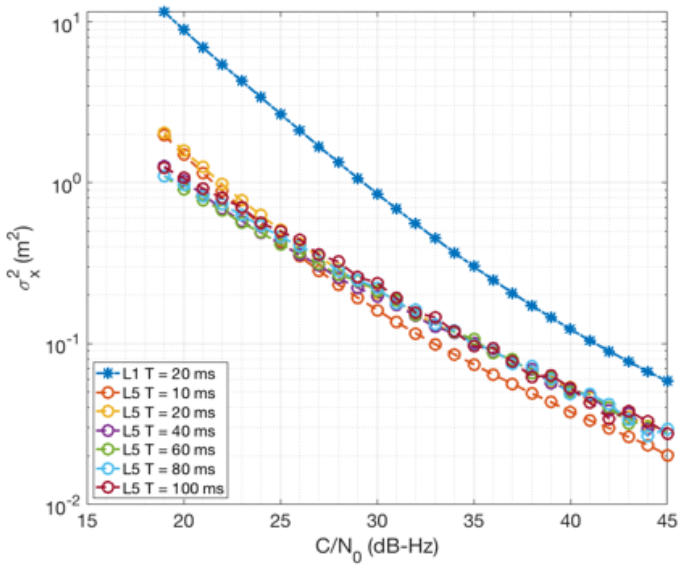

Figure 5.6: Covariance of ECEF X Position as a Function of C/N0 for GPS L1 and L5 In-Phase and Quadrature

This analysis shows that the extension of the integration periods will improve the filtering on the measurements. At low dynamics, having extended integration periods will also decrease variance on the states. However, the dual measurement method will restrict the state covariance from decreasing below where the faster update rate would place it.

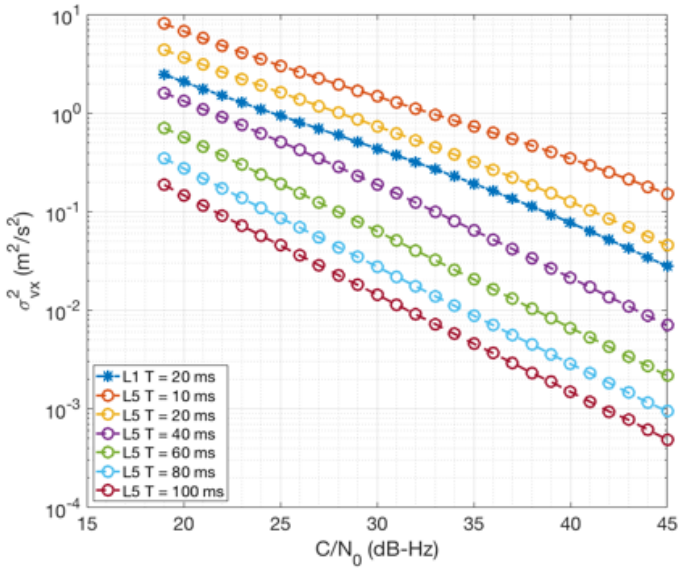

Figure 5.7: Covariance of ECEF X Velocity as a Function of C/N0 for GPS L1 and L5 In-Phase and Quadrature

5.2 Experimental Setup

All live sky and simulated data used in this work was collected as Intermediate Frequency (IF) samples by an IFEN SX3 front-end with a 20 MHz sampling frequency. It was then post processed in MATLAB. There are currently only 14 satellites broadcasting GPS L5, and in Auburn, Alabama, where this data was collected, there are, at most, 6 GPS L5 capable satellites visible. for comparison purposes, the L1 receiver is restricted to using only GPS L5 capable satellites for a more accurate comparative performance analysis.

The first data set is a static test, collected from an antenna mounted on the roof of Auburn University's Woltoz Engineering Research Laboratory. The antenna location has been surveyed and was used to compare position accuracy of the various methods.

The second data set is a dynamic test collected in Auburn University's drive-by-wire Lincoln MKZ with a roof mounted Novatel 703 GGG antenna, which receives both L1 and L5 frequency bands. The data was collected while driving along a neighborhood road in Auburn, Alabama in August of 2020. The road has heavy foliage coverage consistently on each side of the road for the length of the run, and it occasionally has a full canopy completely

covering the road. This data set is meant to test the signal tracking algorithms in common degraded environments.

The last data set to be presented is a simulated data set generated by a Spirent GNSS simulator. The data set is a static position set with the C/N0 set to decrease every five seconds. This set is to test the receivers ability to track consistently in degraded environments.

5.3 Static Live Sky Data

Figures 5.8-5.12 show the positioning quality of the methods compared in this work for the static open sky data set. All methods are initialized with a scalar non-linear weighted least squares and then use an extended Kalman filter once the vector tracking has been initialized. Figure 5.8 shows the results on a East and North scatter plot centered on the surveyed antenna location. In the static open sky scenario, the extended measurements from the GPS L5 in-phase and quadrature separate method allow for the most accuracy, while all GPS L5 methods outperform GPS L1 even after its position converges. The process noise coefficient σ_x^2 used for this data set was $2m^2/s^3$.

In Figure 5.9, the position errors are presented in ECEF coordinates. Here, the slower convergence and increased position variance of GPS L1 can be seen. The GPS L1 solution had a large initial position error from its least squares initialization. Signals from all methods used identical loop filters, integration periods, measurement algorithms, and navigation algorithms for their scalar position initialization. These methods were all shown in Chapter 3. The increased variance on the GPS L1 pseudoranges from the longer code wavelength causes the initial error. The larger variance associated with the measurements also causes the navigation filter to take longer to converge and to oscillate more once the filter has converged.

In Figure 5.10, the up position errors are plotted from the ENU coordinate frame. The majority of the positioning errors are in the vertical direction and are a result of the geometry of the satellites.

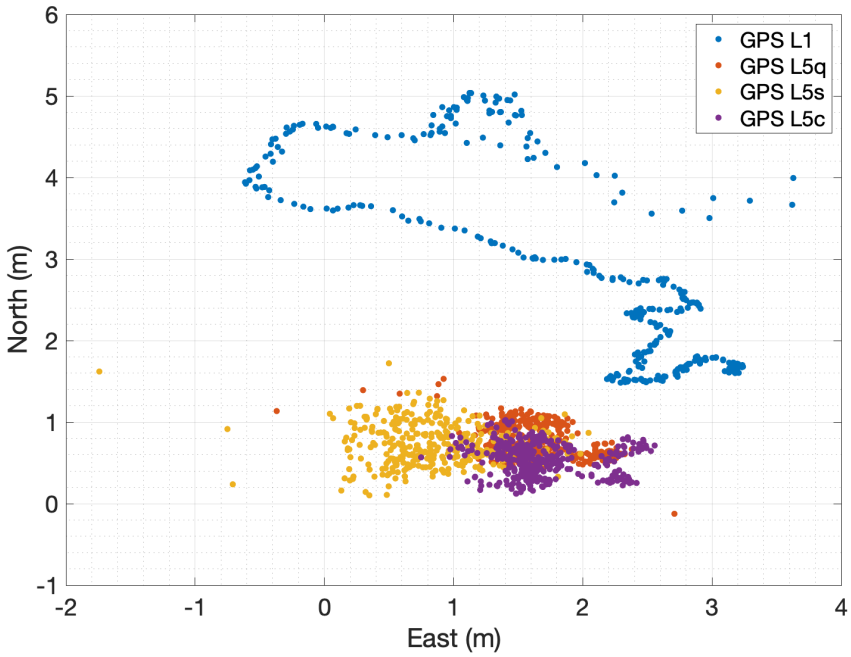

Figure 5.8: Scatter Plot of Receiver Positions in East North Up Coordinate Frame Centered on Surveyed Antenna Position

In Figure 5.11, the velocity errors are presented in ECEF coordinates. The velocity states all converge immediately and the errors are zero mean. The variance on the GPS L1 is the best performing as expected from the covariance analysis performed in the previous section.

In Figure 5.12, the covariance of the position and velocity states are presented. It can be seen here that the GPS L5 position solutions all converge faster than the GPS L1, and the increased integration periods decreased the state variance. The GPS L5 velocity performs equivalently to GPS L1 at identical integration periods with less oscillation. When the GPS L5 separate measurement method applies the extended integration period measurement, there is an order of magnitude decrease in the state variance. In order to show this, the covariance is shown as two lines. The higher line shows the covariance midway through the quadrature integration period, when only the in-phase measurements are being applied, whereas the lower line shows the covariance when the 10 Hz extended quadrature measurement is applied. If the velocity estimate is only considered at points where the

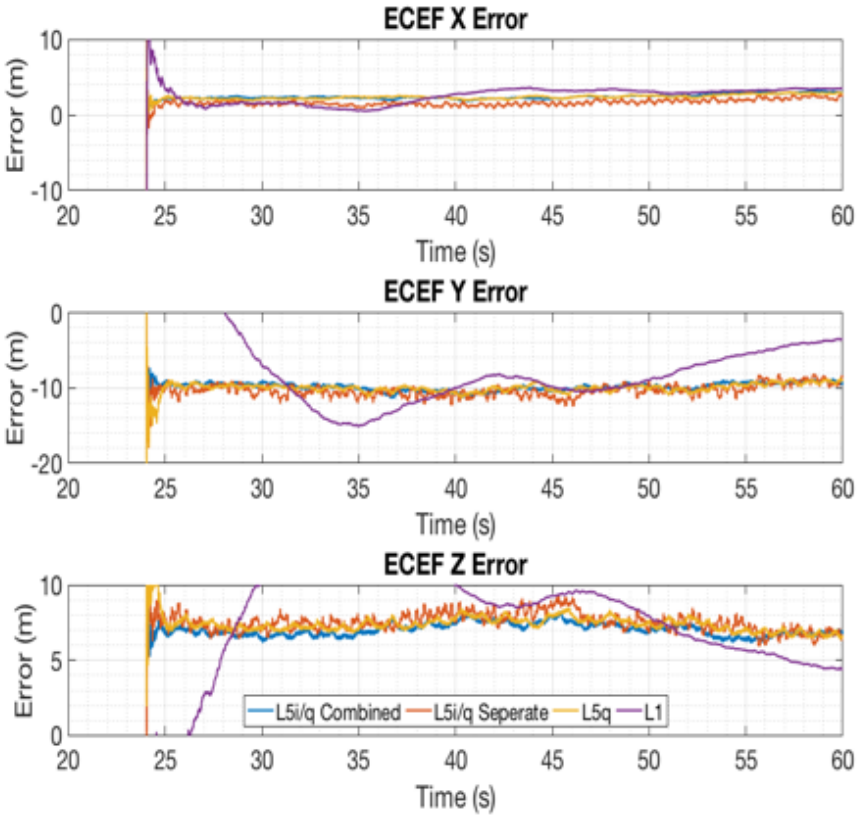

Figure 5.9: ECEF Position Errors

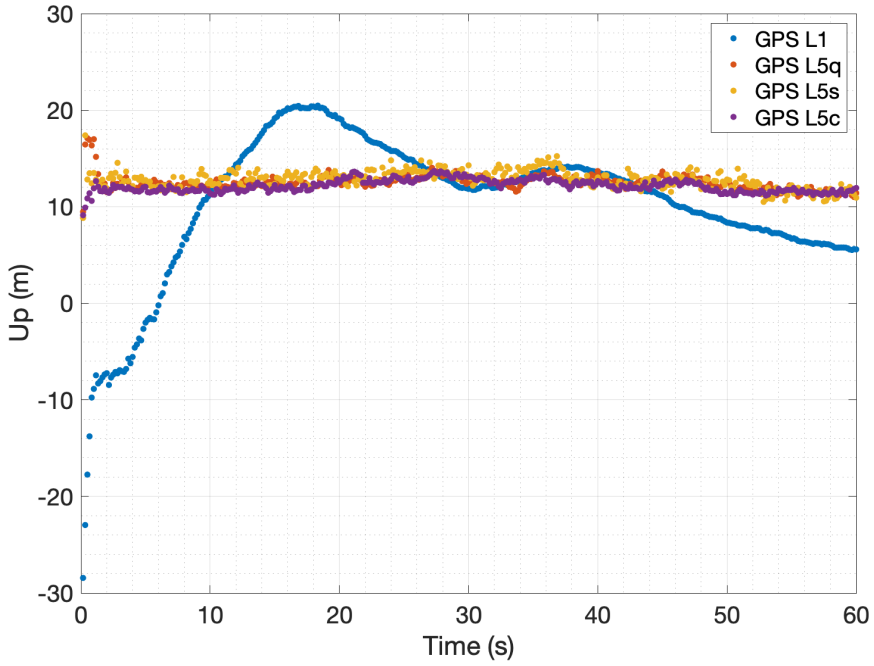

Figure 5.10: ENU Up Position Errors

extended integration period measurements become available, the velocity estimate is much more accurate than all other methods shown.

5.4 Degraded Dynamic Data

In Figure 5.13, the position results of the different methods while driving through a degraded environment are displayed. The route taken begins in a parking lot in the North West corner of the figure. The receivers are given approximately two minutes to initialize position and switch to a vector tracking mode. The route then heads south and east through the foliage heavy route, until emerging out to open sky again. The data set is approximately 7 minutes in total. The process noise coefficient for this data set σ_x^2 was $20m^2/s^3$.

Figure 5.14 shows a zoomed in image of the position results. The driving lane for the data was the lane on the lower left side of the images. All methods maintained a position solution that kept on the road for the entire data set. All solutions except one maintained a position solution in the correct lane the entire data run. The GPS L5 combined channel

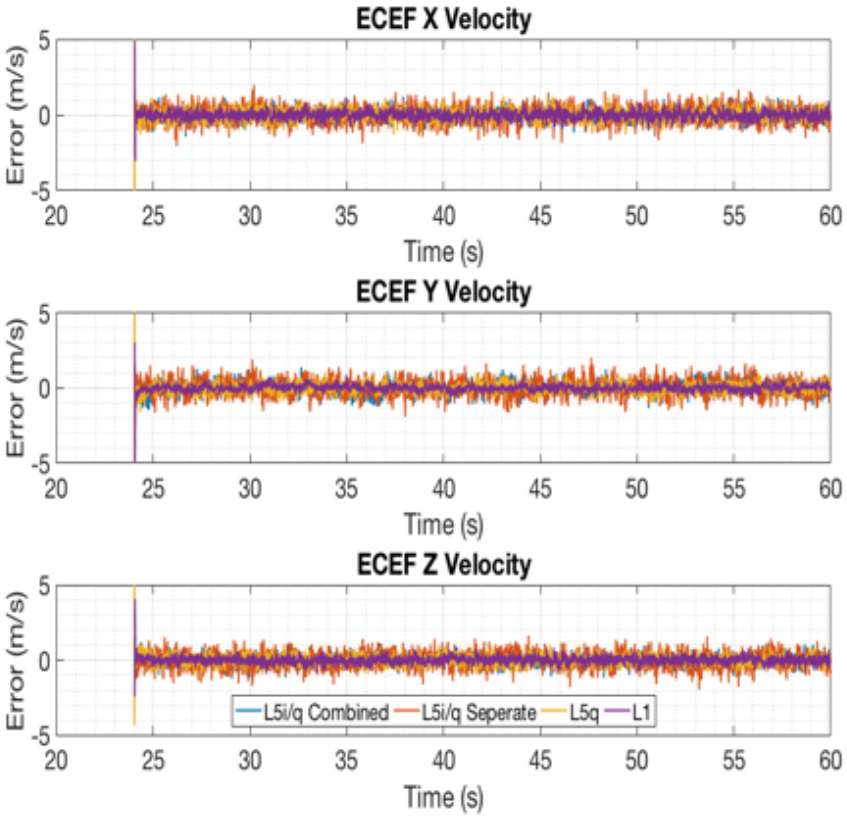

Figure 5.11: ECEF Velocity Errors

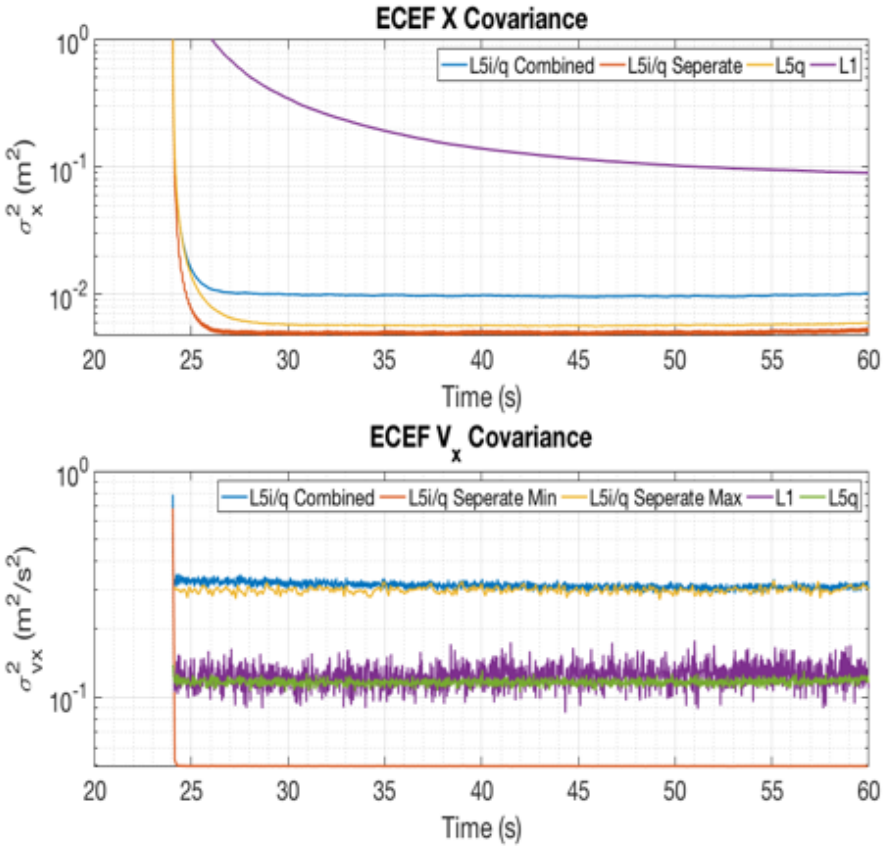

Figure 5.12: ECEF X Dimension Position and Velocity Covariance

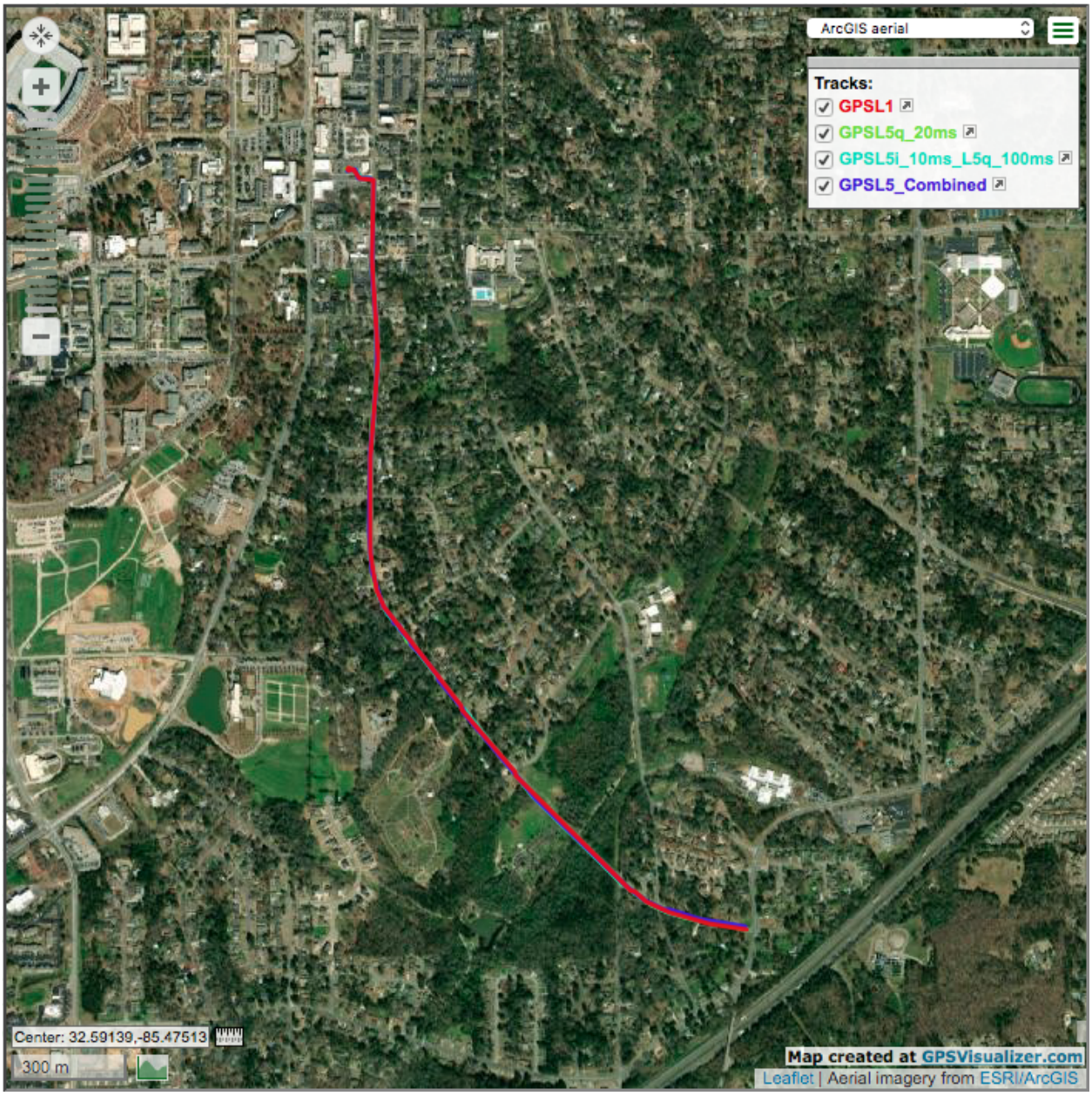

Figure 5.13: Degraded Dynamic Position Results Shown in GPS Visualizer

method had some apparent multipath that biased the position into the oncoming lane for the final few hundred meters of the data set, as shown in the right image. Without a truth reference, it is impossible to determine which method produced the best PVT solution, but all methods were robust to the interference and maintained a quality PVT solution.

While a reference truth could show approximate error of the receivers, the goal of this work is to gauge the robustness of the method rather than the accuracy. The plot shows East and North errors to be on the scale of meters, which is accurate. However, a comparison of robustness between the presented receivers and a commercial receiver is invalid as the commercial receiver is not restricted to the same limited GPS L5 satellite geometry and has unknown tracking and PVT algorithms. The goal of this was only to compare the proposed improvements to GPS L5 vector tracking to methods identical in all ways except the proposed adaptions.

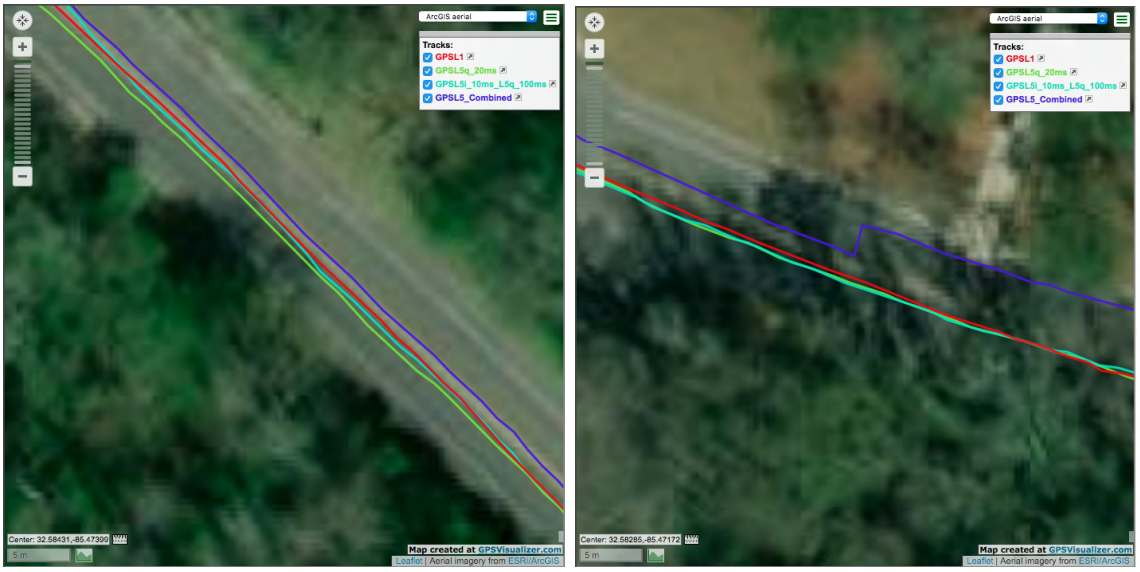

Figure 5.14: Closer View of Degraded Dynamic Position Results Shown in GPS Visualizer

5.4.1 GPS L5 Quadrature Only

This section compares the results of the dynamic data run using the GPS L1 vector tracking method with the GPS L5 quadrature only vector tracking method. The integration

period for the GPS L5 quadrature method is set at 20ms to match the performance of the GPS L1 method. The bandwidth of the vector tracking loop is heavily dependent on integration period length. The differences in these results should be a direct result of signal differences. All receiver algorithms are identical for both methods.

Figure 5.15 shows the pseudorange rate measurement for both GPS L1 and GPS L5 Quadrature for PRN 3. The pseudorange rate is used to show a comparison of the Doppler tracking of both methods. Because the Doppler frequency is carrier frequency dependent, the Doppler frequency will be different for both GPS L1 and GPS L5. By scaling the Doppler frequency into pseudorange rate with the signals carrier wavelength, the Doppler frequencies can be compared since the pseudorange rate will have the same truth value. PRN 3 was the satellite with the weakest received signal for the data set. Both receivers track the signal correctly with similar bandwidths, however, the GPS L1 shorter carrier wavelength provides a slight improvement at equivalent integration periods.

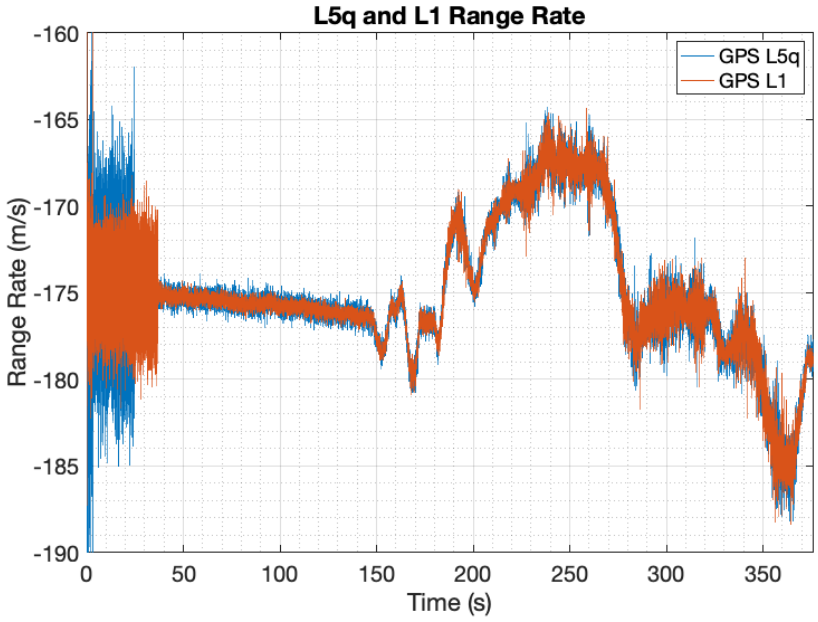

Figure 5.15: Pseudorange Rate for PRN 3 for GPS L5 Quadrature Method and GPS L1

Figure 5.16 shows the pseudorange rate for both GPS L1 and GPS L5 Quadrature for PRN 4. This satellite was the strongest received signal for the data set. Both receivers track the signal with little discernible difference.

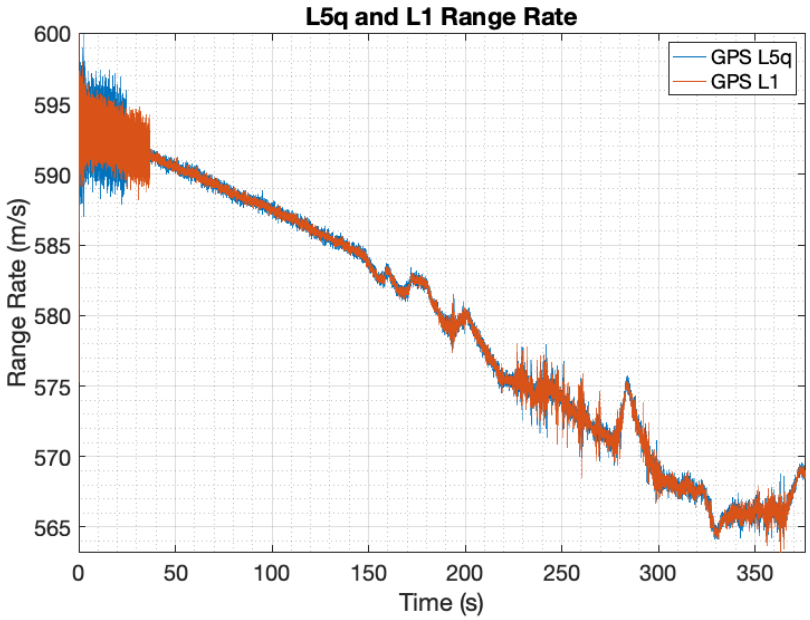

Figure 5.16: Pseudorange Rate for PRN 4 for GPS L5 Quadrature Method and GPS L1

Figure 5.17 shows the C/N0 ratio for both GPS L5 quadrature and GPS L1 on PRN 3. The GPS L5 maintains a higher value on average and drops out in the same places as GPS L1.

Figure 5.18 shows the C/N0 ratio for both GPS L5 quadrature and GPS L1 on PRN 4. The GPS L5 maintains a higher value on average by around 2-3 dB-Hz, and it does not drop as far as the GPS L1 estimate during the points of signal interference.

Figure 5.19 shows the C/N0 ratio for both GPS L5 quadrature and GPS L1 on PRN 27. This satellite has the largest difference in C/N0 estimates, while remaining free of major dropouts. The GPS L5 method approaches and maintains an increase in C/N0 of almost 4 dB-Hz.

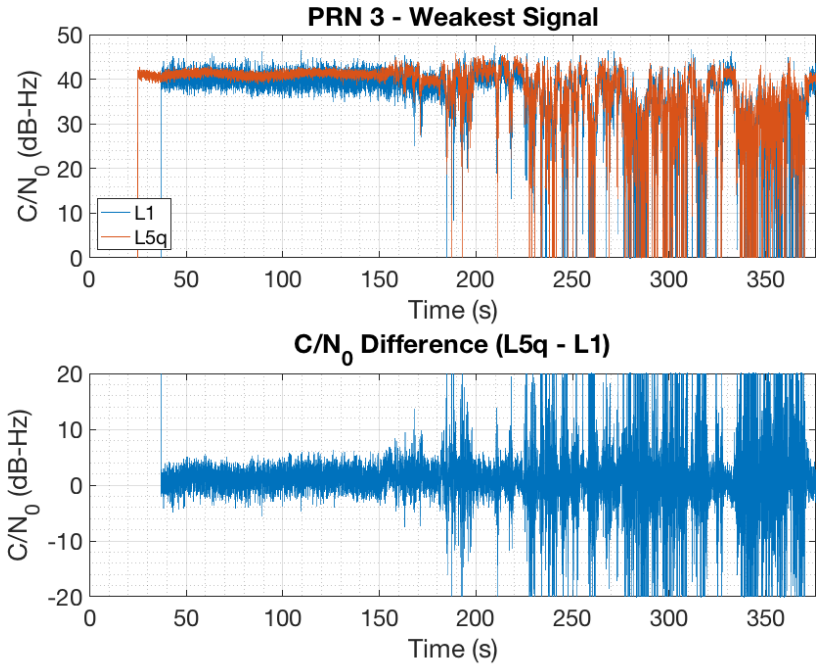

Figure 5.17: C/N0 Estimates for PRN 3 for GPS L5 Quadrature Method and GPS L1

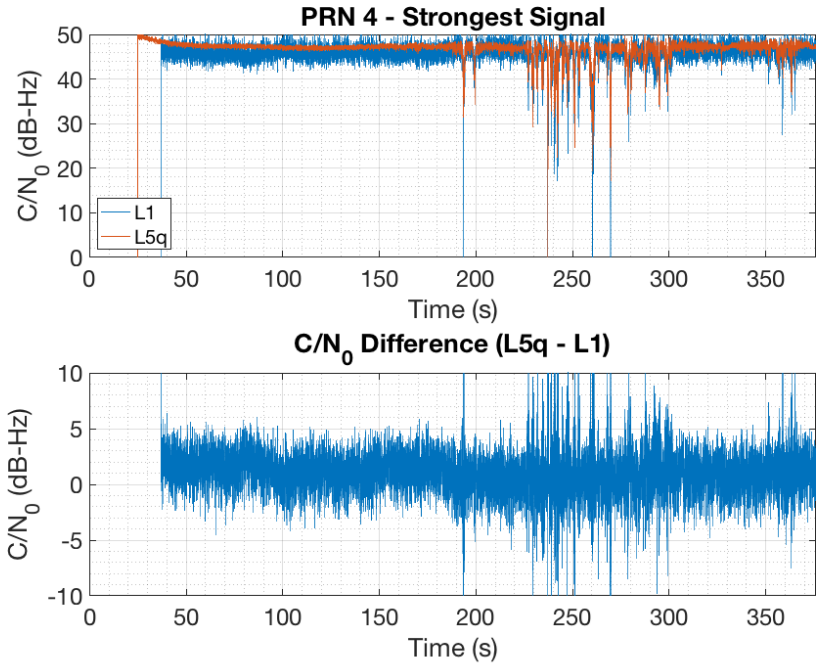

Figure 5.18: C/N0 Estimates for PRN 4 for GPS L5 Quadrature Method and GPS L1

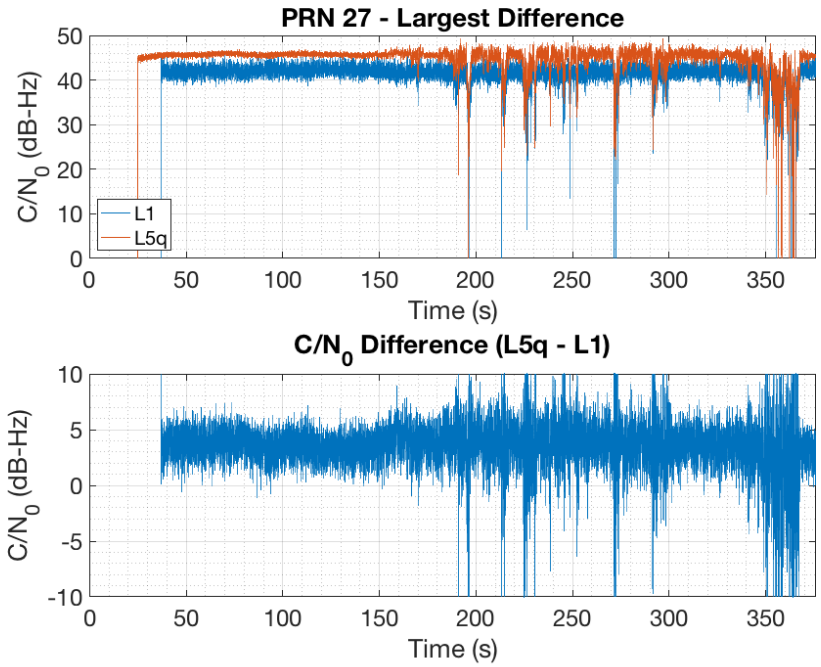

Figure 5.19: C/N0 Estimates for PRN 27 for GPS L5 Quadrature Method and GPS L1

5.4.2 GPS L5 Quadrature and In-Phase Combined

This section compares the results from the GPS L5 Combined method with GPS L1. Here the integration period on the GPS L5 signal is restricted to 10 ms for both in-phase and quadrature due to the data symbol rate for GPS L5.

Figures 5.20 and 5.21 show the pseudorange rate for both methods for the weakest and strongest signals respectively. The effect here of increased integration periods on vector tracking loop bandwidths can be well seen. Both methods maintain a lock on both signals, but the GPS L1 method manages a tighter bandwidth in the open sky areas.

Figures 5.22, 5.23, and 5.24 all show the C/N0 estimates for both methods, as well as a difference between the methods for the same three satellites as in the previous section. The GPS L5 combined method manages to maintain an average of 1-4 dB-Hz improvement over the legacy signal.

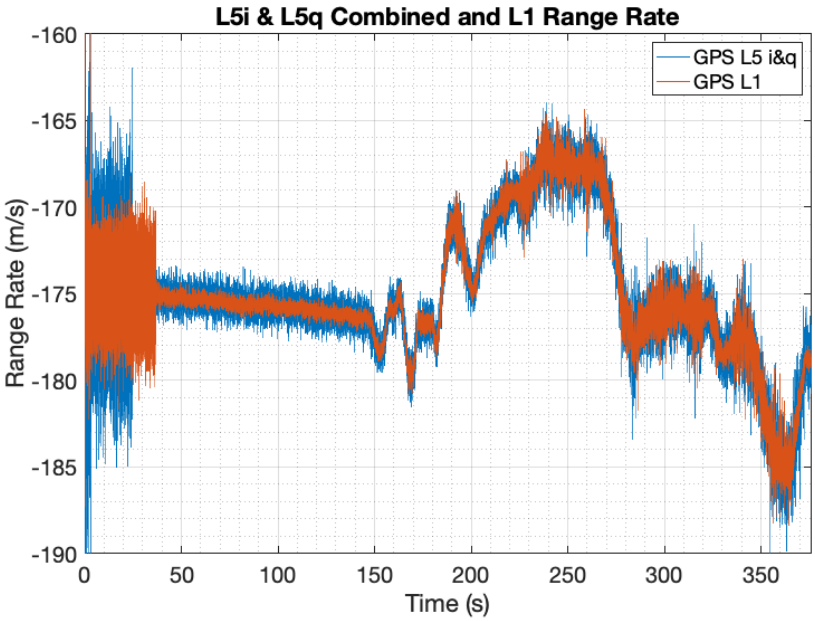

Figure 5.20: Pseudorange Rate for PRN 3 for GPS L5 Combined Method and GPS L1

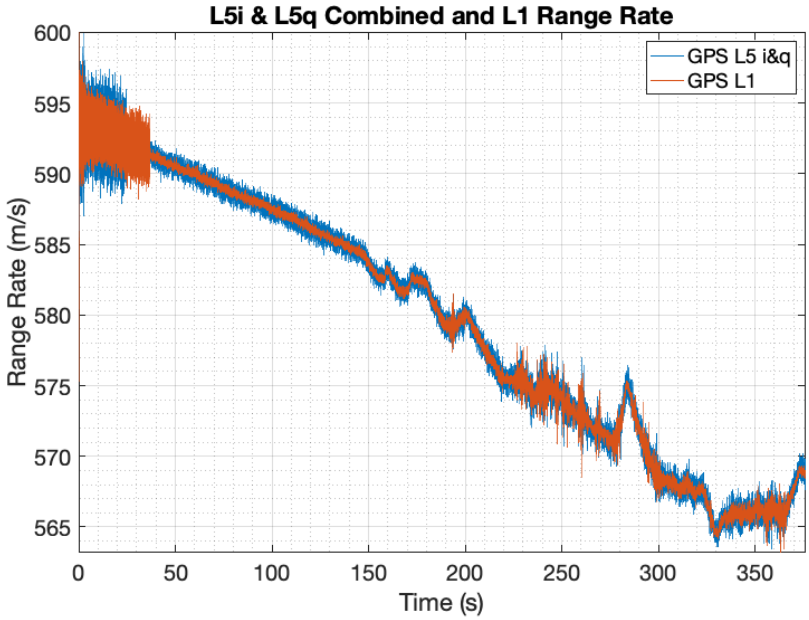

Figure 5.21: Pseudorange Rate for PRN 4 for GPS L5 Combined Method and GPS L1

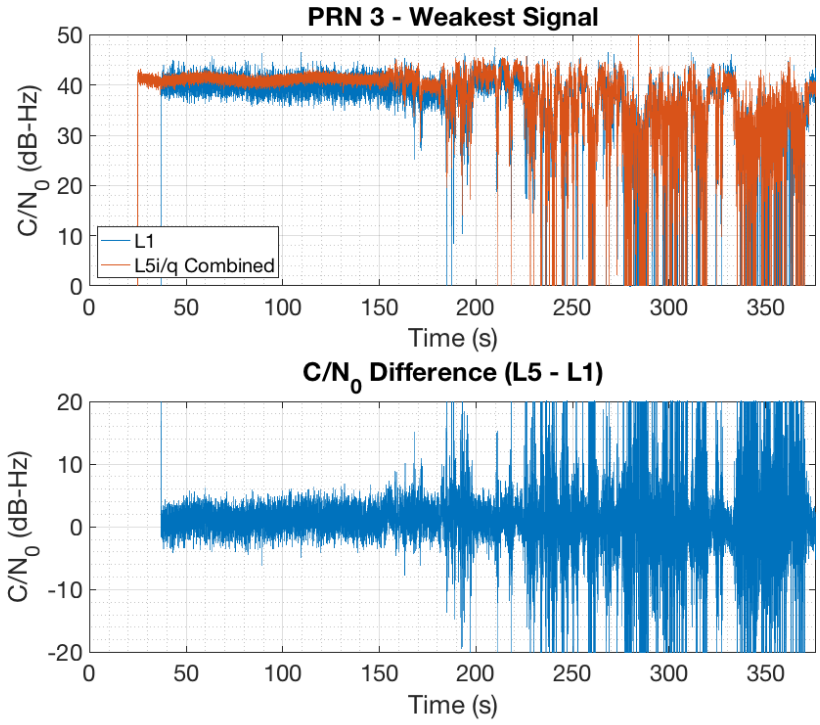

Figure 5.22: C/N0 Estimates for PRN 3 for GPS L5 Combined Method and GPS L1

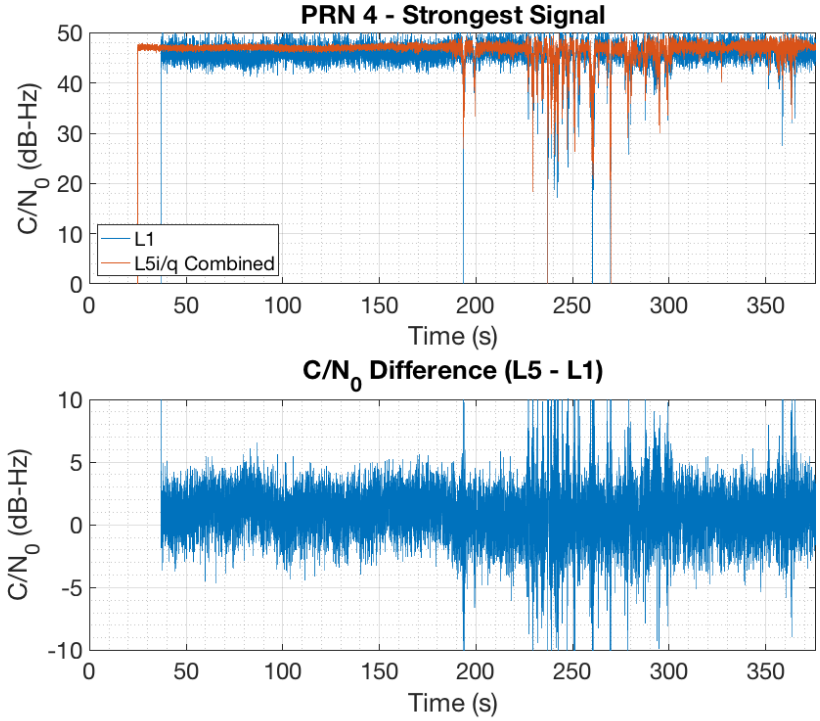

Figure 5.23: C/N0 Estimates for PRN 4 for GPS L5 Combined Method and GPS L1

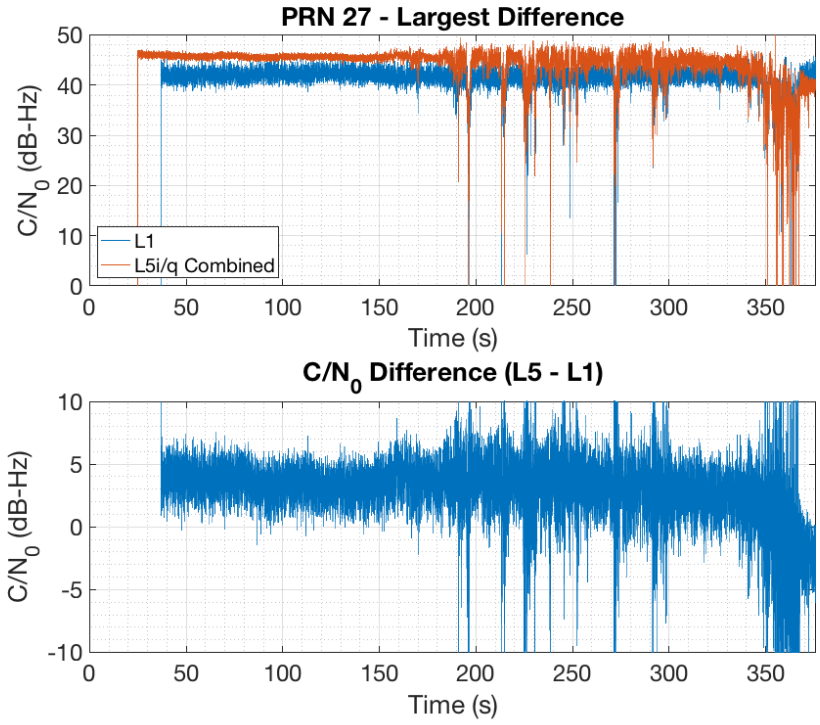

Figure 5.24: C/N0 Estimates for PRN 27 for GPS L5 Combined Method and GPS L1

5.4.3 GPS L5 Quadrature and In-phase Separate

This section shows a comparison between the GPS L5 separate method and the traditional GPS L1 method. The separate method has a 100 ms integration period on the quadrature channel. Three pseudorange rates and C/N0 estimates are presented here: one for GPS L1, one for GPS L5 in-phase, and one for GPS L5 quadrature.

In Figures 5.25 and 5.26, the pseudorange rates are presented with two from the GPS L5 receiver and one from the GPS L1 receiver. The GPS L5 in-phase behaves similarly to the GPS L5 combined, due to the identical integration periods. However, the GPS L5 quadrature was able to achieve the tightest bandwidth of all methods, regardless of channel noise. With a 10 Hz measurement update rate, the quadrature channel managed to fully capture all the receiver dynamics and reject the majority of the noise.

Figures 5.27, 5.28, and 5.29 all show the C/N0 estimates for both methods as well as a difference between the methods for the same three satellites as in the previous section.

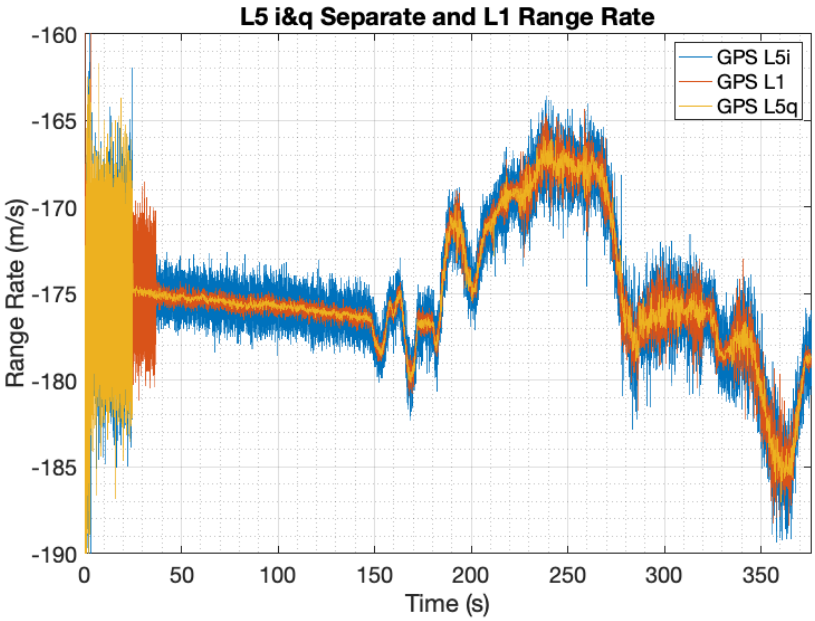

Figure 5.25: Pseudorange Rate for PRN 3 for GPS L5 Separate Method and GPS L1

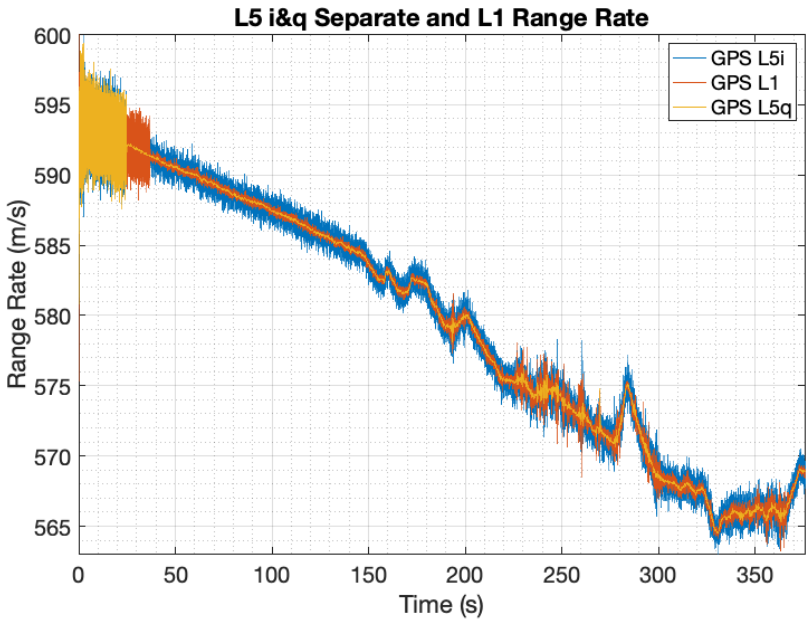

Figure 5.26: Pseudorange Rate for PRN 4 for GPS L5 Separate Method and GPS L1

The GPS L5 in-phase, again, behaves very similarly to the GPS L5 combined method. In strong signal environments, the GPS L5 quadrature channel provides the highest estimate of noise with the smallest variance. However, in noisy environments, the GPS L5 quadrature provides the lowest estimate, but it also suffers from the fewest drop outs of all the other methods. This is because the GPS L5 C/N0 estimate with the extended integration period is actually the most accurate estimate of C/N0. The other methods tend to overestimate C/N0 in noisy environments. This will be shown more explicitly in the simulated results following this section. The GPS L5 quadrature has the fewest drop outs because the extended integration period allows for an accumulation of power that will outlast passing degradation and allow for meaningful updates to be applied.

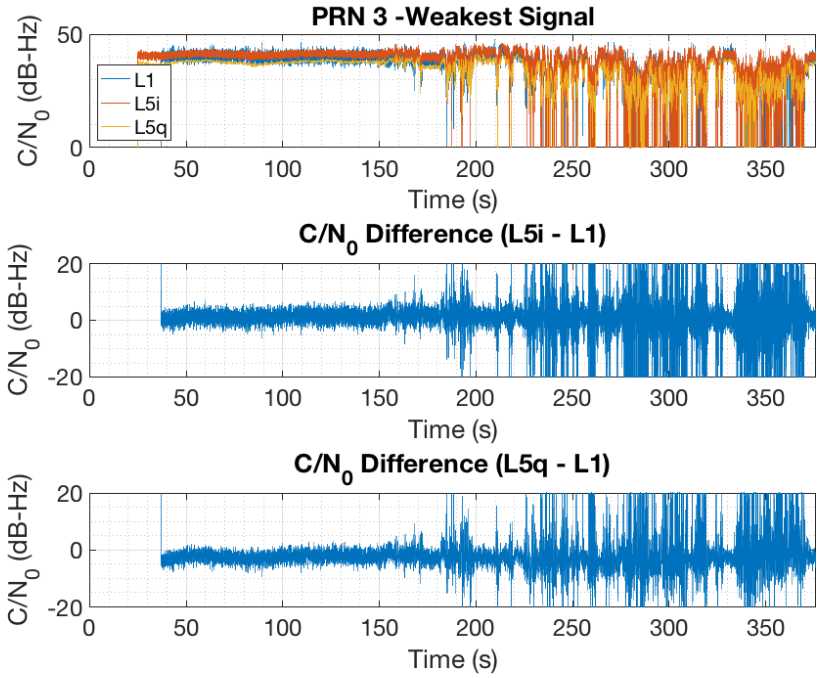

Figure 5.27: C/N0 Estimates for PRN 3 for GPS L5 Separate Method and GPS L1

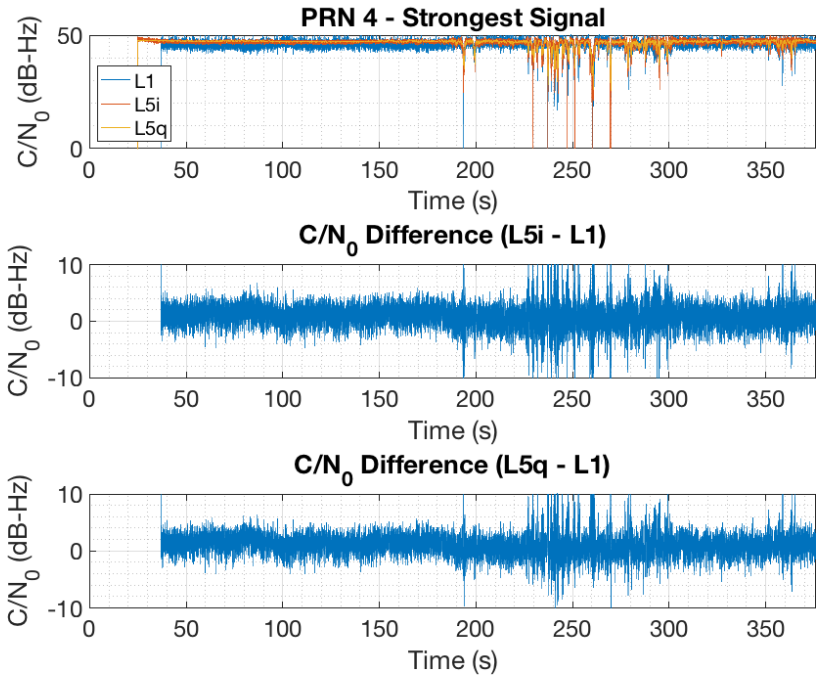

Figure 5.28: C/N0 Estimates for PRN 4 for GPS L5 Separate Method and GPS L1

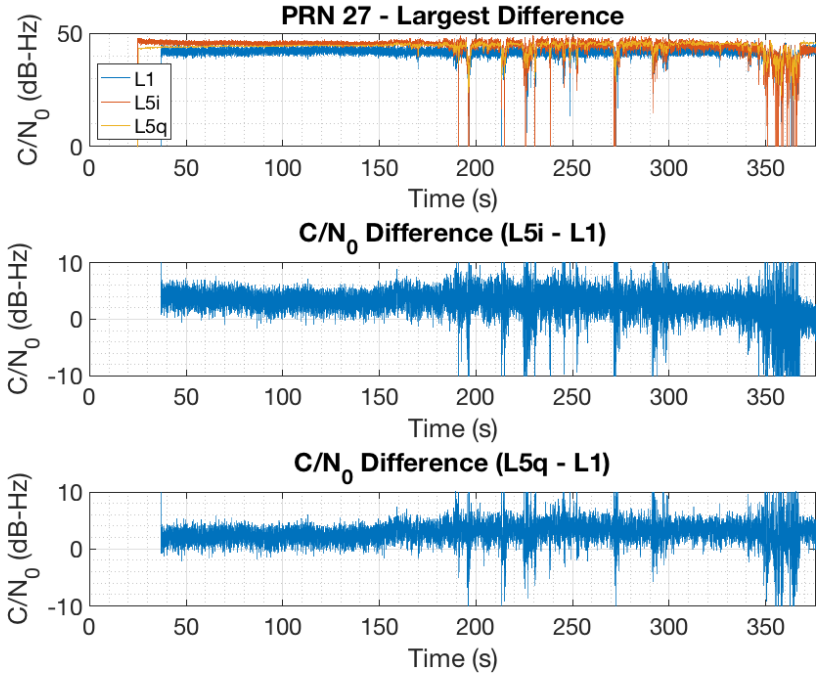

Figure 5.29: C/N0 Estimates for PRN 27 for GPS L5 Separate Method and GPS L1

5.4.4 Robustness Metrics

In order to quantify the robustness of the varying methods, any measurement below 18 dB-Hz is assumed to provide no useful information to the navigation filter. Figure 5.30 shows the number of satellites providing useful updates at the given epoch. Those results are then tabulated into percentages in Table 5.1. In the table, the results are for GPS L1, GPS L5 in-phase and quadrature combined, GPS L5 in-phase separate, GPS L5 quadrature separate, and the GPS L5 quadrature only receiver. The GPS L5 combined method outperformed all other methods by approximately 1-3 %, and it provided more useful measurements to the filter. However all GPS L5 methods outperformed GPS L1.

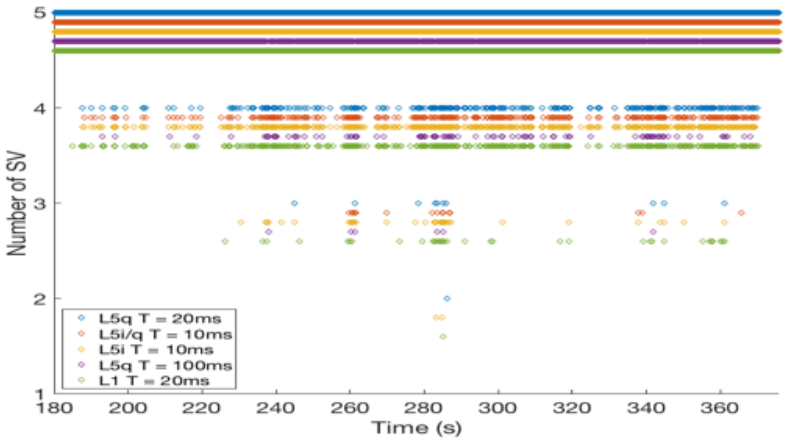

Figure 5.30: Number of Satellites Providing Useful Measurements at each Epoch

	GPS L1	GPS L5 C	GPS L5i S	GPS L5q S	GPS L5q
5 SV	94.90	97.89	95.59	96.52	96.92
4 SV	4.88	2.07	4.22	3.30	3.00
3 SV	0.20	0.04	0.17	0.14	0.07
2 SV	0.01	0.00	0.01	0.00	0.00
1 SV	0.00	0.00	0.00	0.00	0.00
0 SV	0.00	0.00	0.00	0.00	0.00

Table 5.1: Percentage of Time Method had Useful Measurements Provided by X Satellites

5.4.5 PVT and Covariance results

Figure 5.31 shows the velocity estimate of all methods for the dynamic data run. The bandwidth of the Doppler frequency directly relates to the noise rejection in the velocity estimate. The GPS L5 quadrature separate with a 10 Hz update rate provides the most filtered and highly weighted measurement to the navigation filter. If the PVT solution is sampled at the same rate as the extended integration period and in sync with the last arriving signal, the solution will have the filtering of the slower update rate while still benefiting from the stability provided by the faster GPS L5 in-phase updates. This allows for the best velocity estimate of all methods that still can track reasonable dynamics.

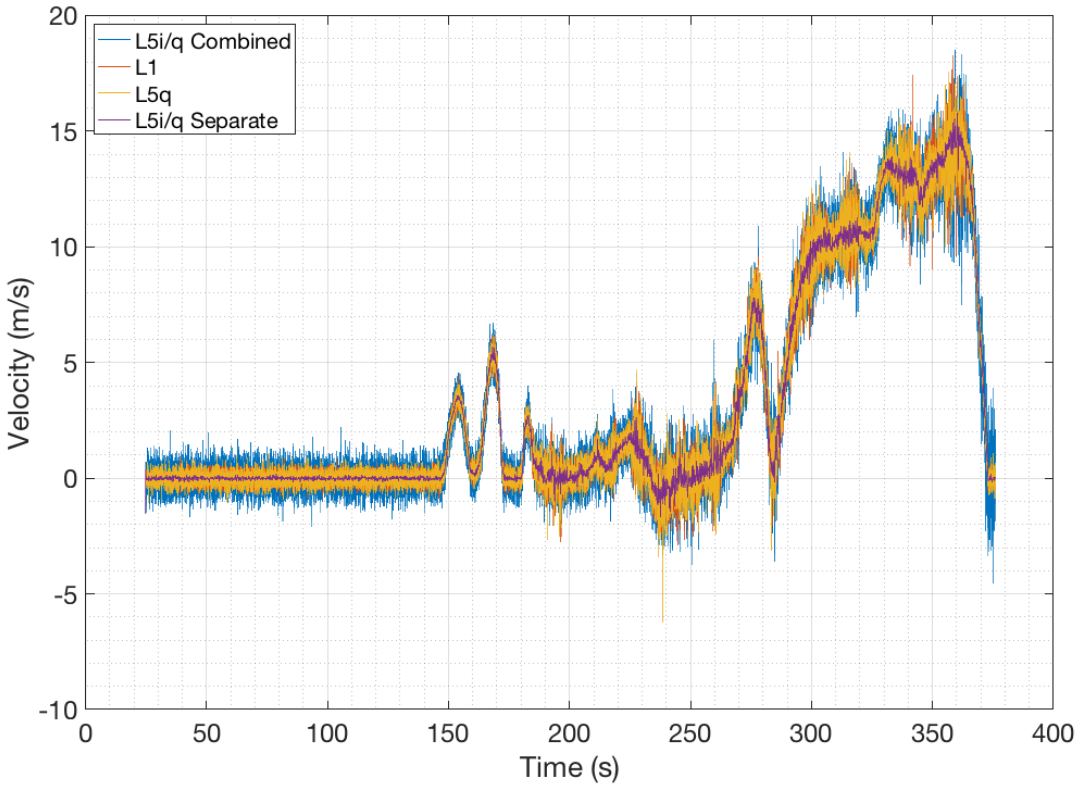

Figure 5.31: ECEF X Dimension Velocity Estimates for Dynamic Data

Figures 5.32 and 5.33 show the covariance of the varying solutions in the ECEF X dimension. The position covariance is similar for all GPS L5 methods, while outperforming GPS L1 by an order of magnitude, even through degraded dynamic environments. The

velocity covariance favors the GPS L1 methods, unless the GPS L5 methods have a greater or equal integration period length. The GPS L5 quadrature has a smaller covariance than the GPS L1 method due to the receiver estimating C/N0 higher for GPS L5 than GPS L1. This 1-3 dB-Hz raise is the difference between the covariance, as seen in the dynamic results and the covariance analysis shown earlier. There are also two velocity covariance lines shown for the GPS L5 separate solution. The lower line comes from sampling the covariance after all the extended channel measurements have been applied. Just as those measurements drive down the noise on the states, they also drive down the variance of the states. The higher line is the covariance sampled at the same sampling rate but offset by half the sampling rate. When the receiver is only receiving the faster update measurements, the covariance and solution quality quickly return to levels more closely associated with other methods of equivalent inegration period.

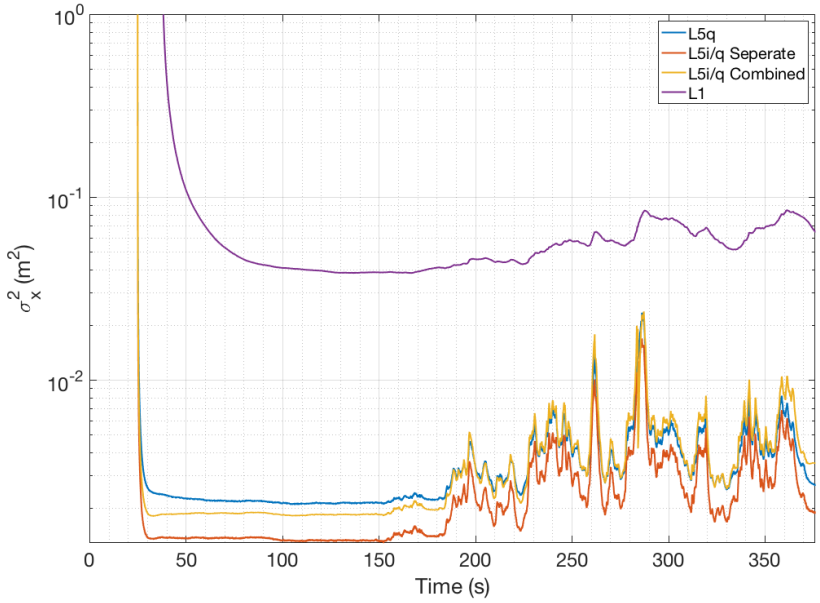

Figure 5.32: ECEF X Dimension Position Covariance For Dynamic Data

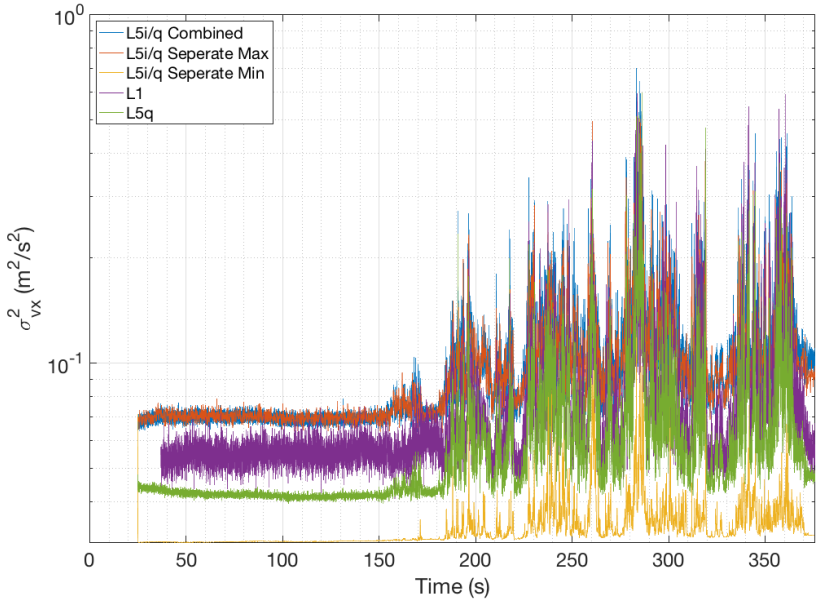

Figure 5.33: ECEF X Dimension Velocity Covariance For Dynamic Data

5.5 Spirent Simulation

These methods were then tested on a full constellation of satellites in simulation. A scenario was generated by a Spirent GNSS Simulator that contained 12 satellites that broadcast both GPS L1 and L5 to a static antenna. After one minute, the broadcast power of each satellite was dropped by a set level at five second intervals. First, all signals dropped by 5 dB-Hz. Then over the next 25 seconds, each signal dropped 2 dB-Hz more every interval. The signals then dropped by 1 dB-Hz every 5 seconds, until the received signal was 31 dB-Hz below its initial value.

Figure 5.34 shows the noise estimate of each method with a solid line showing the timing of the drops. True initial C/N0 values are not known; the Spirent does not report channel noise in terms of receiver C/N0. So, the lines representing the truth are initialized by the average of the C/N0 estimate for that channel during the first minute of the simulation. The timing and depth of the drops are accurately recorded by the "truth" line.

In Figure 5.34, all methods on all channels initially estimate C/N0 in the 45-50 dB-Hz range. The tracking loops begin to report measurements that were rejected by the navigator

beginning at around 17 dB-Hz below the initial value (28-33 dB-Hz). As the C/N0 continues to decrease, the number of measurements rejected continues to increase. Figure 5.35 shows the percentage of useful measurements for each method at each decrease. The extended integration periods on the GPS L5 quadrature separate method allow it to survive the degraded signal environment and consistently provide useful measurements while C/N0s are approaching the cutoff point. Also, the GPS L5 quadrature separate method most accurately estimates the noise at lower levels. Shorter integration periods tend to overestimate C/N0 at lower levels, which shows why the extended integration periods estimated C/N0s lower than other methods in the dynamic data section, while also surviving more blockages and degradation.

5.6 Conclusion

In this chapter, results of various vector tracking architectures on the modern GPS L5 signal were compared to traditional vector tracking architectures on the legacy signal GPS L1. Three scenarios were examined: a static data set with surveyed truth positions, a dynamic data set with heavy foliage, and a simulated static data set with decreasing C/N0 values. A summary of the result is presented below.

In static positioning tests, the GPS L5 methods were all significantly more accurate than the GPS L1 method due to the more precise ranging code. While the GPS L5 methods all performed similarly, the GPS L5 separate method with extended integration periods outperformed the rest. With more precise measurements and high confidence in the dynamic model, the navigation filter is able to more closely approach the true value.

In the dynamic data set, the position did not have a surveyed truth but all position values fell in the correct lane in the satellite image, except for the GPS L5 combined method whose position was biased into the oncoming lane near the end of the run likely due to multipath. All methods survived the heavy foliage environment without failure, but the GPS L5 combined method had the highest percentage of measurements with C/N0 estimates

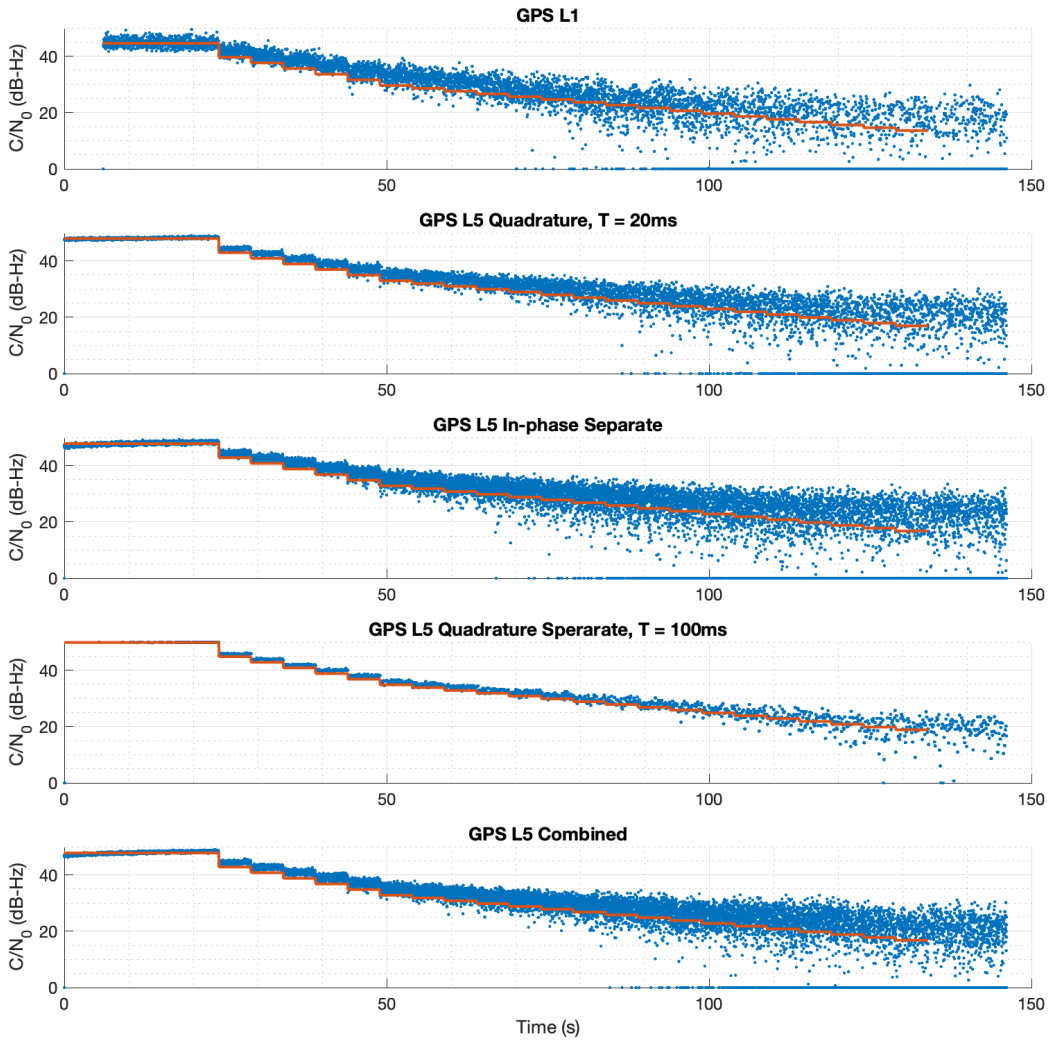

Figure 5.34: C/N0 Estimates for all Methods in the Spirent C/N0 Dropping Simulation

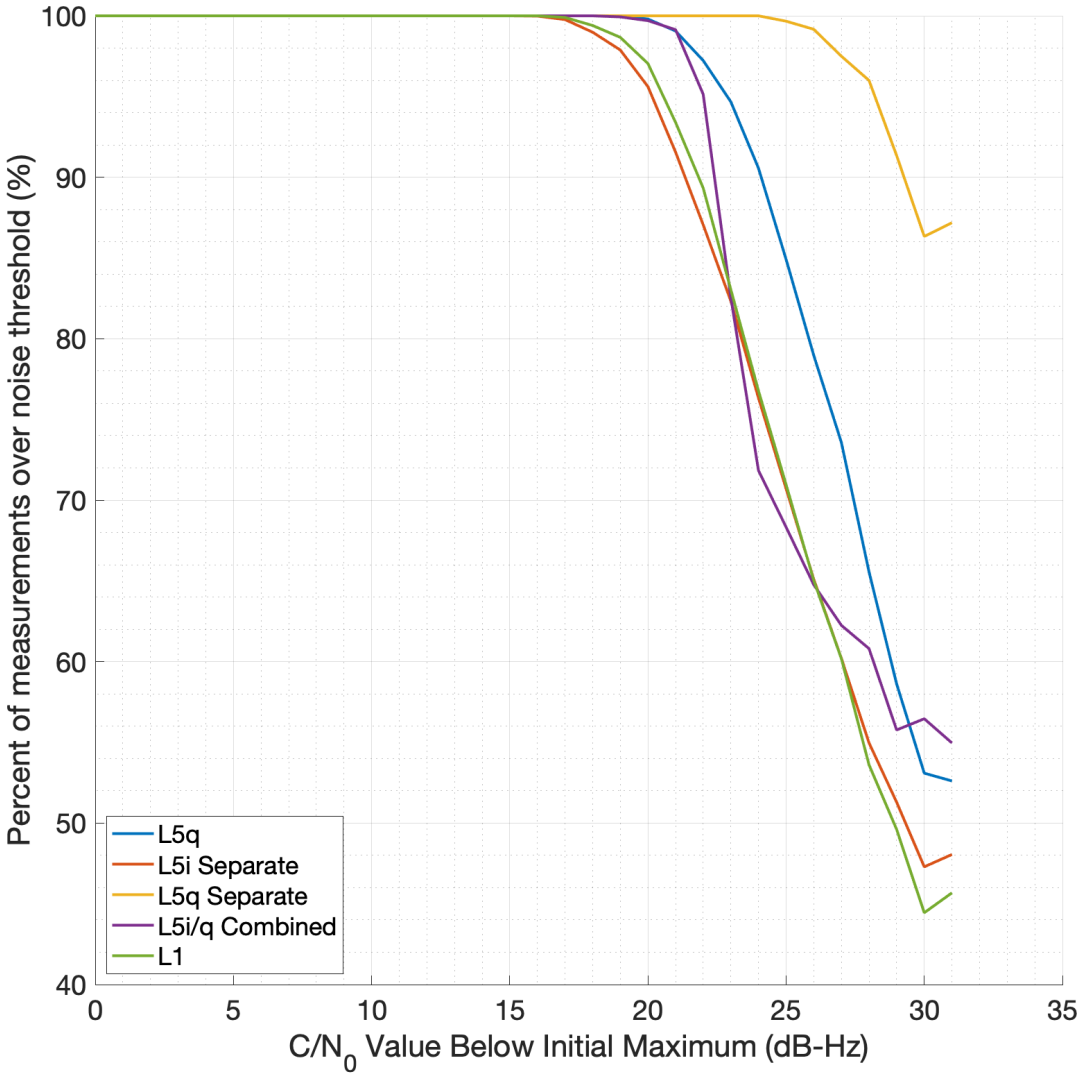

Figure 5.35: Percentage of Useful Measurements Above the Threshold for all Methods in the Spirent C/N0 Dropping Simulation

above the usability threshold. The GPS L5 separate method was able to maintain the most filtering on the carrier frequency estimate. This increased filtering from the extended integration periods allowed for the most precise velocity estimates of all methods and still managed to track all dynamics.

In the simulated static data set, the GPS L5 methods out perform the legacy signal by producing more useful measurements at the same C/N0 degradation levels. In this experiment, extended integration periods dominate the results; the 100 ms GPS L5 quadrature separate provided nearly 90% useful measurements at 31 dB-Hz below the initial noise level. The GPS L5 combined method improves over legacy and equivalent integration period methods but cannot match extended GPS L5 quadrature methods.

In conclusion, the modern GPS L5 signal outperforms the legacy GPS L1 signal, as it was designed to do. The methods proposed in this work allow for more robust tracking and precise PVT estimation than legacy architectures applied to the new signal. The introduction of the pilot channel allow for better navigation performance, as it is no longer limited as the legacy signal was.

Chapter 6

Dual Frequency L1/L5 Vector Tracking and Ionospheric Mitigation

This chapter will look at the potential benefits of a dual frequency GPS L1 C/A and GPS L5 receiver. Both signals are broadcast from the same satellites. Therefore, the measurements generated from the two signals are not independent of one another. However, redundant measurements of different frequencies are capable of mitigating frequency dependent errors, such as some atmospheric ranging delays or some forms of RF interference.

If a GPS L1 C/A receiver was combined with an architecture described in the previous chapter, there could potentially be up to 6 measurements applied to the navigation filter from a single satellite at every epoch. A covariance analysis will be presented to cover potential benefits of adding redundant measurements as well as a brief summary of frequency based errors. The chapter will conclude with a presentation of a dual frequency ionospheric free vector tracking receiver in real and simulated data. The primary focus of this chapter will be on mitigating ionospheric delays, as those delays are frequency dependent.

6.1 Vector Tracking Based Frequency Error Mitigation

The two major atmospheric ranging delays can be seen again in the pseudorange model in equation 3.9. Ionospheric delays are frequency dependent. Troposphere delays are weather dependent and cannot be mitigated by redundant measurements.

The pseudorange measurement is calculated with the assumption that the speed of light is constant across the full range from satellite to receiver. However, the speed of light is dependent upon the refractive index of the medium it travels in. The ionosphere has a larger refractive index than free space due to a high density of free electrons, which

are released primarily by particle collisions with solar ultraviolet radiation. This causes a fluctuating delay that peaks in mid-afternoon [21]. The ionosphere is a dispersive medium, meaning the refractive index is frequency dependent. This delay difference allows the dual frequency user to mitigate the ionospheric effect with a linear combination of the range measurements. The ionospheric error can be assumed to be proportional to the inverse of the carrier frequency squared. There are higher order terms, but they can be safely ignored to develop the ionospheric free pseudorange that is depicted in Equation 6.1 [9].

$$\rho_c = \frac{f_1^2 \rho_1 - f_5^2 \rho_5}{f_1^2 - f_5^2} \tag{6.1}$$

The ionospheric free pseudorange ρ_c is a function of ρ_n and f_n, the pseudorange and carrier frequency of the GPS Ln signal respectively.

In a vector tracking receiver, the code phase error measurement is assumed to represent the pseudorange residual as shown below in Equation 6.2.

$$\delta\rho = \tilde{\rho} - \hat{\rho} \tag{6.2}$$

Given that the estimated pseudorange is geometric in nature and therefore identical for any frequency broadcasting from the same satellite to the same receiver, the measured pseudoranges that are used to create the ionospheric free pseudorange can be replaced with Equation 6.3.

$$\tilde{\rho} = \delta\rho + \hat{\rho} \tag{6.3}$$

This then gives an ionospheric free pseudorange equation that is shown below in Equation 6.4.

$$\delta\rho_c + \hat{\rho} = \frac{f_1^2(\delta\rho_1 + \hat{\rho}) - f_5^2(\delta\rho_5 + \hat{\rho})}{f_1^2 - f_5^2} \tag{6.4}$$

The estimated pseudoranges can then be pulled out of the expression and simplified to Equation 6.5.

$$\delta\rho_c + \hat{\rho} = \frac{f_1^2\delta\rho_1 - f_5^2\delta\rho_5}{f_1^2 - f_5^2} + \frac{f_1^2\hat{\rho} - f_5^2\hat{\rho}}{f_1^2 - f_5^2} \tag{6.5}$$

This expression can then be simplified further to Equation 6.6

$$\delta\rho_c + \hat{\rho} = \frac{f_1^2\delta\rho_1 - f_5^2\delta\rho_5}{f_1^2 - f_5^2} + \frac{f_1^2 - f_5^2}{f_1^2 - f_5^2}\hat{\rho} = \frac{f_1^2\delta\rho_1 - f_5^2\delta\rho_5}{f_1^2 - f_5^2} + \hat{\rho} \tag{6.6}$$

Now the estimated pseudorange can be removed from both sides of the equation, which leaves an ionospheric free pseudorange residual in Equation 6.7.

$$\delta\rho_c = \frac{f_1^2\delta\rho_1 - f_5^2\delta\rho_5}{f_1^2 - f_5^2} \tag{6.7}$$

Now, the vector tracking measurements can be applied to this form of the ionospheric free pseudorange and can provide the navigation filter with a dual frequency ionospheric free measurement that is shown in Equation 6.8.

$$\delta\rho_c = \frac{f_1^2\lambda_{code1}\phi_{DLL1} - f_5^2\lambda_{code5}\phi_{DLL5}}{f_1^2 - f_5^2} \tag{6.8}$$

This measurement can then be corrected by an ionospheric free scalar residual to reduce synchronization errors of vector tracking as covered in Chapter 4. The final form of the corrected measurement, used in the dual frequency receiver to process the data for this chapter, is shown in Equation 6.9.

$$\delta\rho_c = \frac{f_1^2\lambda_{code1}\phi_{DLL1} - f_5^2\lambda_{code5}\phi_{DLL5}}{f_1^2 - f_5^2} + \frac{f_1^2\rho_1 - f_5^2\rho_5}{f_1^2 - f_5^2} - \hat{\rho} \tag{6.9}$$

6.2 Covariance Analysis

This section seeks to present the results of a covariance analysis performed in the manner of the previous chapter. Previously, GPS L5 in-phase and quadrature were combined and

compared to GPS L1 C/A. Now, GPS L1 C/A measurements will be added to the GPS L5 in-phase and quadrature measurements to form a single solution. These results will again be compared to single frequency GPS L1 C/A results.

The results for the position covariance can be seen in Figure 6.1. The addition of the GPS L1 C/A measurements do not significantly change the solution. The GPS L5 range measurements are given more weight, due to the increased precision from the higher code frequency. This results in a position covariance that is roughly identical to that seen in the previous chapter.

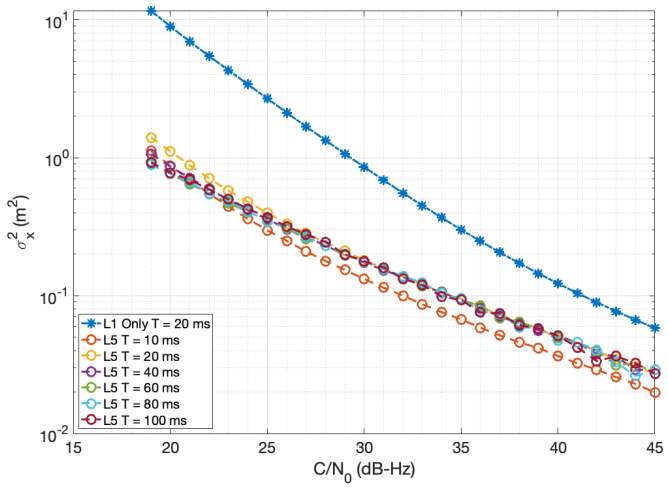

Figure 6.1: ECEF X Position Covariance for GPS L5i/q and GPS L1 C/A combined solution.

The results of the velocity covariance can be seen in Figure 6.2. Here, the addition of the GPS L1 C/A range rate measurements drives the solution performance to the quality of the single frequency GPS L1 C/A solution. GPS L1 C/A has a higher carrier frequency, and therefore a shorter wavelength, giving its range rate measurements increased precision. However, like in the previous chapter, when the GPS L5 quadrature integration period is extended, it provides the superior velocity estimate due to the filtered measurements applied to the navigator.

The addition of GPS L1 C/A as an additional measurement is not worth the computational resources. The filter weights so highly towards the GPS L5 position solution that the

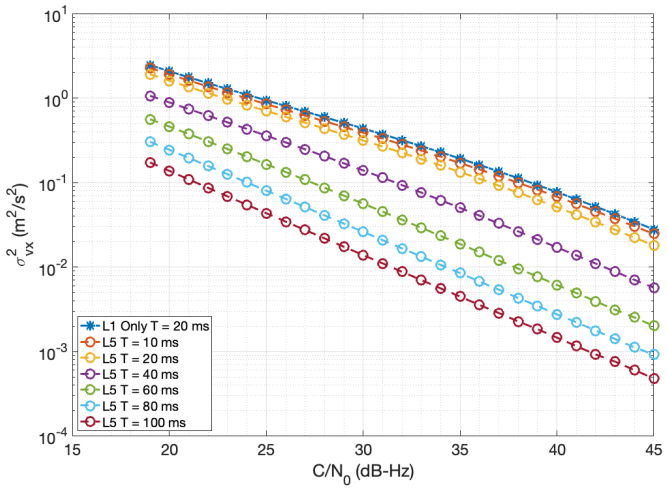

Figure 6.2: ECEF X Velocity Covariance for GPS L5i/q and GPS L1 C/A combined solution.

L1 ranges are functionally ignored. Also, any improvement in velocity estimation offered by GPS L1 can be replicated or bettered by GPS L5 quadrature estimates. If both signals are available from the same satellite, the only benefit from tracking both will be for mitigation of frequency based errors.

6.3 Algorithms and Experimental Setup

The structure of the vector tracking architecture for mitigating frequency based errors will be 20 ms GPS L1 C/A channels, as limited by the data bit, that will close the loop at the same time as 20 ms GPS L5 quadrature channels. The range residual measurement will be formed from as described previously. The variance of the range residual will be given as the sum of the variance on the GPS L5 and GPS L1 measurements. The range rate residual will be the GPS L1 discriminator. The dual frequency ionospheric free range residual vector tracking receiver was run on the same static data set with surveyed truth as in Chapter 5. It is compared against a 50 Hz GPS L5 quadrature only vector tracking receiver with a Klobuchar ionospheric model correction on the scalar residual added to the vector residual. The algorithm for the Klobuchar model can be found in [19] and the parameters for it are given by the GPS data message

6.4 Live Sky Results

The GPS L5 quadrature receiver with the Klobuchar model position results can be seen in Figure 6.3. This can be compared against the results of the receiver without the ionospheric correction in Figure 5.9. Both receivers have identical integration periods and process noise coefficients. Over the same time interval of the first 40 seconds after the first position fix, the ionospheric free has a total error of approximately 5 m, while the standard receiver has a total error of approximately 12 m. The ionospheric free result is able to remove the majority of the altitude error from the initial solution.

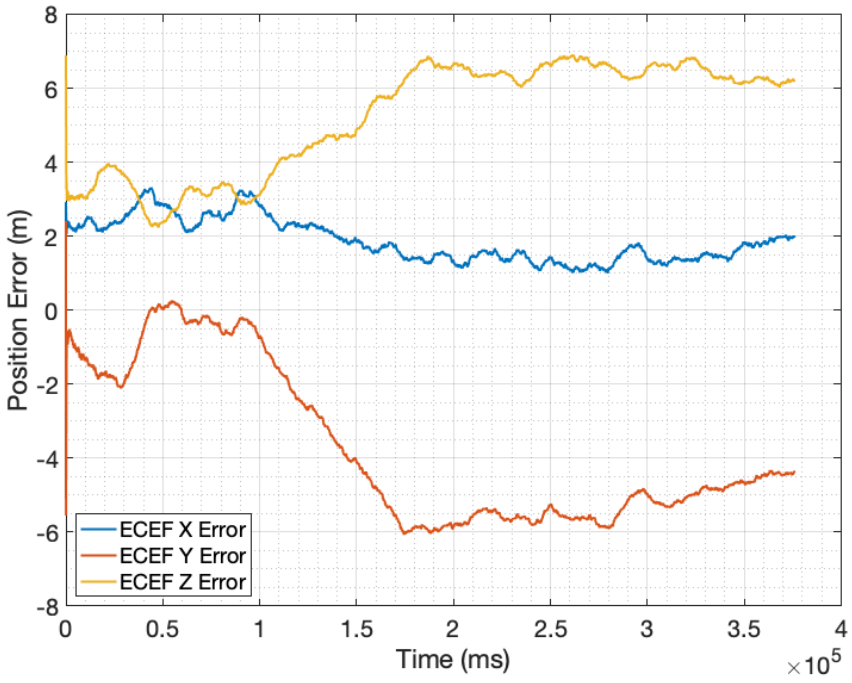

Figure 6.3: Live Sky ECEF Position Errors for a GPS L5 Quadrature Receiver with Ionospheric Model

Figure 6.4 shows the error in the ionospheric free combination receiver. The process noise coefficient is 200 m^2/s^3 rather than the 2 m^2/s^3 of the GPS L5 receiver. Combining the measurements gives the measurements a larger variance. In order for the model to not dominate the state estimation, the process noise was raised to allow the measurements with an increased measurement covariance to drive the solution to zero mean. The solution has

much more variance from the measurements, but it is also closer to zero mean than the single frequency solution.

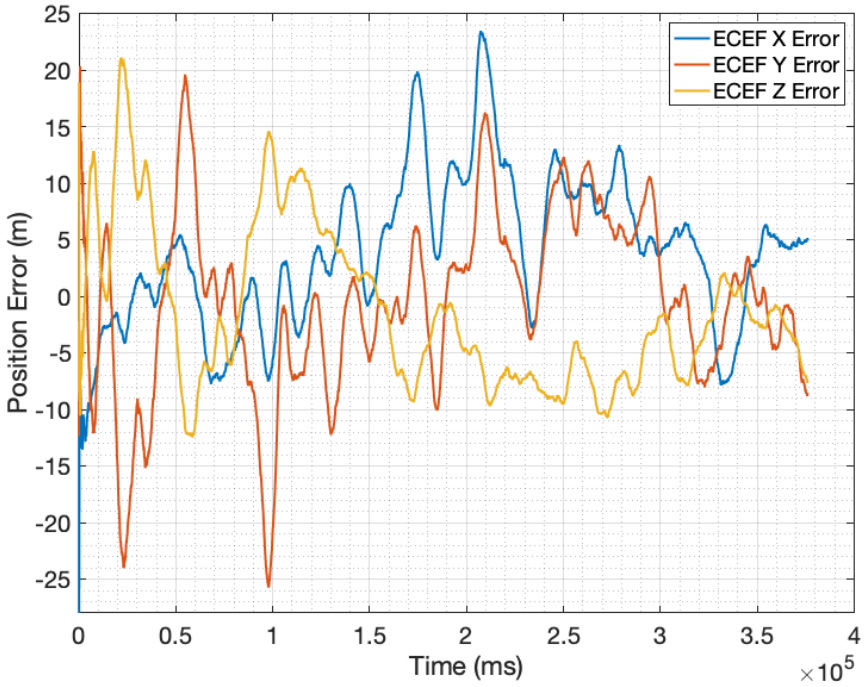

Figure 6.4: Live Sky ECEF Position Errors for a Dual Frequency Receiver with Ionospheric Free Measurement Combinations

Figure 6.5 shows the error between the measured range residual and the true range residual for PRN 10. The true residual was calculated from the true position of the satellite and the antenna at a given epoch. The measured range residual is calculated as shown in Equation 6.9 for the dual frequency receiver and in Equation 4.2 for the single frequency receiver. The dual frequency receiver has discriminators with roughly equivalent variance being applied as measurements. However, the order of magnitude difference in the chipping rate turns an equivalent chip error into an order of magnitude difference in range error. This large variance is only compounded by the linear combination to form the ionospheric free measurement. Thus, the dual frequency measurements are shown to have much higher variance while being closer to zero mean. PRN 10 is the worst performing channel for the dual frequency.

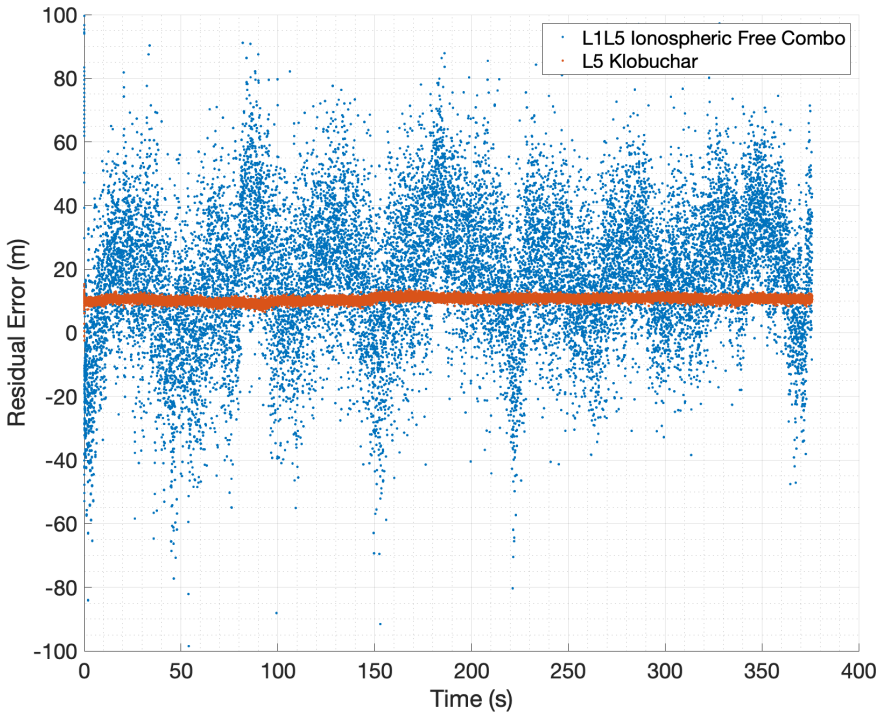

Figure 6.5: Residual Estimate Error for Single and Dual Frequency Methods for PRN 10

Figure 6.6 shows the residual range error for PRN 26. Both receivers preformed well for PRN 26, but dual frequency provided the better mean.

Figure 6.7 provides the mean error and the standard deviation for both receivers residual range error. PRN 10 is channel 2, and PRN 26 is channel 4. The dual frequency can marginally outperform the single frequency receiver, but there is always a drastic increase in measurement variance.

6.5 Simulation Results

The live sky study from the previous section is now repeated in simulation. RF data from a Spirent simulator was recorded by the IFEN SX3 and passed into both receivers in post process. There were 12 satellites broadcasting in the scenario, as opposed to only 5 in the live sky test. It is to be noted that the Spirent simulates the ionospheric errors

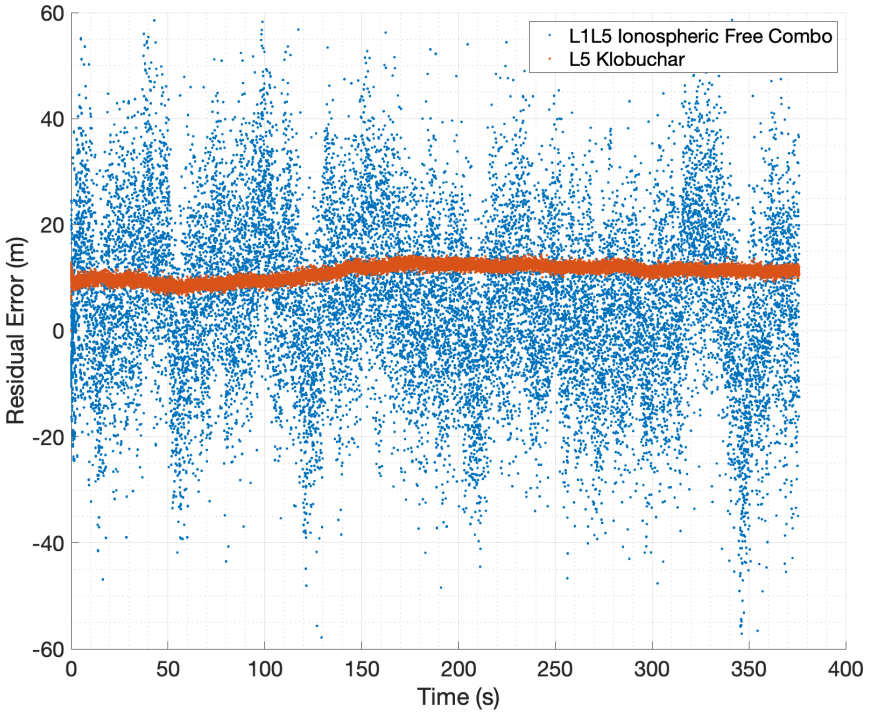

Figure 6.6: Residual Estimate Error for Single and Dual Frequency Methods for PRN 26

with Klobuchar models, but Spirent uses different parameters than what is broadcast in the ephemeris by the simulator.

Figure 6.8 shows the position error for the simulated data set for the single frequency receiver. The error, for ionospheric corrected measurements, was fairly high. For comparison, the position error is plotted for a GPS L5 quadrature vector tracking receiver with no ionospheric model and 50 Hz update rate in Figure 6.9. Similar amounts of error were removed as were in the live sky data. Again the process noise coefficient was 2 m^2/s^3 for both receivers with and without the Klobuchar model.

Figure 6.10 shows the ECEF position errors for the dual frequency receiver. The process noise coefficient was 200 m^2/s^3 again, yet the PVT solution is much more stable than the live sky results.

Figure 6.11 shows the residual range error for PRN 9 in the simulated data set. Both receivers had approximately the same mean error, but the variance was much higher for

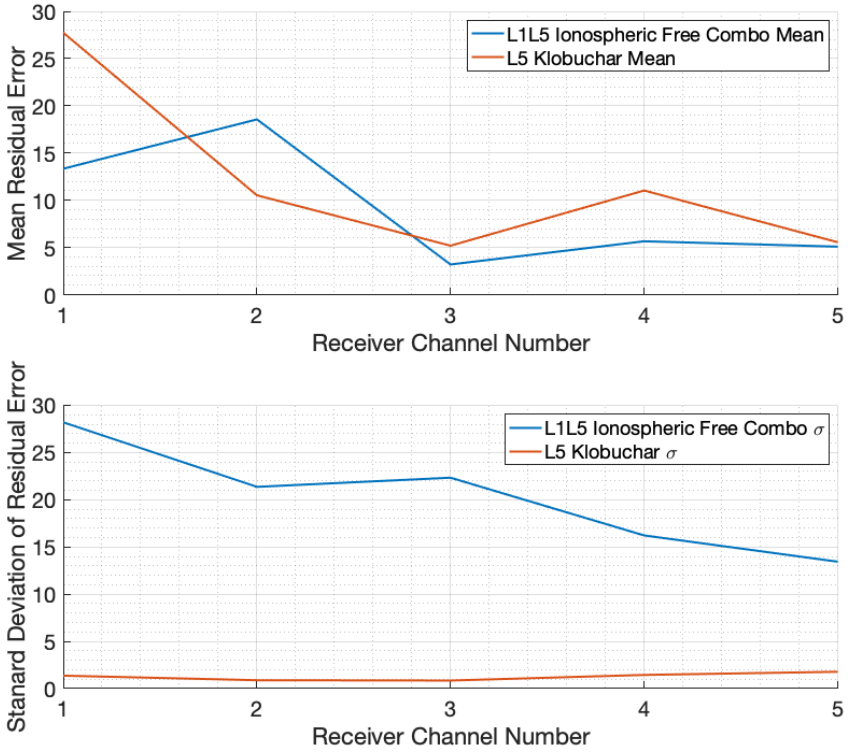

Figure 6.7: Mean and Standard Deviation for Single and Dual Frequency Methods for all Channels

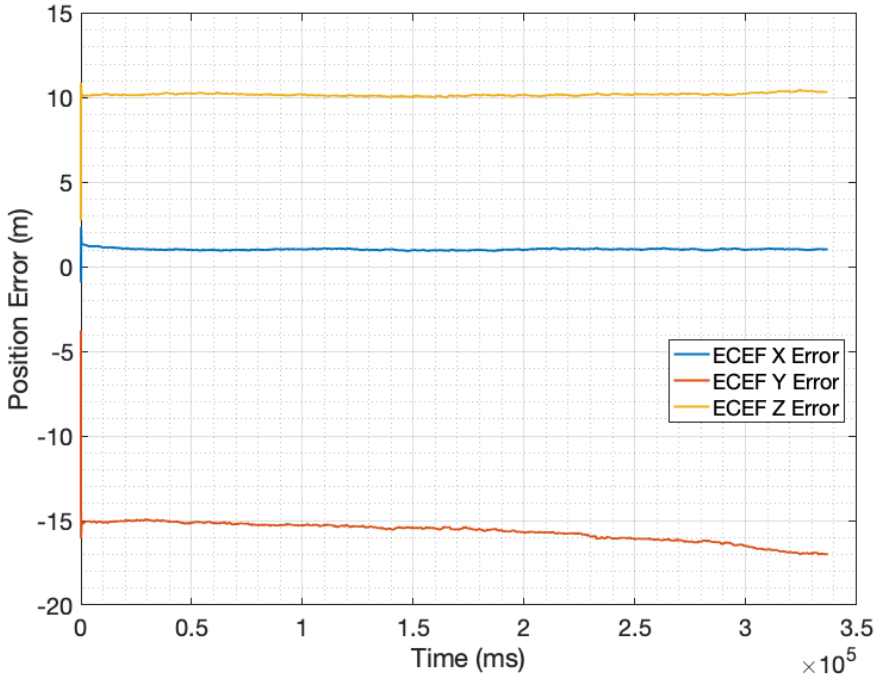

Figure 6.8: Simulated ECEF Position Errors for a GPS L5 Quadrature Receiver with Ionospheric Model

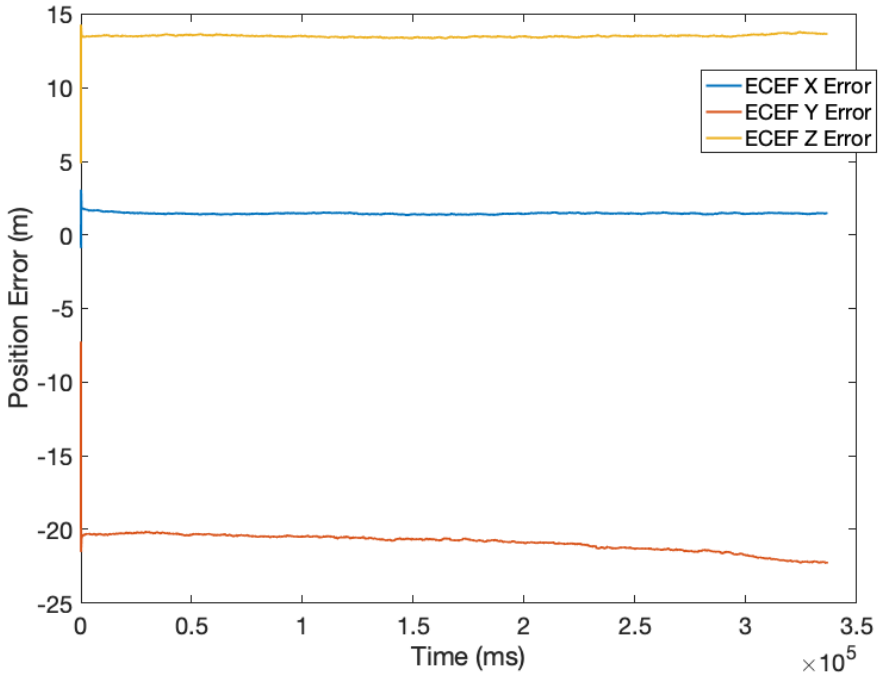

Figure 6.9: Simulated ECEF Position Errors for a GPS L5 Quadrature Receiver without Ionospheric Model

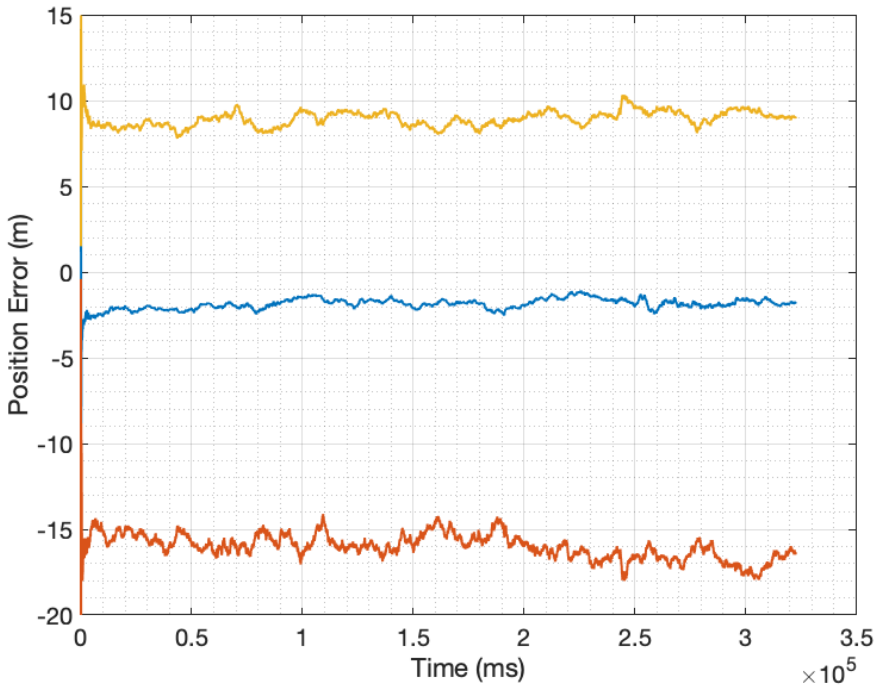

Figure 6.10: Simulated ECEF Position Errors for a Dual Frequency Receiver with Ionospheric Free Measurement Combinations

the dual frequency. It is to be noted that the GPS L1 discriminators have less oscillatory behavior than the live sky data, and this resulted in a lower variance for all channels.

Figure 6.12 shows the residual range error for PRN 17 in the simulated data. This channel had the lowest mean for either receiver and was approximately zero for the dual frequency receiver.

Figure 6.13 provides the mean error and the standard deviation for both receivers residual range error. PRN 9 is channel 2, and PRN 17 is channel 6. The dual frequency consistently outperforms the single frequency receiver in mean, and the variance is consistent and lower than in the live sky tests. However, the variance is still significantly higher than that of the single frequency

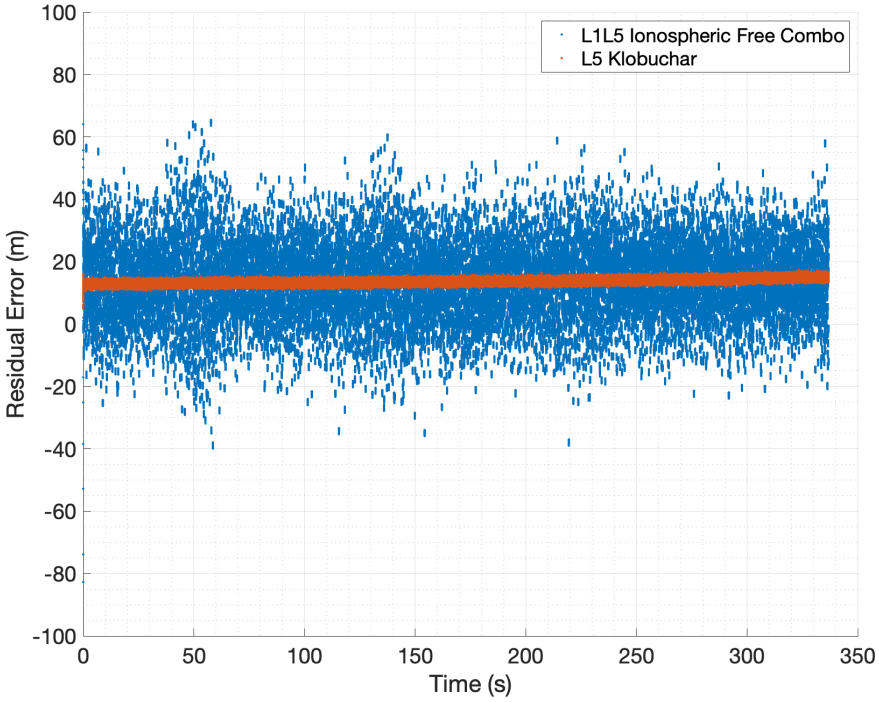

Figure 6.11: Simulated Residual Estimate Error for Single and Dual Frequency Methods for PRN 9

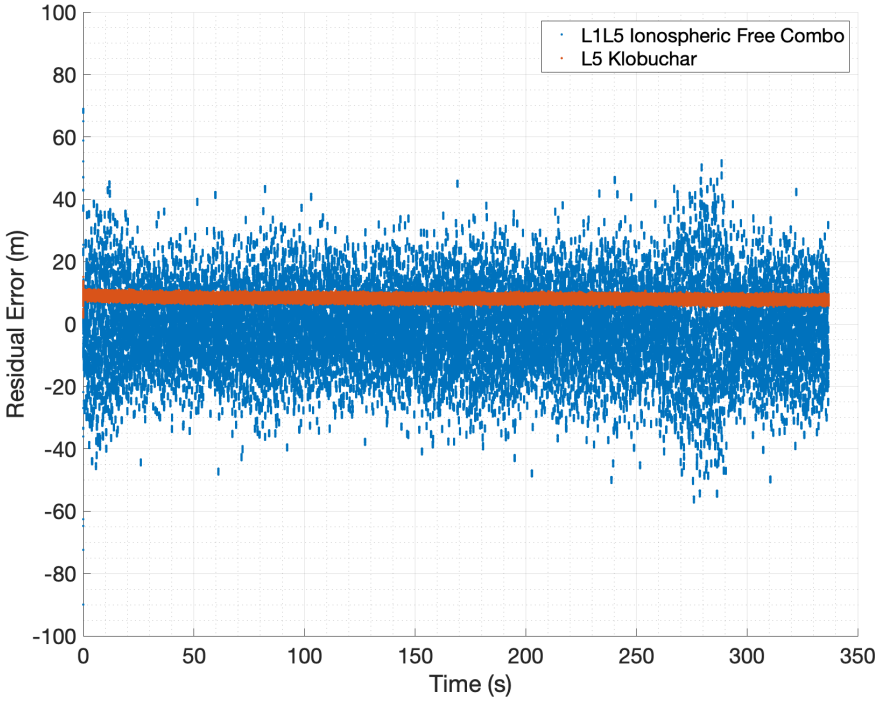

Figure 6.12: Simulated Residual Estimate Error for Single and Dual Frequency Methods for PRN 17

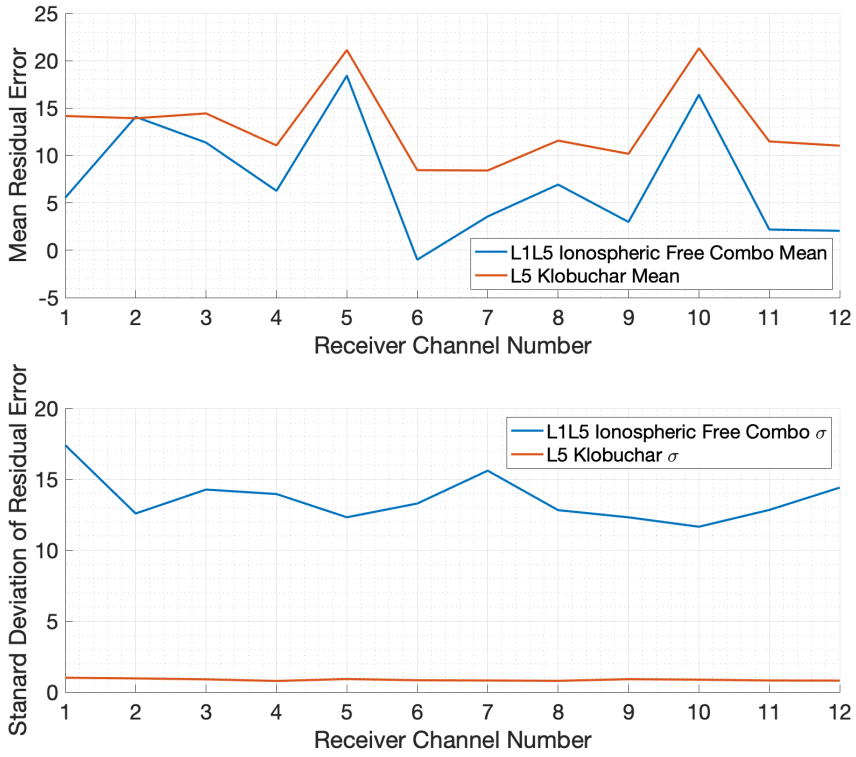

Figure 6.13: Mean and Standard Deviation for Single and Dual Frequency Methods for all Channels in Simulated Data Set

6.6 Conclusion

The inclusion of additional measurements was shown not to make a noticeable improvement to the PVT solution in the covariance analysis. The difference in measurement quality weights so heavily towards GPS L5 that the GPS L1 measurements are almost disregarded.

However, the addition of GPS L1 for the removal of frequency dependent errors is much more useful. The ionospheric free combination can remove the majority of the delay at the price of increased noise on the measurement. This can be counteracted by using more precise measurements, such as carrier ranging. However, vector tracking is unable to generate a carrier phase measurement without infrastructure for RTK [14].

The dual frequency ionospheric receiver has been shown in this chapter to be a viable alternative to models for the reduction in ionospheric errors. While the measurement variance is increased, the linear combination is a simpler implementation that removes true error rather than modeled error. The live sky results are confirmed by the simulation, and, as the GPS L5 constellation becomes fully available, the live sky results are more likely to trend towards the simulated results when the receiver has more measurements.

Chapter 7

Conclusion and Future Work

This work has provided an analysis of a vector tracking architecture on the new GPS L5 signal. The GPS L5 signal has been shown to be an improvement over the legacy signal GPS L1 C/A in both precision and robustness, as expected from the literature. This work extended the state of the art by adapting the vector tracking architecture to the new signal structure. This produced even more performance gains than solely signal improvements. The implementation of the algorithms proposed are shown to have improved the ability of the GNSS vector tracking receiver to survive through degraded conditions and to improve the PVT solution in both live sky and simulated tests. The GPS L5 separate method defined in this work was able to provide useful measurements 85% of the time on signals 31 dB-Hz below its clear sky value while a traditional 50 Hz vector tracking receiver was able to provide useful measurements 45% and 52% of the time for GPS L1 and GPS L5 quadrature respectively. The GPS L5 in-phase and quadrature combined channels at the discriminator level improved the performance in dynamic degraded environments over other methods by providing useful measurements 98% of the time while the traditional GPS L1 receiver was only able to provide useful measurements 95% of the time.

This work also showed the viability of an ionospheric free vector tracking approach. There is an increase in measurement noise on such a signal combination, but a slight improvement in the mean residual error estimate, as opposed to single frequency modeling methods. For future work, signals with higher chipping rates than L1 C/A should be used in the combination. The variance of the L1 signal hurt the results overall. A modern signal such as GPS L2C or L1C could probably make this method more resistant to measurement noise.

For future work, the author recommends further research into a GPS L5 quadrature only receiver that is designed with a variable integration period to be optimally selected to set a bandwidth best suited for the users noise level and dynamics. The extended Kalman filter sets the bandwidth, but the measurement covariance can be changed by the selection of integration period to allow for different EKF results. The draw back of the narrow bandwidth is the potential inability of tracking full signal dynamics. A decision of the next integration length could be made in order to accrue as much signal power as possible to accurately create measurements and filter thermal noise while not sacrificing dynamic tracking potential. Also, this work struggled with the stability of the longer tracking loops without an underlying faster loop updating the states. Potentially eliminating the need for the second loop would free up a significant amount of resources that could be dedicated to tracking another frequency or constellation signal.

Bibliography

[1] Don Benson. Interference Benefits of a Vector Delay Lock Loop (VDLL) GPS Receiver. In *Proceedings of the 63rd Annual Meeting of The Institute of Navigation*, Cambridge, Massachusetts, April 2007. Institute of Navigation.

[2] P. Bolla and K. Borre. Performance analysis of dual-frequency receiver using combinations of GPS L1, L5, and L2 civil signals. *J Geod.* 93, 437–447 (2019).

[3] K. Borre, D. Akos, N. Bertelsen, P. Rinder, and S. H. Jensen. *A Software-Defined GPS and Galileo Receiver: A Single Frequency Approach.* Birkhauser, 2007.

[4] R.G. Brown and P. Y. C. Hwang. *Introduction to Random Signals and Applied Kalman Filtering.* John Wiley & Sons, Inc., 1996.

[5] . J. Geng and C. Shi. Rapid initialization of real-time PPP by resolving undifferenced GPS and GLONASS ambiguities simultaneously. *J Geod.* 91, 361–374 (2017).

[6] C. A. Givhan, D. Bevly, and S. Martin. Performance Analysis of a Vector Tracking Software Defined Receiver for GPS L5. In *Proceedings of the 33rd International Technical Meeting of the Satellite Division of The Institute of Navigation (ION GNSS+ 2020).* September 2020.

[7] T. Humphreys, B. Ledvina, M. Psiaki, B. O'Hanlon, and P. Kintner. Assessing the spoofing threat: Development of a portable GPS civilian spoofer. In *Proceedings of ION GNSS 2008*, 2008.

[8] C. Hyun, K. Hyun, C. Shin, S. Lee and J. Kim. Acquisition and tracking schemes for a GPS L5 receiver. In *Proceedings of the 2008 International Conference on Control, Automation and Systems.* 2008.

[9] E. Kaplan and C. Hegarty. Understanding GPS: Principles and Applications. Artech House, 2006.

[10] M. Lashley and D. M. Bevly. Analysis of Discriminator Based Vector Tracking Algorithms. In *Proceedings of the 2007 National Technical Meeting of The Institute of Navigation.* San Diego, California, January 2007.

[11] M. Lashley, D. M. Bevly, and J. Y. Hung. A Valid Comparison of Vector and Scalar Tracking Loops. In *Proceedings of IEEE/ION Position Location and Navigation Symposium Conference.* Indian Wells/Palm Springs, California, May 2010.

[12] M. Lashley and D. M. Bevly. Comparison in the Performance of the Vector Delay/Frequency Lock Loop and Equivalent Scalar Tracking Loops in Dense Foliage and Urban Canyon. In *Proceedings of the 24[24] International Technical Meeting of the Satellite Division of The Institute of Navigation (ION GNSS)*. Portland, Oregon, September 2011.

[13] M. Lashley. *Kalman Filter Based Tracking Algorithms For Software GPS Receivers*. Master's Thesis, Auburn University, December 2006.

[14] S. Martin. *GPS Carrier Phase Tracking in Difficult Environments Using Vector Tracking For Precise Positioning and Vehicle Attitude Estimation*. PhD Dissertation, Auburn University, 2017.

[15] C. Mongrédien, G. Lachapelle, and M. E. Cannon. Testing GPS L5 Acquisition and Tracking Algorithms Using a Hardware Simulator. In *Proceedings of the 19th International Technical Meeting of the Satellite Division of The Institute of Navigation (ION GNSS 2006)*. Fort Worth, Texas, September 2006

[16] C. Mongrédien, M. E. Cannon, and G. Lachapelle. Performance Evaluation of a GPS L5 Software Receiver Using a Hardware Simulator. In *Proceedings of the 20th International Technical Meeting of the Satellite Division of The Institute of Navigation (ION GNSS 2007)*. Fort Worth, Texas, September 2007.

[17] C. Mongredien, M. E. Cannon, G. Lachapelle. Performance Evaluation of Kalman Filter Based Tracking for the New GPS L5 Signal. In *Proceedings of the 20th International Technical Meeting of the Satellite Division of The Institute of Navigation (ION GNSS 2007)*. Fort Worth, Texas. September 2007.

[18] Navstar GPS Joint Program Office. Interface specification IS-GPS-200L, 2020.

[19] Navstar GPS Joint Program Office. Interface specification IS-GPS-705G, 2020.

[20] M. Roi, Z. Yoav, and K. Dror. Analyzing Tesla's Level 2 Autonomous Driving System Under Different GNSS Spoofing Scenarios and Implementing Connected Services for Authentication and Reliability of GNSS Data. In *Proceedings of the 33rd International Technical Meeting of the Satellite Division of The Institute of Navigation (ION GNSS+ 2020)*. September 2020.

[21] B. Parkinson and J. Spilker. The global positioning system: theory and applications volume I. Aiaa, 1996.

[22] M. Psiaki and H. Jung. Extended Kalman Filter Methods for Tracking Weak GPS Signals. In *Proceedings of ION GPS 2002*. Portland, Oregon. September 2002.

[23] L. Ries, C. Macabiau, O. Nouvel, Q. Jeandel, W. Vigneau, V. Calmettes, and J. Issler. A software receiver for GPS-IIF L5 signal. In *Proceedings of the 15th International Technical Meeting of the Satellite Division of The Institute of Navigation (ION GNSS)*. Portland, Oregon, September 2002.

[24] J. Spilker. Vector Delay Lock Loop Processing of Radiolocation Transmitter Signals. Stanford, California, March 1995. US Patent 5,398,034.

[25] J. Spilker and A. Van Dierendonck. Prop. osed New L5 Civil GPS Codes. *NAVIGATION, Journal of The Institute of Navigation*. 48(3):135-144, 2001.

[26] S. A. Stephens and J. B. Thomas. Controlled-Root Formulation for Digital Phase-Locked Loops. In *IEEE Transactions on Aerospace and Electronic Systems*, 31(1):78-95, 1995.

[27] M. Tran and C. Hegarty. Receiver Algorithms for the New Civil GPS Signals. In *Proceedings of The Institute of Navigation's National Technical Meeting*. San Diego, California, January 2002.

[28] M. Tran. Performance Evaluations of the New GPS L5 and L2 Civil (L2C) Signals. *Navigation: The Journal of the Institute of Navigation*, 51(3):199-212, 2004.

[29] University of Texas at Austin. Spoofing a Superyacht at Sea. https://news.utexas.edu/2013/07/30/spoofing-a-superyacht-at-sea. 2013.

[30] P. Ward. Performance Comparison Between FLL, PLL, and a Novel FLL-Assisted-PLL Carrier Tracking Loop Filter Under RF Interference Conditions. In *Proceedings of The Institute of Navigation International Technical Meeting*. Nashville, Tennessee, September 1998.

[31] T. Watts. *A GPS and GLONASS L1 Vector Tracking Software-Defined Receiver*. Master's Thesis, Auburn University, 2019.

[32] S. Zhao and D. Akos. An Open Source GPS/GNSS Vector Tracking Loop - Implementation, Filter Tuning, and Results. In *Poceedings of the 2011 International Technical Meeting of The Institute of Navigation*. San Diego, California, January 2011.

[33] B. Zheng and G. Lachapelle. Acquisition Schemes for a GPS L5 Software Receiver. In *Proceedings of the 17th International Technical Meeting of the Satellite Division of The Institute of Navigation (ION GNSS 2004)*. Long Beach, Califonia. September 2004.